NASA CR-
144364

DEVELOPMENTS IN CONVECTIVE HEAT TRANSFER MODELS FEATURING SEAMLESS AND SELECTED- DETAIL SURFACES, EMPLOYING ELECTROLESS PLATING

(NASA-CR-144364) DEVELOPMENTS IN CONVECTIVE HEAT TRANSFER MODELS FEATURING SEAMLESS AND SELECTED DETAIL SURFACES, EMPLOYING ELECTROLESS PLATING (ITV Aerospace Corp.) 101 p HC $5.25 CSCL 20D G3/34
N75-29356
Unclas
31985

BY C. J. STALMACH , Jr.

30 June 1975

TECHNICAL REPORT 2-57110/5R-3227

Prepared under Contract No. NAS9-13692 by
Vought Systems Division
LTV Aerospace Corporation
Dallas, Texas

For

National Aeronautics and Space Administration

FORWARD

This report covers the program conducted under contract No. NAS9-13692 with NASA, Lyndon B. Johnson Space Center. The contract time span was November 1973 to June 1975 during which time the contract was dormant for approximately six months (October 1974 to April 1975) awaiting availability of government furnished model under CCA No. 1.

The contract objective was to develop improved methods of fabricating heat transfer wind tunnel models. The program was divided into a Phase A, development of concepts, and Phase B, fabrication of an Orbiter model applying Phase A experience. Phase A experiments included evaluation of a plated slab model concept and feasibility study of plating controlled roughness on a model surface. Based on NASA technical priorities and cost estimates of Phase B options, a Change Order, CCA No. 1, was issued October 3, 1974 which directed the remaining funds to the selective plating of scaled heatshield tiles on an existing Orbiter model.

Dr. Winston D. Goodrich, NASA-JSC program technical monitor, provided valuable suggestions and encouragement which are greatly appreciated. Many other individuals provided assistance; particular recognition and thanks are given to:

- Dr. Richard N. Claytor, Consultant on electroless plating
- Mr. Jim M. Holland, laboratory co-worker
- Mr. William K. Lockman, NASA Ames, for tunnel tests of Phase A Models
- Mr. Howard MacKay, Shipley Company representative, for suggesting the ECAN process
- Mr. Thomas C. Pope, for computer studies of instrumentation concepts

TABLE OF CONTENTS

LIST OF SYMBOLS

A	Area
b	Thickness of metallic skin
erfc	Complementary error function, $\frac{2}{\sqrt{\pi}} \int_{\beta}^{\infty} e^{-\lambda^2} d\lambda$
C, Cp	Specific heat at constant pressure
h, H	Aerodynamic heat transfer coefficient
k, K	Thermal conductivity
M	Free-stream Mach number
P	Pressure
$\dot{q}$, Q	Heat transfer rate
R	Radius, or free-stream Reynolds number
S	Surface Distance
T	Temperature
t	Time
β	$= \frac{h\sqrt{t}}{\sqrt{\rho C K}}$
ρ	Density
λ	Dummy variable of integration
μ	Micro-

DEVELOPMENTS IN CONVECTIVE HEAT TRANSFER MODELS FEATURING SEAMLESS AND SELECTED - DETAIL SURFACES, EMPLOYING ELECTROLESS METALLIC PLATING

By C. J. Stalmach, Jr.
Vought Systems Division
LTV Aerospace Corporation
Dallas, Texas

SUMMARY

Several model/instrument concepts employing electroless metallic skin were considered for improvement of surface condition, accuracy and cost of contoured-geometry convective heat transfer models. A plated semi-infinite slab approach was chosen for development and evaluation in a hypersonic wind tunnel. The plated slab model consists of an epoxy casting containing fine constantan wires accurately placed at specified surface locations. An electroless alloy is deposited on the plastic surface that provides a hard, uniformly thick, seamless skin. The chosen alloy forms a high-output thermocouple junction with each exposed constantan wire, providing means of determining heat transfer during tunnel testing of the model. A set of stringent model objectives were met except that maximum surface smoothness and maximum operating temperatures were demonstrated independently but not simultaneously. Plated epoxies with nominal 15 microinch RMS surface withstood approximately 350°F temperature and with nominal 60 microinch RMS surface withstood 550°F (which is approximately the limit for the epoxy material). The plated slab model demonstrated good data accuracy in the tunnel test. Further development effort is justified for electroless plated semi-infinite material and thin-skin calorimeter approaches.

A selective electroless plating procedure was used to deposit scaled heatshield tiles on the lower surface of a 0.0175-scale Orbiter model. Twenty-five percent of the tiles were randomly selected and plated to a height of 0.001-inch. The purpose is to assess heating effects of surface roughness simulating misalignment of tiles that may occur during manufacture of the spacecraft.

INTRODUCTION

During the aerothermodynamic development of the Space Shuttle Orbiter the need for improved methods of fabricating heat transfer models of contoured geometries was again apparent. Model/instrument demands were increased by the geometry, and high structural strength and resistance of the surface to particle damage were required by high Reynolds number hypersonic tests.

Problems with conventional machined thin-skin calorimeter models include the difficulty of instrumenting tight quarters such as leading edge radii and the inaccuracy of the measured heat transfer distribution in such areas caused by lateral heat conduction in the skin. Accessibility requirements for welding thermocouple wires to the skin inner surface implies high cost of machining and joints in the model surface. Local roughnesses from mechanical joints and attachment hardware influence the heating results, particularly at conditions near natural boundary layer transition.

Use of temperature-sensitive, phase-change paints applied to plastic models provides valuable data on heating distribution, however not without shortcomings. The optical recording of the melt-line progression causes this method to have inherent problems in providing quantitative data at all discrete model locations of interest over the surface of a contoured body. The paint layer also adds surface roughness that may influence the results. The surviability of the plastic models is often marginal to the temperature and particle environment of hypersonic wind tunnels.

This program evaluated promising new fabrication concepts of heat transfer models that employ an electroless deposition of a metallic alloy to the model surface. Electroless plating is a means of depositing metal through controlled autocatalytic chemical reduction. An electroless deposition of metal was discovered in 1844 by Wrentz, improvements (resulting in a patent) were accomplished by Roux in 1916, however the process was not practical until about 1946 when Brenner and Riddell developed a controllable autocatalytic reduction process (Refs. 1, 2, 3). Since electrical current is not involved in the deposition, the surface of non-conductors such as plastics may be plated by seeding the surface with a catalyst. The growth of the deposit originates from multitudinous point sources (catalytic centers) on the surface. On a properly prepared surface, the number of nuclei is so large that growth proceeds as a plane front parallel to the original surface. Thus electroless plating produces a plate of uniform thickness wherever the solution may reach, including blind holes and sharp corners that give problems in conventional electroplating. Most of the electroless nickel alloys contain phosphorous which results in a very hard plate comparable to chrome. Hardness and abrasion resistance can be increased further to about Rockwell C70 by heat treatment at 750°F. The nickel phosphorous alloy has very low thermal conductivity which can be used to great advantage in models that have high surface temperature gradients. Shipley Company, in its Niculoy 22, improved the ductility of the alloy while retaining hardness with the addition of one percent copper.

The inherent properties of electroless plating that are of particular importance to fabricating heat transfer models are: (1) uniform plate thickness regardless of the surface contour, (2) seamless coating over many materials including plastics or combinations of surface materials, (3) abrasion resistance, (4) low thermal conductivity and (5) automatic formation of thermocouple junctions when plated to surfaces equipped with thermocouple wires. An outstanding feature discovered during this study is that a high output, repeatable thermocouple junction results when the chosen electroless alloy (Niculoy 22) is plated to a single (constantan) wire. The one-wire junction greatly improves the accuracy and cost of instrumentation.

A Phase A effort studied several model/instrument fabrication ideas employing electroless plating. A plated, semi-infinite slab approach was chosen for laboratory and wind tunnel evaluations. In this method epoxy models are cast with constantan wires protruding at desired model locations. Two layers of electroless nickel totalling approximately 0.0015-inch thickness are applied. The ends of the wires are polished flush to the first layer surface so that the second layer provides a continuous skin over the surface. Such models provide accurate data in a hypersonic tunnel to maximum surface temperatures of approximately 550°F. Experimental evaluations of two other concepts and further refinement of the reported method are recommended.

Phase B effort began with application studies of Phase A results to current Orbiter test requirements. The chosen Phase B hardware product was to modify an existing Orbiter model to simulate the surface roughness resulting from heatshield tiles that may be misaligned in surface height during normal manufacturing and assembly practice. A selective electroless nickel plating procedure was used to precisely raise the randomly selected scaled tiles above the mean of the lower surface of a 0.0175-scale Orbiter model. This model is scheduled for test by NASA in the AF AEDC Tunnel F in the fall of 1975 where the same model was previously tested in a smooth surface configuration. The use of selective electroless plating to provide precise control of surface detail on wind tunnel models has significant application potential.

This report describes the model/instrument concepts studied, wind tunnel evaluations of one method and tables of the electroless plating procedures applied in this effort.

PROGRAM OBJECTIVES

New Model Methods

The objective for Phase A and part of Phase B was to develop techniques for fabricating aeroheating models that: (1) have a minimum of surface joints, (2) reproduce very closely the surface contours of the hardware, (3) have a smooth surface finish suitable for boundary layer transition studies, (4) are instrumented with thermocouple wires which can be predictably located, (5) possess hard surfaces that have good resistance to abrasion by particles normally encountered in hypersonic facilities, (6) have sufficient structural strength to withstand hypersonic flows at high dynamic pressures, (7) permit customizing the sensor sensitivity to the model location and the facility conditions, (8) allow instrument placement anywhere on the model surface, (9) are effective in measuring local heat transfer in areas of high temperature gradients, (10) can be fabricated in less time than conventional machining methods, and (11) can be fabricated at costs not to exceed conventional machining methods.

The technical characteristics (1-9) were demonstrated in varing degrees of success for the plated slab, model/instrument method evaluated. Detailed grading relative to the above list will be presented later. The item giving the most difficulty for the chosen approach was item (3). The surface smoothness objective was met, however with a reduction of temperature resistance of the plate bond to the substrate. Certain objectives are more sensitive to the choice of model/instrument concept. The troublesome objective may be better met by other methods to be discussed. Cost objectives (10-11) remain as expected benefits once the model techniques are fully developed. Test results indicate merits and potential of electroless plated model methods that justify further evaluation.

Selective Plating of Controlled Roughness

The objective of Change Order CCA No. 1 was to simulate the roughness of random misalignment of heatshield tiles that may exist on the lower surface of the Orbiter by selective electroless plating of tiles on an existing scaled model of the Orbiter.

This objective was met completely by plating the specified pattern and height on a 0.0175-scale stainless steel model. This successful application should encourage further uses of this method to control surface detail in aerothermodynamic models.

MODEL DEVELOPMENT PROGRAM

The development of improved methods of heat transfer modeling was begun with a review of past experiences in the literature. After the review a list was composed of promising concepts. A semi-infinite slab method employing an electroless nickel skin was chosen for laboratory development based on analytical, previous experience and cost considerations. After evaluating several fabrication procedures, sample models were made and evaluated in a hypersonic wind tunnel. Fabrication refinements after the tunnel test and cursory experiments with other concepts completed the development portion of the effort.

Trade Studies

Library Research. - Requests were issued to Defense Documentation Center and NASA Scientific and Technical Information Facility for computer literature search, including limited distribution references, from the period 1965 to the request date of September, 1973 for the following subjects:

Electroless Plating of Plastics
Casting of Wind Tunnel Models
Heat Transfer Measurements

The results of the computer searches and private searches are presented in Appendix I, after screening for applicability. The bibliographies are not exhaustive but should be representative of the work published during this period that best applies to the subject effort.

No evidence was found in the literature of any previous attempts to use electroless plating in fabricating a heat transfer model (except for the author's preliminary work (Ref. 4)). Review of instrumentation developments was very helpful in both stimulating and culling design concepts for this program.

Model/Instrument Concepts. - Three instrumentation approaches that have the potential of meeting the program objectives are:

Calorimeter
Gardon
Semi-Infinite Material

Example sketches of how these instrumentation approaches may be incorporated into a jointless heat transfer model are shown in Figure 1.

A method of measuring temperature with the electroless nickel skin at each point that it plates to a wire is shown for each of the concepts. The one-wire method contributes significantly to meeting the objectives, therefore one of the first laboratory experiments was to assess the thermocouple characteristics of the plate and various wire alloys. It was found that Shipley's electroless nickel Niculoy 22 plated to constantan wire provided an excellent thermocouple as shown in Figure 2. The Niculoy/constantan output is similar to the copper/constantan output which may be due to the one percent copper contained in the Niculoy 22 alloy. The thermoelectric characteristics of

Niculoy and its improved ductility and surface smoothness resulted in it being the primary plate material evaluated in the laboratory experiments.

The calorimeter approaches of Figure 1a include a free-standing, thin-skin shell shown as Style A. The advantages of a shell plated by the electroless method compared to machining or electroforming include: (1) plating to one wire rather than welding of two wires, (2) jointless surface, (3) uniform plate thickness (inherent for electroless, difficult in electroplating and machining), (4) harder surface than heat treated stainless steel and (5) lower thermal conductivity. Several fabrication approaches appear feasible. For one example, a replica of the model could be cast with a low melting temperature alloy such as Cerrotru (a product of Cerro de Pasco Corporation). The casting would include the thermocouple wires and sting/model adapter. After plating, the replica would be melted and removed leaving a thin-skin, free-standing shell plated to the support and wires.

Style B provides sensitivity adjustment for long run facilities with a slug that is cast in an insulative substrate. A thin electroless nickel plate provides a jointless surface.

Style C would be more suitable for short run duration tunnels where a thin skin is desired for sensitivity and where high dynamic pressures require a solid backing except for local areas. The air gap reduces heat losses to the substrate at the sensor location for a short run time.

Style D is an attempt to thermally isolate a slug calorimeter from the substrate using an air gap.

Air spaces could be achieved by suitable placement of a low melting temperature material into the mold prior to puring the casting material. The disposable material would extend to the rear of the model to permit removal after the plating operation. Wax or Cerrotru wires are example materials and electroless plating was demonstrated for both. Hard "file-a-wax" was plated after first polishing the surface with boron nitride.

A Gardon gage (Ref. 5) is a steady state instrument that has been successfully used in heated blowdown tunnels (Ref. 6). The measurement required is the delta temperature from the center of a thin disc to its outer edge. The disc edge is cooled by a heat sink. Figure 1b shows possible ways to use this instrument with electroless nickel to form an instrumented, seamless model for use in long run duration tunnels.

Style A could make use of a machined steel model in which short constantan tubes are placed. The sleeve would contain a small constantan wire cast into its center, using a material such as Cerrotru. After plating, the Cerrotru would be melted and drained. The model could be cast with Gardon gages for Styles A, B, and C. Style C reduces the complexity of melting and removing materials, however the substrate under the disc needs to be addressed for effects on sensor accuracy.

Two classes of semi-infinite material gages incorporating electroless plating are shown in Figure 1c. The plated slab of Style A is similar to the cast models used for the phase-change paint method except that for the plated slab the surface temperature is measured with thermocouple wires that are joined to a thin metal skin during deposition of the skin.

Variations in material property have been experienced when fillers are used in epoxy castings (Ref. 7, for example) whereas the thermal properties are known and repeatable for thermocouple wire. The wire gage concepts shown as Styles B and C attempt to either isolate a wire from the substrate (Style B) or use a substrate that has thermal properties similar to the wire. The wire gages measure heat transfer using the surface thermocouple output and the wire material properties. The material in Style C may be cast or machined steel. For a steel model, the wire would have a thin electrically insulative coat. The electroless nickel would form the thermocouple junction and provide a seamless surface. Style C employing a steel model should give results similar to the coaxial gage (Ref. 8) and has the advantages of requiring only one thermocouple wire per junction and exhibiting a continuous surface.

Analytical Heat Flow Study. - An analytical program was conducted to assess the effects of the geometric and thermal property variations on the design and accuracy of the various model/instrument concepts. A two-dimensional computer routine was programmed (Appendix II) and representative results are given in Figures 3 through 8. The input heating condition shown in these figures represents a flow condition in the NASA Ames 3-1/2 Foot Hypersonic Wind Tunnel. The one inch diameter hemisphere represents the model size chosen for the Phase A test. Properties of the candidate materials are given in Table I. Some property values were assumed based on literature values for similar materials.

Effects of an air gap around a wire is indicated in Figure 3. The air gap locally increases the plate temperature which increases the temperature of the plate over the wire. The wire was not isolated by the gap because of the heat conduction in the plate. (Perfect isolation of the wire would approach the case shown for the infinite wire diameter). For these initial computer runs, the electroless plate properties were not known and therefore a pure nickel plate, 0.0015-inch thick, was assumed. As shown in Table I, the conductivity of nickel is over an order of magnitude greater than electroless nickel. Although electroless nickel would provide better isolation than indicated in Figure 3, a high degree of isolation with practical skin thickness does not appear likely. The results of Figure 3 and fabrication complexity eliminated all design concepts involving air gaps early in the study.

After the runs of Figure 3, the computer routine was refined to include calculation of the temperature at the interface between the plate and wire (or substrate if a wire was not present). Niculoy 22 had been chosen as the plate material and its properties were incorporated in the routine.

Figures 4 and 5 show effects of wire and plate dimensions for low and moderate conductivity substrate materials. The low conductivity of Isochem's Novimide results in a steep temperature rise, more than desired for application in a heated blowdown tunnel (Figure 4). The high thermal expansion of this material also often caused failures in the plate during laboratory evaluations and therefore Novimide 700/55 was not evaluated further. The Novimide material could prove advantageous in areas of low heat transfer and short run duration tunnels.

The results shown in Figure 5 for Emerson Cuming's Stycast 2762FT indicate that such a material coupled with practical electroless plate thickness and wire diameter will provide reasonable temperature histories for a plated slab gage in the designated NASA Ames facility. The effects of a 0.001-inch plate and a 0.003-inch diameter wire are noted as being small and essentially constant after the time interval required to insert the model into the test stream (~1/2 second). Larger wire diameters around 0.032-inch may be used as semi-infinite wire gage if the Niculoy plate is sufficiently thin as indicated for the 0.00025-inch case in Figure 5.

Figure 6 shows calculated temperature distributions in the materials after 2.5-seconds of heating. It is observed that the temperature along the axis of the 0.003-inch constantan wire that is cast within a Stycast substrate and topped with a 0.001-inch Niculoy plate is similar to the temperature distribution of the pure Stycast substrate.

Figures 7 and 8 were prepared to examine the possible use of Niculoy plate as a thin-skin calorimeter (Figure 1a). As discussed in Reference 8, a calorimeter gage will exhibit a straight line for the relation of Figure 8 up to the time that conduction errors become significant. The 0.003-inch diameter thermocouple wire had a negligible effect on the calorimeter gages. A 0.010-inch thick plate backed by Novimide (a very low conductivity substrate) indicates conduction errors after about a half second of heating. Figure 8 indicates that a thin skin calorimeter supported by a low conductivity substrate may be employed in a short run duration tunnel such as a hotshot type, however a "free-standing" shell (i.e. a thin shell held by minimum contact with support structure) would be more suitable for heated blowdown facilities.

Grading of Concepts. - Funding considerations necessitated an early judgement as to which one of the model/instrument concepts of Figure 1 would best demonstrate the program objectives in a hypersonic wind tunnel. The above discussed library and computer studies, predicted availability of required materials and fabrication complexities were used to help anticipate relative grades for the model/instrument concepts. Table II presents the grading results and indicates that the plated slab gage of Figure 1c had the highest anticipated relative grade (8.8 out of 10). Laboratory work from this point concentrated on developing and testing this model/instrument method.

The anticipated grade for the plated slab concept was lowered as shown in Table II after completion of the experiments because the substrate-material/plating-procedure combination did not fully meet the projected results. Table II will be reviewed further when discussing recommendations.

Technique Development

Initial Material/Technique Evaluations. - After review of vendor information and initial laboratory evaluations, the following materials were chosen and proved to be adequate to meet the described needs of this study:

(1) Molds - Requires a castable material that faithfully reproduces the surface of the master or sub-master models. The mold must maintain diminsional accuracy while high temperature plastics are being cured in the mold and must permit release of the cured plastic replica. Silastic J by Dow Corning was chosen.

(2) Sub-master model - Requires a castable material that faithfully reproduces the surface of the master model and that can be readily drilled to locate each thermocouple station. (Sub-master is not required if surface drilling is permitted on master model or pattern). Epocast 11B, an iron-filled room temperature epoxy by Furane Plastics was chosen.

(3) Model Skin - Requires a smooth, hard, ductile and uniform plate that is suited for plating of plastics and that forms a reliable thermocouple junction with a standard wire. Niculoy 22 electroless alloy by Shipley was chosen. Desired improvements would be a plating solution that operates at a lower temperature and exhibits lower plating stress than the chosen alloy.

(4) One-wire thermocouple - Requires a sensitive, repeatable output from a standard thermocouple wire joined to an electroless plate. Niculoy 22/constantan junction proved to be quite adequate (Figure 2).

Sensitize Smooth Plastics Nickel Plate (SSPN). - Table III lists three representative plating procedures used in the initial laboratory evaluation of the candidate substrate materials of Table I. Because of the objective of a smooth surface, chemical etching of the plastic surface was only briefly evaluated in these initial experiments. A concentrated effort was made to obtain sufficient plate adherence to a smooth plastic surface through use of cleaners, ultrasonic agitation and wetting agents. Light sanding of the surface with wet 400 to 600 grit paper was added to the procedure to break the high gloss of the castings. The polishing improved adherence while retaining a sufficiently smooth surface. Several variations of the procedures were evaluated including a room temperature bath suggested by Feldstein (Ref. 9) and baking of the deposited palladium catalyst prior to nickel plating.

Evaluation of the casting and plating results for the SSPN procedure brought the disappointing results shown in Table IV. The three hydraulic-setting refractories evaluated exhibited surfaces considered too rough for this study. LO-XA125 by Duramics is the most promising of those evaluated and should be reconsidered if extreme temperature service is required. Large volume castings with hard surface molds produced an acceptable surface;

however small volume castings in RTV molds did not. The plating adherence to the refractories was good.

The Novimide 700/55 material plated the best of the plastics evaluated in the SSPN procedure, followed by Stycast 2762FT. None, however, had adequate adherence to survive the heating in a hypersonic facility.

The SSPN development was terminated and emphasis directed to an innovative aluminum transfer method discovered during this study.

Aluminum Transfer Zinc Aid Nickel Plate (ATZN). - Significantly improved plating bonds to epoxy substrates were achieved and with a very smooth plated surface by use of an aluminum transfer casting method followed by a Zinc Aid and nickel plating procedure summarized as follows:

(1) Aluminize the RTV mold surface by lightly rubbing "leafy" aluminum powder into the surface with cotton and blowing away all excess not adhered to the mold

(2) Insert the thermocouple wires into the holes cast in the mold

(3) Pour the epoxy (or other castable plastic) into the mold

(4) Aluminum layer is bonded to the epoxy casting while curing

(5) Remove the casting from mold, aluminum film is transferred to the casting

(6) Post cure casting

(7) Clean and condition surface for plating

(8) Plate surface and exposed wires to 2/3 of plate thickness

(9) Clip and polish wires to plated surface

(10) Reactivate plate (Shipley 1424)

(11) Plate to final thickness

Smooth nickel and copper electroless platings were achieved with all of the epoxy materials evaluated. Oven tests demonstrated however that the temperature resistance of the plate-to-epoxy bond is sensitive to the material composition and plating procedure. The material should have a coefficient of thermal expansion near that of the plate material. The cast material should develop a high bonding strength to the inner surface of the aluminum powder without wetting the outer aluminum surface.

Table V shows the material samples that were cast, plated and evaluated in an oven. Stycast 3070 material proved best in the "as received" mixture and thus was used as the base material with which optimization with additional fillers was attempted. Optimization of the plating procedure was also conducted and resulted in the procedure for depositing the first layer of electroless nickel shown in Table VI. The best material/plating combination of those evaluated for the ATZN process is indicated in Tables V and VI. This optimum combination will normally survive an oven test of 350 F. Most other combinations would exhibit diamond-pattern wrinkles in the plate when cooled from 350°F because of inadequate bonding and high compressive stress in the plate. Additional improvements in the basic metallic film transfer concept is certainly possible.

Personnel within the local (Dallas) and home offices of Shipley Company were interested in assisting in this program and were supplied sample castings for their independent evaluation. Their study suggested an etch process that will be dicussed next.

Etch, Catalyst, Accelerator, Nickel Plate (ECAN). - The mechanical strength of the plate attachment to a plastic is greatly increased if the surface is slightly porous to permit the plate to mechanically latch into these pores. Certain materials, such as the ABS plastics used extensively for plated plastics in industry, have a constituent that is readily removed by etching. The contorted, tiny tunnels become plated in the electroless process and securely lock the plate to the surface. Unfortunately the ABS plastics do not have the temperature resistance required in this study. Most epoxies do not etch readily and generally develop a rough, pitted or grainy surface.

It was discovered at Shipley that an etched surface of Stycast 3070 castings was more suitable for plating than normally considered for epoxies, possibly explained by the calcium carbonate powder filler. Calcium carbonate reached by an acid will be dissolved leaving random, fine-grain voids in the epoxy surface. Oven evaluation demonstrated that the Phase A ECAN process of Table VI would permit plated Stycast 3070 to withstand temperatures up to 550°F. This exceeds the quoted limit temperature for the epoxy material. The surface was not nearly as smooth as the ATZN process, however.

Wind tunnel test models were fabricated and evaluated for both ATZN and ECAN processes as will be discussed. After the tunnel test an optimization study was conducted to improve the surface smoothness of the ECAN process. This resulted in the Phase B ECAN plating procedure of Table VI and an optimum material of those evaluated in Table VII. The surface condition is very sensitive to the temperature, dwell time, and degree of nitrogen agitation of the Shipley PM-930 solution. The etch process partially exposes the fine glass fibers in the optimum material which provides additional "roots" for the plating. The Phase B ECAN process produced improved surface smoothness compared to Phase A ECAN but the surface is not as smooth as the ATZN process.

Nickel Transfer to Epoxy Cast (NTEC). - Another approach to obtain a smooth plated surface on an epoxy substrate is to first plate the skin and then cast the epoxy into the shell. The bond strength of an epoxy cured to a plate may be greater than the adherence obtained by plating to a smooth surface. Futhermore, the bond would not be subjected to the plating stresses of the plate. The approach was not fully exploited, however some effort was given to the following ideas with promising results. The primary problem was casting a Cerrotru surface free of air bubbles.

(1) Internal plating - Cast a female mold with a disposable material that has a smooth surface and that plates well, such as Cerrotru. Insert the thermocouple wires into the cast holes. Plate internal surface with electroless nickel to about half to two-thirds the final plate thickness. Pour epoxy into model cavity and cure. Post cure the epoxy to a higher temperature which will also melt away the Cerrotru mold. Polish the thermocouple wires to the surface. Chemically clean and activate the surface. Plate skin to final thickness.

(2) External plating - Cast a male replica including the thermocouple wires with a disposable material that has a smooth surface and that plates well, such as Cerrotru. Plate the surface to about two-thirds the final plate thickness. Polish the wires to the surface, activate and plate the surface to the final plate thickness. Cast around the outer surface of the model with a disposable material such as plaster of Paris. Melt and drain the Cerrotru, chemically clean the inner surface and pour epoxy into the cavity. After final curing of the epoxy, the plaster becomes brittle from the oven temperatures and can be broken away from the plate.

Free-Standing Thin-Skin Nickel Plate (FTSN). - A brief laboratory evaluation was given to the free-standing, thin-skin calorimeter model as depicted by Style A of Figure 1a. This concept is given a high anticipated rating in Table II. The generation of the uniform thickness shell would be similar to that discussed for the NTEC process except that a thicker shell is required (0.005 to 0.020-inch depending on facility conditions) and the shell would be supported at minimum number of contact points. The support could be joined to the skin during the plating process or later bonded to the skin for maximum isolation.

A feasibility experiment was conducted by plating Niculoy 22 to a thickness of 0.012-inch on a contoured piece of Cerrotru material. The Cerrotru was melted and drained and the inner plate surface was cleaned with caustic soda. The resultant free-standing contoured shell is strong, hard, uniform thickness, smooth and continuous.

The primary difficulty experienced with this process was casting the Cerrotru free of surface air bubbles. Cerrotru casting was attempted in the Silastic molds used for the epoxy castings and the hot metal appeared to cause an out-gassing in the RTV material.

EVALUATION OF PLATED SLAB MODEL

Results of the development program were evaluated continuously and had a daily effect on the course of the development. The major evaluation of the semi-infinite slab method, however, was accomplished by subjecting sample instrumented and non-instrumented models to M = 7.32 tunnel flow in the NASA Ames 3-1/2 Foot Hypersonic Wind Tunnel.

Wind Tunnel Test Program

Models. - The two model geometries of Figure 9 were tested in the wind tunnel. The hemisphere cylinder provides ease of comparison to existing data and theory. The flat face cylinder geometry provides a good assessment of the instrumentation accuracy in areas of high surface temperature gradients and assessment of the particle resistance of the plate. A master thin-skin model was machined for each shape out of 17-4PH stainless steel. The steel models served as mold masters from which the epoxy replicas were derived. The steel masters were instrumented and tested simultaneously with the plastic models to help gauge the data effectiveness of the plastic models.

Table VIII lists and briefly defines the Phase A test models. Figure 10 shows the models prior to shipment to the test facility.

Test Procedure. - Two master models and eight plastic models were tested simultaneously by using the mount shown in Figures 10 and 11. The shadowgraph of Figure 12 and oil flow patterns on the centerbody confirmed that the model assembly was in fully started flow. Eight runs were conducted at M = 7.32 at a nominal total temperature of 1500°R. The test began at low Reynolds number (0.8×10^6 per foot) and progressed to 4.0×10^6 per foot which exceeded the target value for the evaluation of 3.6×10^6 per foot.

The models were inserted into the flow stream and then retracted after about two seconds. Digital temperature data from the models were recorded on magnetic tape. Notes and photographs were made of a visual inspection of the models after each run (Table IX). Models whose plating wrinkled or otherwise failed were replaced during the model inspection.

Data Reduction. - The data reduction procedure for the plated semi-infinite slab model is rather simple if sphere data are obtained and used to determine the thermal property of the substrate-plate-wire combination. The data reduction made use of the semi-infinite slab solution as expressed by Jones and Hunt (Ref. 10):

$$\bar{T} = 1 - e^{\beta^2} \operatorname{erfc}\beta$$

$$\bar{T} = \frac{T_w - T_i}{T_{aw} - T_i}$$

$$\beta = \frac{h\sqrt{t}}{\sqrt{\rho C K}}$$

For simplicity, assume $T_{aw} = T_T$. The effects of this assumption and the effects of the plate and thermocouple wire on the in-depth heating of the substrate are lumped into the material property term $\sqrt{\rho CK}$ which is determined from a plastic hemisphere model for which the heat film coefficient, h, is known from measurements with the master model. This effective $\sqrt{\rho CK}$ term is then applied to determine h for the flat face cylinder test model. The flat face model was fabricated in the same manner and encountered a similar range of heating as the hemisphere model.

The step-by-step procedure followed:

(1) Establish h for a sphere in the test conditions using the master sphere model (Table X, Average values shown in Figure 13)

(2) Determine temperature-time data for the plastic models

(3) Plot temperature-time data (See Figures 14 and 15 for examples)

(4) Determine the effective time zero (t_i) and initial wall temperature (T_{wi}) (Figures 14 and 15)

(5) Calculate $\overline{T}$ at selected times

(6) Determine β from $\overline{T}$ (Ref. 10)

(7) For the plastic sphere models determine $\sqrt{\rho CK}$ at each station and time by using the measured values of h obtained with the master sphere model

(8) Plot $\sqrt{\rho CK}$ as a function of $\sqrt{t}$ for all model positions, all times and all runs for a given sphere model (Figure 16)

(9) Calculate h for the flat face plastic models using the faired values of $\sqrt{\rho CK}$ from a sphere model composed of the same materials

The relation of $\sqrt{\rho CK}$ to $\sqrt{t}$ was suggested by Reference 7. An attempt was made to more closely define the $\sqrt{\rho CK}$ term by relating it to a second term. It appears that the term β can be related to $\sqrt{\rho CK}$ for selected times as is indicated in Figure 17. The Figure 17 faired values are within ±10% of the Figure 16 fairings. The Figure 16 fairings were used in the data reduction.

Data reduction of the flow conditions and heat transfer rates for the thin-skin master models were provided by NASA-Ames. Millivolt-time digital data were also provided for the plastic model thermocouples.

Tunnel Data. - Evaluation data from the tunnel test began with notes on model survivability as shown in Table IX. Thermocouple data from selected ECAN and ATZN models were reduced and the results are given in Tables X and XI and Figure 18.

The averaged stagnation values for the hemisphere and flat face master models were in excellent agreement with theory as noted in Table XI. The plastic model data compare well with the master flat face model data and expected distribution as shown in Figure 18. The surface of the ECAN Model CC was rougher than the ATZN Models G and I. The ATZN models generally failed after one or two runs, however. The sensitivity of the fairing of $\sqrt{\rho CK}$ on the comparison was examined. Calculations of h for Model CC were made for the lower fairing of Figure 16. The results are presented in Table XI and are 8% lower.

The increasing value for $\sqrt{\rho CK}$ as time approaches zero in Figure 16 is attributed to the influence of the wire and plate (review also Figure 5). The indicated influence is independent of the local geometry. Checks were made to see if using the experimentally determined $\sqrt{\rho CK}$ (that combined the wire, plate and substrate properties) resulted in any time dependency in the calculated values of the film coefficient, h. The coefficient was calculated at each model station for several selected times between the interval 0.1 to 1.75 seconds. The calculations were found to agree well with the average and did not indicate a time dependency. Further proof of the validity of the data procedure is given through the good agreement of the computer prediction of temperature to the measured temperature shown in Figure 14. The average experimental value of $\sqrt{\rho CK}$ at time one second was input in the routine for the substrate property. The routine assumes the value to be constant. The average experimental value of h was also a constant computer input. The effects of the wire and plate on the thermocouple temperature are taken into account in the routine through thermal balance of the finite elements of the various materials.

The slope of the material property $\sqrt{\rho CK}$ with time after about one second (where the wire and plate effects become negligible) are comparable with results for a similar substrate material without a plate or wire (Ref. 7). The reduction of the substrate value of $\sqrt{\rho CK}$ can explain why the predicted temperature in Figure 14 falls below the measured for times greater than one second.

Figures 14 and 15 indicate the agreement in temperature measurements between the new Niculoy/constantan and standard copper/constantan thermocouples. Stations 002 and 012 are both located thirty degrees from stagnation but along different rays. The agreement was particularly good for the smoother models such as Model BB of Figure 15 and the ATZN models.

Evaluation Results

The combined laboratory and tunnel results for the plated slab method are compared to the technical program objectives. The plastic modeling research did not extend through a phase B model and therefore the cost objectives (10 and 11) remain as expected benefits.

Compliance with Objectives. - Combined laboratory and tunnel results demonstrate that the plated slab concept fully meets the following program objectives:

(1) No surface joints
(2) Good surface detail reproduction
(4) Accurate instrument location
(6) Sufficient strength
(8) Instrument placement anywhere
(9) Effective in areas of high thermal gradients

The plated slab possesses a very hard surface that is resistant to particle damage and therefore meets in principal the model objective number (5). However, particle damage did occur in the pebble-bed heater facility used in this evaluation. Figure 19 shows post-test magnified views of the flat face of ECAN Model CC compared to the heat treated (190,000 psi) flat face of the master Model A. Both models were subjected to all eight runs in the hypersonic tunnel and both were still providing data without any loss of instrumentation. Figure 19 and Table IX indicate particle damage resistance of the ECAN models is comparable to a heat treated stainless steel model. The softer copper coating of the ATZC process had more severe particle damage as noted in Table IX.

The customization of sensor sensitivity, objective (7), was restricted to materials that provided good plate-to-substrate bond strength. The best materials for bond strength fortunately also provided good data sensitivity. Areas of low heating impose less demand on the plate bond and therefore less restriction on the choice of materials for increased sensitivity (if required).

Data accuracy (not listed as a specific objective) obviously must be adequate if the plated slab concept is to be practiced. The tunnel results of this preliminary test proved that this model method will provide accurate data. Further improvements in accuracy can be expected as material, process and data reduction improvements are made. Discovery of the Niculoy/constantan thermocouple greatly enhances the data accuracy and overall attractiveness of this modeling approach.

Problem Areas. - A smooth surface finish (objective (3)) could be provided, however, for marginal operating temperatures. The principal problem area was finding an acceptable compromise between surface smoothness, plate hardness and maximum operating temperature of the model.

Figure 20 is a photograph comparing the surface smoothness of master, ATZN and ECAN models. The smoothness of ATZN models are considered adequate for applications involving natural hypersonic boundary layer transition. Figure 21 shows magnified views of the ATZN surfaces compared to the master and the aluminum transfer film. Note that polishing marks of the master are reproduced in the plated plastic models which attests to the faithful reproduction of surface detail of this process. The thicker plate of Model M shows some pores caused by hydrogen bubbles forming on the surface during plating. This problem can be reduced by better control of the nitrogen agitation in the plating solution.

The ATZN process in the current state of development is restricted to maximum temperatures of about 300 to 350°F. This maximum is based on both oven and tunnel evaluations. One ATZN model, Model F, failed after run four and experiencing a stagnation temperature exceeding 500°F (Table IX). The ATZN models generally fail in the cool-down process when the compressive stress in the plate overcomes the bond strength of the plate. The compressive stress results from the deposition process and from the difference in coefficient of thermal expansion of the plate and substrate.

An aluminum transfer method that meets both the temperature and surface smoothness requirements is ATZC. The difference of ATZC with ATZN is that an electroless copper (Shipley CP-74) is deposited rather than nickel. The CP-74 copper alloy is harder than pure copper and plates smoothly, although not as glossy as Niculoy 22. Table IX shows that Model V with the ATZC process survived all eight runs at stagnation temperatures exceeding 650°F without a temperature induced failure. The bond strength of the electroless copper is not considered to be higher than electroless nickel, therefore the lack of wrinkling is assumed to mean lower plating and thermal expansion stresses exist at the interface. Nickel coatings over the copper, ATZCN, failed whereas ATZC did not. The ATZC models were not instrumented; however no problems in obtaining data with the ATZC process are expected. Valid one-wire/plate thermocouple of copper/constantan should be possible. The ATZC method lacks particle resistance.

The surface finish of ECAN models are shown in Figures 20 and 22. Model CC represents the roughness of the Phase A ECAN models, and Model FFF represents the improved surface finish obtained in a Phase B optimization study conducted after the tunnel test. Table IX shows the ECAN models generally survived all eight runs at stagnation temperatures exceeding 650°F. Oven tests (where the models were heat soaked and cooled to progressively higher temperatures) generally caused local plate blistering in ECAN models when cooling from 550°F. The manufacturer's rating of Stycast 3070 is 500°F. Therefore, the ECAN demonstrated operating temperatures exceeding the plastic substrate rated temperature.

Models AA and CC provided valid heating data for the model geometries of this study in spite of the undesirable roughness. The improved surface finish of Phase B ECAN may prove adequate for many model applications, however further improvements should be sought.

APPLICATIONS STUDIES

The Phase A development results indicate applications and modeling concepts that justify further effort. Some of the recommended effort may have progressed within a Phase B of this contract except that a reassessment of priorities directed the remaining funds to the selective plating effort to be described.

Orbiter Model Requirements in Tunnel B

Phase B was begun with the intent of fabricating a 0.0175-scale model of the Orbiter with the improved ECAN process and test in the AF-AEDC Tunnel B. The Phase A tests in the NASA-Ames facility were conducted at heating conditions exceeding Tunnel B at its maximum Reynolds number. The model insertion mechanism is not as rapid in Tunnel B as is possible in the NASA-Ames 3-1/2 Foot Hypersonic Tunnel. Figure 23 shows the computer prediction of maximum temperatures that are expected for Orbiter and hemisphere models during the nominal five to seven second insertion time of Tunnel B. The shown extrapolations were made to conserve computer time. Considering the temperature predictions, Phase A results, and the lower particle contamination of Tunnel B, it appears Phase B ECAN models could be tested successfully in Tunnel B. The "durability" factor of safety for the models would be essentially one, however, unless: (1) the operating temperature of the plated slab model is increased through improvements, (2) the insertion time of the facility is decreased, or (3) the test is conducted in the Mach 6 capability of the facility. If the model insertion time in Tunnel B could be reduced to the nominal two seconds of the Ames facility then the ECAN models could be used with confidence of survival in Tunnel B and the smooth-surface ATZN models would have a fair probability of survival.

Recommended Efforts

Based on the difficulty in finding a substrate-plating combination for the plated slab method that meets both the smoothness and temperature criteria, the "grade" in Table II was reduced for the plated slab approach. Further material and process studies could raise this grade and should be conducted because of the attractiveness of this method if the material problem is solved.

Review of Table II and Figure 1 indicates that the semi-infinite wire concept Style C and calorimeter concept Style A currently have the highest predicted ratings. Laboratory and tunnel evaluations of both are recommended.

The wire gage would be easily evaluated with an existing model machined from 17-4PH stainless steel or similar material. Instrumentation holes would be filled with a length of constantan wire that has a coating of electrical insulator. The surface would be plated with Niculoy 22 to provide a smooth, jointless surface and establish Niculoy/constantan thermocouples at each sensor location. The material property term $\sqrt{\rho CK}$ of constantan differs from 17-4 stainless steel by only one percent (Table I) which should result in good accuracies. This approach is not suitable for areas of high thermal gradients where the material conduction would quickly distort the surface heating distribution.

The free-standing thin-skin calorimeter (FTSN) concept requires more laboratory development. The electroless plated thin-skin heat transfer model has several advantages over machined or electroformed models that make it worthy of development. The concept also has application to dynamic stability testing where low model inertia and freedom from energy absorbing structural joints are important. A successful material-technique optimization for the FTSN process would also permit fabrication and evaluation of the NTEC process that could conceivably help the plated slab method pass all of the objectives.

SELECTIVE PLATING
HEATSHIELD TILE ROUGHNESS

The feasibility of electroless nickel providing a controlled surface roughness on wind tunnel models was demonstrated during Phase A. This process promised an accurate assessment of heatshield heating on the Orbiter as affected by misalignment of tiles resulting from manufacturing. This assessment is important to current NASA project and therefore, the remaining contract effort was devoted to this task.

Specifications

The specifications for simulating misaligned heatshield tiles on the lower surface of the Orbiter were:

(1) Tile Pattern - The herringbone tile pattern planned for the centerline portion (as defined in Rockwell drawing VL70-399043) will be used over the total area of interest

(2) Tile Area of Interest - Begin tile pattern 2% length aft of nose, covering the lower orbiter area up to the tangent line of the chines and wing leading edge, extending rearward to 80% length of the model

(3) Selection of Tiles to be Raised - Random selection of tiles to provide 25% of raised tiles in the tile area of interest. The plated tile pattern will be symmetrical about the longitudinal centerline (instrumentation is located only on one side of centerline)

(4) Tile Size - All selected tiles will be plated to within 0.0009 to 0.001 inch height. The tiles are 0.105 inch square for the 0.0175-scale model

Technique Development

A positive-resist method of selective electroless nickel plating was chosen. Development tasks included a negative of the plating pattern and customization of the selective plating method for the material, geometry and specifications of this effort.

A negative was generated by first accurately drawing all of the lower Orbiter tiles existing on one side of centerline to 0.04167-scale with a Gerber computer driven drafting machine. A table of random numbers (Ref. 13) was used to designate which 25% of the tiles would be raised. The tiles and the selection are shown in Figure 24. The selected tiles were covered with 0.250-inch flat black tape on the drawing and then photographic processes were employed to provide a 0.0175-scale negative of the plating pattern with symmetry about the longitudinal centerline.

The basic steps of the selective plating process are:

(1) Clean surface
(2) Apply resist
(3) Expose and develop resist
(4) Activate exposed surface
(5) Electroless plate exposed surface
(6) Remove resist

The process used for the subject model is given in Table XII. The nickel strike improved adhesion to the polished stainless surface. Two coats of resist were necessary for it to endure the activation and relatively long plating time. A vacuum bagging technique was used to tightly hold the negative over the model surface during resist exposure. The model is shown in Figure 25 with the exposed and baked resist prior to the activation and plating steps.

Model Results

The plating of simulated heatshield tile roughness on a scaled model was successfully accomplished. Figure 26 is a photograph of the completed model. This existing model had a welded nose section and weld fills. Weld heat-lines became vivid during the mild etching of the activation process as shown; however, they did not cause any surface roughness. The plated pattern duplicates the negative with good fidelity. The plated height is within the requested tolerance; the plate surface is bright and the tiles are well adhered.

NASA has scheduled a test in the AF AEDC Tunnel F where this same model was previously tested in a smooth-surface condition.

This demonstration of controlled roughness suggests application of the technique to provide special model surface details in other aerothermodynamic requirements.

CONCLUSIONS AND RECOMMENDATIONS

1. A plated slab concept demonstrated the technical model objectives in varying degrees of success. Objectives such as a jointless surface and accurate placement of instruments were readily achieved. Good surface smoothness and model operating temperatures to the limits of the substrate material were demonstrated individually but not simultaneously.

2. The plated slab concept may be applied to hypersonic wind tunnel models if the maximum, momentary surface temperature is restricted to approximately 500°F for the ECAN and 300°F for the ATZN processes.

3. Experimental results indicate that further development work is required and justified for two modeling methods employing electroless nickel: (1) semi-infinite material and (2) free-standing thin-skin calorimeter

4. Controlled surface roughness was successfully accomplished on a scaled wind tunnel model using a selective electroless plating method. Selective electroless plating is an effective method for providing special surface details on wind tunnel models.

5. This research resulted in four innovations considered as new technology items: (1) a plated slab model method of measuring convective heat transfer. This method is a new approach for obtaining highly instrumented, seamless-surface models regardless of external geometry, (2) a one-wire Niculoy/constantan thermocouple that is formed during electroless plating of the model surface. This instrumentation improves accuracy and cost and makes practical the plated slab model concept, (3) an aluminum transfer procedure whereby a thin layer of aluminum powder is bonded to the plastic surface during the casting process. The film is readily plated with electroless nickel or copper to excellent surface brightness and with temperature resistance up to 350°F for nickel and 550°F for copper coating and (4) selective electroless plating of scaled surface detail on aerothermodynamic models. The use of photo resist and selective electroless plating (or etching) to control surface roughness on wind tunnel models is considered a new application of an existing technology.

REFERENCES

1. Brenner, A.: History of the Electroless Plating Process. Symposium on Electroless Nickel Plating, ASTM Special Technical Publication No. 265, 1959, pp. 1-2.

2. Gorbunova, K. M. and Nikiforova, A. A.: Physicochemical Principles of Nickel Plating. National Science Foundation Publication TT63-11003, 1963, translated in Jerusalem from a publication by the Institute of Physical Chemistry, Academy of Sciences of the U.S.S.R., 1960.

3. Goldie, W.: Metallic Coating of Plastics. Electrochemical Publications Limited, Middlesex, England, Volume 1, 1968.

4. Stalmach, C. J., Jr.: Plating Methods for Thin-Skin Heat-Transfer Models. LTV Aerospace Report 2-59700/2R-2986, February 1972, Rev. A May 1972.

5. Gardon, R.: An Instrument for the Direct Measurement of Intense Thermal Radiation. The Review of Scientific Instruments, Vol. 24, No. 5, May 1953.

6. Hube, F. K.: An Experimental Method for Determining Heat Transfer Distributions on Blunt Bodies at Hypersonic Mach Numbers. AF AEDC-TR-69-20, June 1969.

7. Matthews, R. K., Eaves, R. H., Jr., and Martindale, W. R.: Heat-Transfer and Flow-Field Tests of the McDonnell Douglas-Martin Marietta Space Shuttle Configurations. AF AEDC-TR-73-53, April 1973.

8. Trimmer, L. L., Matthews, R. K., and Buchanan, T. P.: Measurement of Aerodynamic Heat Rates at the Von Karman Facility. International Congress on Instrumentation in Aerospace Simulation Facilities, September 1973.

9. Feldstein, N.: Two Room-Temperature Electroless Nickel Plating Baths - Properties and Characteristics. RCA Review, Princeton, N. J., June 1970.

10. Jones, R. A. and Hunt, J. L.: Use of Fusible Temperature Indicators for Obtaining Quantitative Aerodynamic Heat-Transfer Data. NASA TR R-230, February 1966.

11. Zoby, E. V. and Sullivan, E. M.: Effects of Corner Radius on Stagnation-Point Velocity Gradients on Blunt Axisymmetric Bodies. NASA TM X-1067, March 1965.

12. Jones, R. A.: Heat-Transfer and Pressure Distributions on a Flat-Face Rounded-Corner Body of Revolution with and without a Flap at a Mach Number of 8. NASA TMX-703, September 1962.

13. Selby, S. M.: Standard Mathematical Tables. The Chemical Rubber Company, Cleveland, Ohio, 16th Edition, 1968.

TABLE I

PROPERTIES OF MATERIALS CONSIDERED FOR MODEL AND INSTRUMENTATION

Material (Trademark & No.)	Thermal Conductivity X 10^4 (Cal)(cm)/(sec)(cm^2)(°C)	Specific Gravity	Specific Heat Cal/gm °C	Maximum Surface Temperature °C	Thermal Expansion Coef.X10^6/°C	Tensile Strength PSI	Flexural Strength PSI	Compressive Strength PSI	Shrinkage Linear, %
2762 FT	32.0	2.1	.2	300	38		18,500		
Stycast 3070				260	20	9,000	16,000	12,000	
1095	4.48	.80		260	40		4,200		NIL
2850 KT	103.3	2.8		200	29		16,000		
Eccobond Paste 99	40.3			230	32				
Solder 58C	241.			260	32		9,700		
Novimide 700/55	5.0	1.94		540	64	10,300		18,000	.05
LO-XA 125	40.0	1.80		1260	1.20			4,000	.00
Thermo-Sil 120	14.8	1.88		1650	.81			5,000	.10
Kaolite 2200	5.68	.90		1200				700	.3
Air (Standard Atmosphere at Rest)	.57	.00123	.24						
Quartz	34.0	2.2	.18	1100	.56				
Wax (Nominal)	6.0	.9	.69	120					
Electroless Nickel (Literature)	105 to 135	7.85		890	13.				
(RCA)				1240					
(Niculoy 22)	135*	8.20	.13*	1000	13.5				
Nickel (200)	1819 to 1600	8.89	.13	1450	15.3 to 13.5	48,000			
Stainless S. (17-4PH)	430	7.78	.13	1400	10.8	145,000			
Chromel	460	8.73	.107	1430	13.1	95,000			
Constantan	506	8.92	.094	1220	14.9	80,000			

* Measurement not available; value shown assumed for computer program

TABLE II GRADING OF MODEL/INSTRUMENT CONCEPTS EMPLOYING JOINTLESS ELECTROLESS NICKEL SURFACE

	PGRM OBJ. NO.	CALORIMETER CONCEPTS				GARDON CONCEPTS				SEMI-INFINITE MATERIAL CONCEPTS				
		A	B	C	D	A CAST	A MACH	B	C	A* ATZN	A* ECAN	B	C CAST	C MACH
MODEL/INSTRUMENT FABRICATION		7.8	6.6	6.4	5.6	5.6	7.6	5.0	6.0	8.4	8.4	6.2	6.8	8.4
Model Fabrication														
Instrument Fabrication														
Availability of Suitable Materials														
Reproduction of Surface Detail	2													
Ease of Instrument Placement	8													
ELECTROLESS PLATING (To Required Thickness)		8.8	6.8	7.3	6.8	6.8	9.5	6.8	6.8	7.5	7.3	6.8	7.3	8.5
Lack of Joints	1													
Lack of Mold Lines, Localized Roughness	1													
Overall Surface Smoothness	3													
Process Complexity														
ACCURACY OF DATA		8.3	5.6	6.8	5.5	7.3	7.3	7.3	5.9	8.6	9.1	6.3	7.9	7.8
Suitable Theory to Process Data														
Calibration or Property Determination														
Heat Loss/Gain Errors with Time														
Influence of Model Radii (Thermal Gradients)	9													
Instrument Effect on Surface Temp. Dist.														
Instrument Effect on Surface Roughness														
Customize Sensor Sensitivity	7													
Accuracy of Inst. Location	4													
MODEL/INSTRUMENT DURABILITY		9.0	6.7	8.7	6.7	4.3	5.0	4.3	8.0	5.0	6.7	4.3	6.7	9.3
High Pressures and Vibrations	6													
Particle Impingement	5													
Surface Temperature Rise														
AVG. GRADE OF MAJOR HEADINGS		8.5	6.4	7.3	6.2	6.0	7.4	5.9	6.7	7.4*	7.9*	5.9	7.2	8.5

NOTES: (1) Refer to Figure 1 for concepts; Text for objectives.

(2) Grading criteria: 1 = poor or very difficult
5 = acceptable or difficult
10 = excellent or simple

(3) Each major heading grade is an average of subheading grading.

(4) Grading is conjectured, based on library and computer studies and general experience to date. The * columns include laboratory and wind tunnel experience on samples (anticipated ~ 8.8 prior to recent experience)

TABLE III

REPRESENTATIVE PLATING PROCEDURES FOR SENSITIZED SMOOTH PLASTICS (SSPN)

Process			Solution	Temperature	Time (Min.)	Agitation
1	2	3				
o	o	o	Sand with wet 400 to 600 grit paper			
o	o	o	Xylene	RT	10	Ultrasonic
o	o	o	Shake off			
o	o		Alconox	RT	10	Ultrasonic
o	o		Rinse water + spray	RT	1	Ultrasonic
		o	Hydrolyzer (Shipley)	140	5	
		o	Rinse water + spray	RT	5	
		o	Neutralizer, PM-950 (Shipley)	110	3	
		o	Rinse + spray rinse	RT	2	
o			Sensitizer (Stannum Chloride)	120	1	Ultrasonic
	o	o	Catalyst 9F (Shipley)	RT	5	
o	o	o	Spray rinse	RT		
o			Activator (Palladium Chloride)	120	1	Ultrasonic
	o	o	Accelerator PM-960 (Shipley)	RT	2	
o	o	o	Spray rinse	RT		
o			Repeat Sensitizer and Activator steps			
o	o	o	PM-980 Nickel (Shipley)	RT	5	
o	o	o	Spray rinse	RT		
o	o	o	Niculoy 22 (Shipley)	195	As req'd $\sim$ 10 μ inch/min.	N_2
o	o	o	Rinse water	195	2	
o	o	o	Spray rinse (optional)	RT		

TABLE IV

EVALUATION OF CANDIDATE SUBSTRATE MATERIALS WITH SSPN (TABLE III) PLATING PROCEDURES

Material (Trademarks)	General Casting Characteristics	Air Pores, Roughness	Hardness	Compatability With Waxed Wires	Plating Results
Stycast 2762FT	Ø	Ø	ØØ	-	-
3070	Ø	Ø	ØØ		X
1095	Ø	Ø	Ø		-
2850KT	Ø	Ø	Ø	-	X
Eccobond 99	X	X	ØØ		
58C	X	Ø	X		
Novimide					
700/55-F18	Ø	/	Ø	-	/
700/55-F19	Ø	ØØ	-	X	-
700/55-P19	Ø	ØØ	Ø	X	-
700/55-F18/P19	Ø	Ø	Ø	X	-
LO-XA 125	-	X	-		Ø
Thermo-Sil 120	X	X	-		Ø
Kaolite 2200	X	X	X		Ø

grading (relative, based on the samples evaluated and not to be considered an absolute conclusion)

ØØ	excellent
Ø	good
/	fair
-	marginal
X	unsatisfactory
(blank)	not evaluated

TABLE V

MATERIAL SAMPLES EVALUATED WITH ATZN PLATING PROCESS

	SUBSTRATE MATERIAL				
Filler Material	Emerson Cuming Stycast 2762FT	Emerson Cuming Stycast 3070 +% Filler	Furane Epocast 21 +% Filler	Shell 828 +% Filler	Dow 438 +% Filler
None	0	0	0	0	0
Graphite		2, 3, 4*, 5, 8, 16	20, 40		
1/16" Long Fiber Glass		2, 4, 6, 8, 12, 18	18, 35, 44		
PVA Fibers		.625, 1.25			
Quartz		4, 8, 11, 22	44, 51	79	24
Aluminum		8, 16	116		

* Considered best with the ATZN process

TABLE VI

PLATING PROCEDURES FOR ALUMINUM TRANSFER (ATZN) AND ETCHED SURFACE (ECAN) PLASTICS

ATZN *	Phase A ECAN	Phase B ECAN **	Solution	Temperature (°F)	Time (Min.)	Agitation
o			Xylene	RT	10	Ultrasonic
o			Shake off			
o			Alconox	RT	10	Ultrasonic
o			Rinse water + spray	RT	1	Ultrasonic
o			10% Nitric Acid	RT	1	Ultrasonic
o			Zinc Aid	RT	1/2	
	o		Concentrated Sulfuric Acid	RT	25	
	o		Rinse water + spray	RT	2	
	o		Etch PM-930 (Shipley)	140	5	N_2
		o	Etch PM-930 (Shipley)	150	7	N_2
	o	o	Rinse water	RT	2	
	o	o	Rinse water + spray	RT	2	
	o	o	Neutralizer PM-950 (Shipley)	110	5	
	o	o	Rinse water + spray	RT	2	

TABLE VI (CONTINUED)

ATZN *	Phase A ECAN	Phase B ECAN **	Solution	Temperature (°F)	Time (Min.)	Agitation
	o	o	25% Hydrochloric Acid	RT	1	
	o	o	5-2-1 mix catalyst 9F (Shipley)	RT	3	Ultrasonic
	o	o	Rinse water + spray	RT	2	
	o	o	Accelerator PM-960 (Shipley)	105	2	Stir
o	o	o	Rinse water + spray	RT	1	
o	o	o	Niculoy 22 (Shipley)	195	As req'd ~ 10 μ inch/min.	N_2
o	o	o	Rinse water	195	2	
o	o	o	Spray rinse (optional)	RT		

* Optimized for Stycast 3070 + 4% graphite with bonded aluminum powder on surface

** Optimized for Stycast 3070 + 4% glass fibers

TABLE VII

MATERIAL SAMPLES EVALUATED WITH ECAN PLATING PROCESS

Filler Material	Substrate Material Emerson Cuming Stycast 3070 + % Filler	 Dow 431 + % Filler
None	0	
Graphite	4, 6	6, 16, 32
Boron Nitride	4	
1/16" Long Fiber Glass	4*, 8, 12	
Quartz	8	
Calcium Carbonate	2, 4	
Aluminum	4, 16, 32	
Copper	4, 16	
Carbolized Iron	4, 16, 32	
Pure Iron	8, 16	

* Considered best with the ECAN process

TABLE VIII

ONE INCH DEVELOPMENT MODELS

A. PHASE A

FLAT FACE	DOME FACE	SUBSTRATE MATERIAL	INSTRU-MENTED	SKIN MATERIAL	SKIN THICKNESS	PLATE PROCESS	TUNNEL TESTED	FABRICATION REMARKS
A	B		Yes	17-4 PH	.03 (Nom)	Machine	Yes	Master Models, 4.8 to 9.8 rms
	C	Stycast 3070	Yes	Ni 22-9-M	.001	ATZN	No	Isolated wrinkle on cylinder, void
	D	3070 + 2% Gr.	Yes	Ni 22-9-0	.0015	ATZN	No	Blistered, void
	E	3070 + 3% Gr.	Yes	Ni 22-9-M	.001	ATZN	Yes	OK
	F	3070 + 4% Gr.	Yes	Ni 22-9-M	.0015	ATZN	Yes	.001 + .0005, OK
G		3070 + 4% Gr.	Yes	Ni 22-9-M	.0015	ATZN	Yes	.001 + .005, surface 11 to 20 rms
H		3070 + 4% Gr.	Yes	Ni 22-9-M	.003	ATZN	Yes	.002 + .001, 2 piece mold
I		3070 + 4% Gr.	Yes	Ni 22-10-N	.0015	ATZN	Yes	.0005 + .001, No Agitation Plate Rougher than G
J		3070 + 4% Gr.	No	Ni 22-9-0	.001	ATZN	No	Al. dull, plate spotty, One Blister, void
K		3070 + 4% Gr.	No	-	-	-	No	Al. dull, did not plate, void

TABLE VIII (CONTINUED)

FLAT FACE	DOME FACE	SUBSTRATE MATERIAL	INSTRU-MENTED	SKIN MATERIAL	SKIN THICKNESS	PLATE PROCESS	TUNNEL TESTED	FABRICATION REMARKS
L		3070	No	Ni 22-9-0	.001	ATZN	No	OK
M		3070	No	Ni 22-9-0	.0035	ATZN	No	.003 + .005, face loose after plating, surface 12 to 33 rms
N		3070 + 2% Gr.	No	Ni 22-9-0	.001	ATZN	No	Al. dull, spotty plate, Question
O		3070 + 3% Gr.	No	-	-	-	No	Al. dull, did not plate, void
P		3070	No	CP-74 + Ni 22-9-M	.001	ATZCN	Yes	.0008 + .0002, Al. dull, plate spotty, Question
	Q	3070 + 2% Gr. + 2% Gl.	No	Ni 22-9-M	.001	ATZN	No	Al. dull, plate spotty, Question
	R	3070	No	CP-74	.001	ATZC	Yes	OK
NOTE: New RTV Molds were used for subsequent non-instrumented models to solve dull Al. problem								
	S	3070 + 4% Gl.	No	Ni 22-9-M	.0015	ATZN	Yes	Plate spotty
	T	3070 + 2% Gr. + 2% Gl.	No	Ni 22-9-M	.0015	ATZN	Yes	Plate spotty
	U	3070 + 4% Gr.	No	CP-74 + Ni 22-9-M	.00125	ATZCN	Yes	.001 + .00025, OK

TABLE VIII (CONTINUED)

FLAT FACE	DOME FACE	SUBSTRATE MATERIAL	INSTRU-MENTED	SKIN MATERIAL	SKIN THICKNESS	PLATE PROCESS	TUNNEL TESTED	FABRICATION REMARKS
	V	3070 + 4% Gr.	No	CP-74	.001	ATZC	Yes	OK
W		3070 + 4% Gr.	No	-	-	-	No	Did not plate, surface 13 to 25 rms
X		3070 + 4% Gr.	No	Ni 22-9-M	.0005	ATZN	Yes	OK
Y		3070 + 4% Gr.	No	Ni 22-9-M	.002	ATZN	Yes	OK
	AA	3070	Yes	Ni 22-9.5-N	.0015	ECAN	Yes	.001 + .0005, surface like CC
	BB	3070 + 4% Gr.	Yes	Ni 22-9.5-N	.0015	ECAN	Yes	.001 + .0005, not as rough as CC
CC		3070	Yes	Ni 22-9.5-N	.0015	ECAN	Yes	.001 + .0005, surface 70 to 140 rms
DD		3070	No	Ni 22-9.5-N	.003	ECAN	Yes	.0015 + .0015, surface like CC
	EE	3070	No	Ni 22-9.5-N	.003	ECAN	No	.0015 + .0015, surface like CC
	FF	3070	No	-	-	-	No	Did not plate, surface 10 to 17 rms

TABLE VIII (CONTINUED)

B. PHASE B

FLAT FACE	DOME FACE	DATE CAST	SUBSTRATE MATERIAL	INSTRU-MENTED	SKIN MATERIAL	SKIN THICKNESS	PLATE PROCESS	TUNNEL TESTED	FABRICATION REMARKS
	FFF	9/16	3070 + 4 Gl.	No	Ni 22-9.5M	.001	ECAN	No	Surface improved, 40 to 78 rms
	GG	9/16	3070 + 4 Gl.	No	Ni 22-9.5M	.001	ECAN	No	Surface like FFF
HH		9/16	3070 + 4 Gl.	No	Ni 22-9.5M	.001	ECAN	No	Surface like FFF
II		9/16	3070 + 4 Gl.	No	Ni 22-9.5M	.001	ECAN	No	Surface like FFF

<u>Footnotes for Table VIII</u>

Ni 22-	Niculoy 22, Nickel Alloy by Shipley
CP74 -	Copper Alloy by Shipley
9-0	90% strength, old solution
9-M	90% strength, old and new solution mixed
10-N	100% strength, new solution
Gr	Graphite, powder
Gl	Glass, chopped fibers
ATZN	Aluminum Transfer cast process with Zinc Aid, Nickel plate procedure
ATZC	Aluminum Transfer cast process with Zinc Aid, Copper plate procedure
ATZCN	ATZC with Nickel plated over the copper
ECAN	Etch, Catalyst, Accelerator treatment of plastic with Nickel plate

TABLE IX
Model Surviability Results
M = 7.32 Tests

Run No.	hS* BTU / Ft^2-Sec-^{o}R	MAX.** Model Temp. at $\theta=30^o$, ^{o}F	Insertion*** Time Sec.	Mount Position	Model Letter	Model Condition After Run
1	.020	355	2	1	B	good
				2	A	good
				3	AA	good
				4	CC	good
				5	BB	good
				6	I	good
				7	H	good
				8	F	good
				9	G	face wrinkled after run
				10	E	face wrinkled after run
2	.028	395	1	1	B	slight particle abrasion at stagnation on all models
				2	A	
				3	AA	
				4	CC	
				5	BB	
				6	I	face loose after run
				7	H	
				8	F	
				9	DD	
				10	V	

TABLE IX
Model Surviability Results
M = 7.32 Tests

Run No.	hS* BTU / Ft^2-Sec-^{o}R	MAX.** Model Temp. at θ=30^o, ^{o}F	Insertion*** Time Sec.	Mount Position	Model Letter	Model Condition After Run
3	.034	445	1	1	B	particle abrasion more noticeable on all models
				2	A	
				3	AA	
				4	CC	
				5	BB	
				6	U	particle pitting more apparent due to copper under nickel
				7	H	wrinkle and spalling on face
				8	F	two fine cracks in plate from particle pits
				9	DD	
				10	V	particle pitting more apparent on copper
4	.040	490	1	1	B	particle pitting continues on all models
				2	A	
				3	AA	
				4	CC	
				5	BB	
				6	U	
				7	Y	most of plate on face lost
				8	F	some spalling of plate on face
				9	DD	
				10	V	

TABLE IX
Model Surviability Results
M = 7.32 Tests

Run No.	hS* $\frac{BTU}{Ft^2\text{-Sec-}^\circ R}$	MAX.** Model Temp. at $\theta=30^\circ$, °F	Insertion*** Time Sec.	Mount Position	Model Letter	Model Condition After Run
5	.038	540	2	1	B	particle pitting very noticeable
				2	A	particle pitting very noticeable
				3	AA	some particles penetrating plate, local damage only
				4	CC	some particles penetrating plate, local damage only
				5	BB	practically no particle penetration, very little abrasion
				6	U	face area very pitted and rough
				7	X	most of plate on face lost
				8	T	plate peeling at stagnation area
				9	DD	two small blisters and a crack in plate on face, very little particle penetration
				10	V	most particles penetrating through plate and deep into substrate
6	.043		2	1	B	pitted, rough face
				2	A	pitted, rough face
				3	AA	hit by a large particle leaving a crater and local plate damage, fine cracks in plate at stagnation
				4	CC	particle pitting of plate noticeably increased

TABLE IX
Model Surviability Results
M = 7.32 Tests

Run No.	hS* $\frac{\text{BTU}}{\text{Ft}^2\text{-Sec-}^{o}\text{R}}$	MAX.** Model Temp. at $\theta=30^o$, ^{o}F	Inser-tion Time Sec.***	Mount Posi-tion	Model Letter	Model Condition After Run
6 (Cont'd)	.043	615	2	5	BB	two small blisters in plate near stagnation
				6	U	fine cracks in plate in addition to heavy pitting
				7	P	wrinkles in plate on face
				8	R	stagnation area blue and purple from heat
				9	DD	more cracks in plate, particle penetration low
				10	V	stagnation area blue and purple from heat
7	.039		2	1	B	no apparent change (except more particle hits)
				2	A	no apparent change
				3	AA	no apparent change
				4	CC	no apparent change
		560		5	BB	no apparent change
				6	U	most of plate on face lost, peeled back
				7	S	local spalling and blistering of plate on face
				8	R	no apparent change
				9	DD	cracks in plate increased, lost a spot of top coat of plate
				10	V	no apparent change

TABLE IX
Model Surviability Results
M = 7.32 Tests

Run No.	hS* $\frac{\text{BTU}}{\text{Ft}^2\text{-Sec-}^o\text{R}}$	MAX.** Model Temp. at $\theta = 30^o$, ^{o}F	Insertion*** Time Sec.	Mount Position	Model Letter	Model Condition After Run
8	.040	470	2	1	B	no apparent change in any of models
				2	A	
				3	AA	
				4	CC	
				5	BB	
				6	-	models in mounts 6-9 removed and mount rotated 90° so that position 5 is top, an objective of run was to get best shadowgraph view of shock system on each type of model
				7	-	
				8	-	
				9	-	
				10	V	

* Measured value on Model B, 1.0 inch diameter hemisphere

** Measured on Model BB, 30° off stagnation, 1.0 inch diameter hemisphere; this model mounted such that it was first into and last out of flow, maximum temperature reached during retraction cycle.

*** Delta time between beginning of insertion to beginning of retraction

TABLE X SUMMARY OF PHASE A MODEL TEST RESULTS
M = 7.32, AMES 3-1/2 FOOT HYPERSONIC TUNNEL

Run No.	P_T Psia	T_T ^oR	R_e/ft $x\,10^{-6}$	Model Face & Type	Model T/C	S/R	T_{Wi} ^oR t = 0	Q $\frac{Btu}{ft^2\text{-sec}}$ t = 0	h $\frac{Btu}{ft^2\text{-sec-}^oR}$	$\frac{h}{h_s}$ Flat	$\frac{h}{h_s}$ Sphere
1	202.8	1548.7	.813	Dome Master	B001	0	562.0	19.494	.01976		1.0
					B002	.524	560.4	17.185	.01738		.8796
					B003	1.047	559.0	8.907	.00906		.4585
					B004	1.571	557.2	2.083	.00210		.1063
				Flat Master	A001	0	563.0	11.491	.01166	1.0	.5901
					A002	.50	563.2	12.854	.01304	1.1184	.6599
					A003	1.146	562.8	12.888	.01307	1.1209	.6614
					A004	3.092	561.9	1.137	.00115	.0986	.0582
				Flat ECAN	CC012	.50	552		.01189	1.0200	
					CC002	.50	552		.01628	1.3962	
					CC003	1.146	552		.01446	1.2401	
					CC004	3.092	552		.00136	.1166	
				Flat ATZN	I012	.50	545		.01399	1.1998	
					I002	.50	545		.01283	1.1003	
					I003	1.146	545		.01256	1.0772	
					I004	3.092	545		.00139	.1192	
				Flat ATZN	G012	.50	540		.01374	1.1784	
					G002	.50	540		.01328	1.1389	
					G003	1.146	540		.01256	1.0772	
					G004	3.092	540		.00151	.1295	

TABLE X SUMMARY OF PHASE A MODEL TEST RESULTS
M = 7.32, AMES 3-1/2 FOOT HYPERSONIC TUNNEL

Run No.	P_T Psia	T_T ^oR	R_e/ft $x10^{-6}$	Model Face & Type	Model T/C	S/R	T_{Wi} ^oR t = 0	Q $\frac{Btu}{ft^2\text{-sec}}$ t = 0	h $\frac{Btu}{ft^2\text{-sec-}^oR}$	$\frac{h}{h_{s}}$ Flat	$\frac{h}{h_{s}}$ Sphere
2	399.3	1561.1	1.579	**Dome Master**	B001	0	572.4	27.800	.02812		1.0
					B002	.524	570.6	24.713	.02495		.8873
					B003	1.047	569.1	13.217	.01332		.4737
					B004	1.571	567.1	2.901	.00291		.1035
				Flat Master	A001	0	573.5	15.977	.01619	1.0	.5754
					A002	.50	573.9	18.283	.01852	1.1448	.6587
					A003	1.146	573.4	18.129	.01836	1.1346	.6528
					A004	3.092	570.9	1.672	.00169	.1044	.0601
				Flat ECAN	CC012	.50	555		.01797	1.1099	
					CC002	.50	555		.02347	1.4500	
					CC003	1.146	555		.01916	1.1834	
					CC004	3.092	555		.00171	.1056	
				Flat ATZN	I012	.50	550		.01957	1.2088	
					I002	.50	550		.01777	1.0976	
					I003	1.146	550		.01658	1.0241	
					I004	3.092	550		.00172	.1062	

TABLE X SUMMARY OF PHASE A MODEL TEST RESULTS
M = 7.32, AMES 3-1/2 FOOT HYPERSONIC TUNNEL

Run No.	P_T Psia	T_{oT} °R	$R_e/ft \times 10^{-6}$	Model Face & Type	Model T/C	S/R	T_{Wi} °R t = 0	Q $\frac{Btu}{ft^2\text{-sec}}$ t = 0	h $\frac{Btu}{ft^2\text{-sec-}^oR}$	$\frac{h}{h_s}$ Flat	$\frac{h}{h_s}$ Sphere
3	599.2	1597.8	2.277	Dome Master	B001	0	566.7	34.666	.03362		1.0
					B002	.524	564.2	31.005	.02999		.8920
					B003	1.047	562.0	16.614	.01603		.4848
					B004	1.571	559.7	3.663	.00352		.1047
				Flat Master	A001	0	568.2	20.205	.01962	1.0	.5836
					A002	.50	568.4	22.769	.02212	1.1274	.6579
					A003	1.146	568.0	22.471	.02182	1.1121	.6490
					A004	3.092	567.8	2.007	.00195	0.0994	.0580
				Flat ECAN	CC012	.50	555		.02250	1.1468	
					CC002	.50	555		.02916	1.4862	
					CC003	1.146	555		.02375	1.2105	
					CC004	3.092	555		.00257	.1310	
4	850.2	1616.3	2.638	Dome Master	B001	0	580.1	41.390	.03994		1.0
					B002	.524	577.2	36.959	.03556		.8902
					B003	1.047	574.6	19.783	.01899		.4754
					B004	1.571	572.2	4.462	.00427		.1069
				Flat Master	A001	0	581.7	24.153	.02335	1.0	.5844
					A002	.50	581.6	26.840	.02594	1.1112	.6494
					A003	1.146	581.1	27.025	.02611	1.1183	.6536
					A004	3.092	582.9	2.446	.00237	.1014	.0593
				Flat ECAN	CC012	.50	570		.02616	1.1203	
					CC002	.50	570		.03452	1.4784	
					CC003	1.146	570		.02802	1.2000	
					CC004	3.092	570		.00294	.1259	

TABLE X SUMMARY OF PHASE A MODEL TEST RESULTS
M = 7.32, AMES 3-1/2 FOOT HYPERSONIC TUNNEL

Run No.	P_T Psia	T_T ^oR	R_e/ft $x10^{-6}$	Model Face & Type	Model T/C	S/R	T_{Wi} ^oR t = 0	Q $\frac{Btu}{ft^2\text{-sec}}$ t = 0	h $\frac{Btu}{ft^2\text{-sec-}^oR}$	$\frac{h}{h_{s_{Flat}}}$	$\frac{h}{h_{s_{Sphere}}}$
5	848.0	1562.4	3.349	Dome Master	B001	0	569.3	37.940	.03821		1.0
					B002	.524	566.7	33.929	.03407		.8917
					B003	1.047	564.3	18.471	.01850		.4844
					B004	1.571	561.9	4.356	.00435		.1138
				Flat Master	A001	0	571.6	23.230	.02344	1.0	.6135
					A002	.50	571.7	25.222	.02546	1.086	.6663
					A003	1.146	571.4	24.720	.02494	1.064	.6527
					A004	3.092	571.4	2.318	.00234	.0998	.0612
				Flat ECAN	CC012	.50	560		.02268	.9676	
					CC002	.50	560		.03025	1.2906	
					CC003	1.146	560		.02680	1.1433	
					CC004	3.092	560		.00286	.1220	
6	997.1	1617.7	3.709	Dome Master	B001	0	571.7	45.142	.04316		1.0
					B002	.524	568.8	40.320	.03844		.8906
					B003	1.047	564.8	22.032	.02092		.4847
					B004	1.571	561.5	5.293	.00501		.1161
				Flat Master	A001	0	573.0	26.626	.02540	1.0	.5905
					A002	.50	574.6	29.240	.02803	1.0999	.6495
					A003	1.146	573.7	28.759	.02755	1.0808	.6383
					A004	3.092	573.1	2.725	.00261	.1024	.0604
				Flat ECAN	CC012	.50	550		.02462	.9693	
					CC002	.50	550		.03347	1.3177	
					CC003	1.146	550		.03039	1.1965	
					CC004	3.092	550		.00340	.1339	

TABLE X SUMMARY OF PHASE A MODEL TEST RESULTS
M = 7.32, AMES 3-1/2 FOOT HYPERSONIC TUNNEL

Run No.	P_T Psia	T_T °R	R_e/ft x 10^{-6}	Model Face & Type	Model T/C	S/R	T_{Wi} °R t = 0	q $\frac{Btu}{ft^2\text{-}sec}$ t = 0	h $\frac{Btu}{ft^2\text{-}sec\text{-}°R}$	$\frac{h}{h_{s_{Flat}}}$	$\frac{h}{h_{s_{Sphere}}}$
7	848.0	1549.3	3.397	Dome Master	B001	0	575.8	37.658	.03871		1.0
					B002	.524	573.5	33.625	.03445		.8900
					B003	1.047	570.3	18.381	.01877		.4849
					B004	1.571	567.6	4.421	.00450		.1162
				Flat Master	A001	0	577.4	22.666	.02332	1.0	.6023
					A002	.50	578.9	24.805	.02556	1.0961	.6602
					A003	1.146	577.9	24.338	.02506	1.0744	.6471
					A004	3.092	576.9	2.297	.00236	.1013	.0610
				Flat ECAN	CC012	.50	558		.02287	.9807	
					CC002	.50	558		.02995	1.2843	
					CC003	1.146	558		.02753	1.1805	
					CC004	3.092	558		.00296	.1269	
8	846.7	1415.9	3.952	Dome Master	B001	0	563.9	34.131	.04006		1.0
					B002	.524	564.1	30.320	.03559		.8647
					B003	1.047	562.2	16.431	.01924		.4674
					B004	1.571	560.3	3.870	.00452		.1098
				Flat Master	A001	0	561.2	20.044	.02342	1.0	.5845
					A002	.50	559.9	22.155	.02588	1.1053	.6461
					A003	1.146	557.1	21.896	.02550	1.0888	.6364
					A004	3.092	553.9	2.045	.00237	.1012	.0592
				Flat ECAN	CC012	.50	547		.02271	.9697	
					CC002	.50	547		.02965	1.2660	
					CC003	1.146	547		.02778	1.1862	
					CC004	3.092	547		.00306	.1307	

TABLE XI AVERAGED VALUES OF PHASE A MODEL TEST RESULTS
M = 7.32, AMES 3-1/2-FOOT HYPERSONIC TUNNEL

Model Face and Type	Model T/C	S/R	$\left(\frac{h}{h_s}\right)_{Sphere}$	$\frac{h_s}{h_{s_{Theory}}}$	$\left(\frac{h}{h_s}\right)_{Flat}$	Runs Averaged
Dome Master	B001	0	1.0000	1.020***		1-8
	B002	.524	.8864			
	B003	1.047	.4767			
	B004	1.571	.1097			
Flat Master	A001	0	.5906	1.011****	1.0000	1-8
	A002	.50			1.1111	
	A003	1.146			1.0990	
	A004	3.092			0.1011	
Flat ECAN	CC002 & CC012	.50			1.2034*	1-8
	CC003	1.146			1.1937*	
	CC004	3.092			0.1240*	
Flat ECAN	CC002 & CC012	.50			1.1057**	1-8
	CC003	1.146			1.093**	
	CC004	3.092			0.1141**	
Flat ATZN	I002 & I012	.50			1.1516*	1-2
	I003	1.146			1.0874*	
	I004	3.092			.1127*	
Flat ATZN	G002 & G012	.50			1.1587*	1
	G003	1.146			1.0772*	
	G004	3.092			.1295*	

* Using mid fairing of $\sqrt{\rho CK}$

** Using lower fairing of $\sqrt{\rho CK}$ (See Figure 16)

*** Fay-Riddell theory (Calculated each run by NASA Ames)

**** Zoby-Sullivan theory, Ref. 11

TABLE XII SELECTIVE PLATING PROCESS ON STAINLESS STEEL MODEL

	Solution or Treatment	Temperature (°F)	Time** (Min.)
	* Nickel Chloride Plate	140	Strike Coat
	Preheat in Oven	175	60
	Clean 1424 (Shipley)	165	12
	Water Rinse and Spray	RT	
	Dry in Oven	175	30
DARK ROOM OPERATIONS	Resist AZ111 (Shipley)	RT	Dip
	Air Dry	RT	30
	* Resist AZ111 (Shipley)	RT	Dip (Opposite End First)
	Airdry	RT	30
	Cure in Oven	175	60
	Expose Pattern Through Negative with Ultraviolet Lamps	RT	15
	Develop AZ-303A (Shipley)	RT	10
	Water Rinse and Spray	RT	
	Bake in Oven	400	60
	Preheat Model	200	60
	Activate 1424 (Shipley)	165	13
	Water Rinse and Spray	165	2
	Plate Niculoy 22 (Shipley)	195	As Required ~10 μ in./min. ***
	Remove Resist 1112A (Shipley)	170	60
	Water Rinse and Spray	RT	

* Optional, Depending on Plate Thickness Required

** Approximate Times; Actual Times Dependent on Specific Condition, i.e. Model Size, Light Intensity, Resist Thickness, etc.

*** Two Coats of Resist Will Withstand Activation and Plating to Approximately 0.001 Inch Thickness

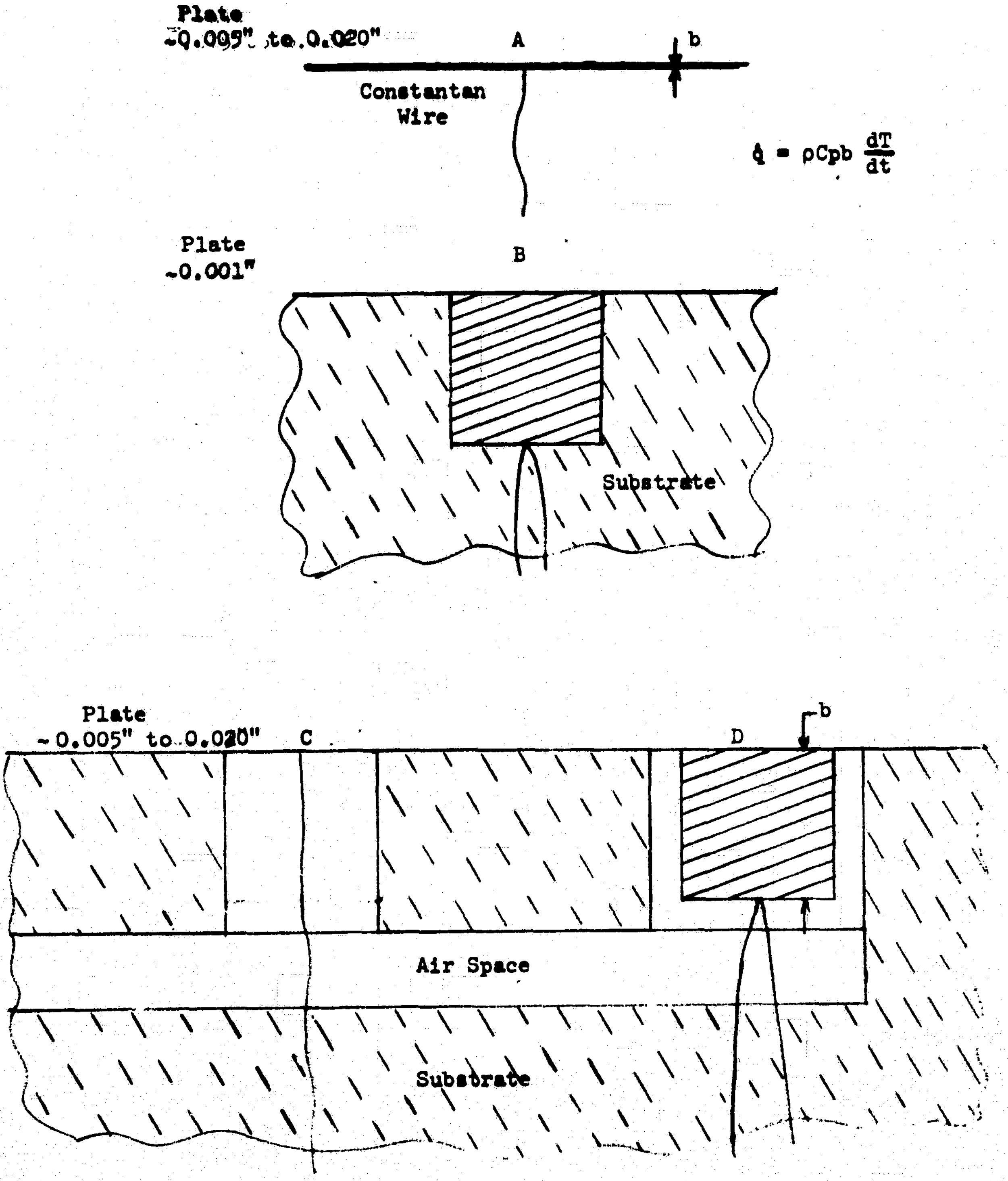

Figure 1 Model/Instrumentation Concepts Employing Electroless Nickel Surface a. Calorimeter Gages

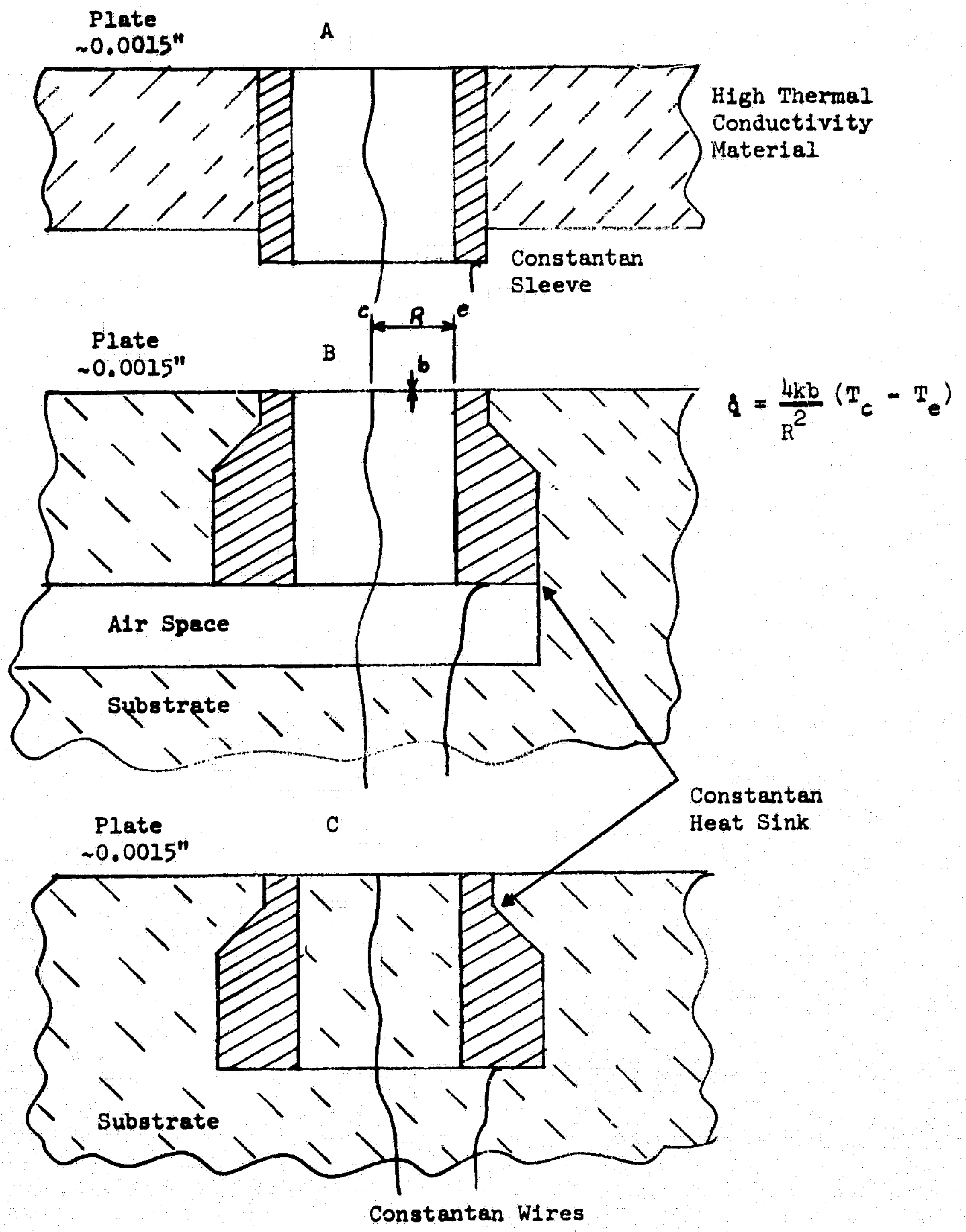

Figure 1 Model/Instrumentation Concepts Employing Electroless Nickel Surface b. Gardon Gages

Slab Gage

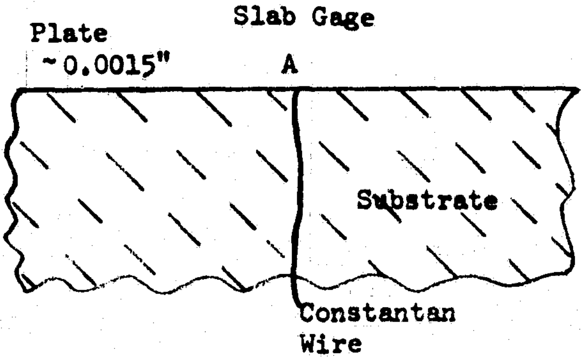

$$h = \frac{\beta\sqrt{\rho c k}}{\sqrt{t}}$$

$$\frac{T_w - T_i}{T_{aw} - T_i} = 1 - e^{\beta^2}\operatorname{erfc}\beta = \overline{T}$$

Wire Gages

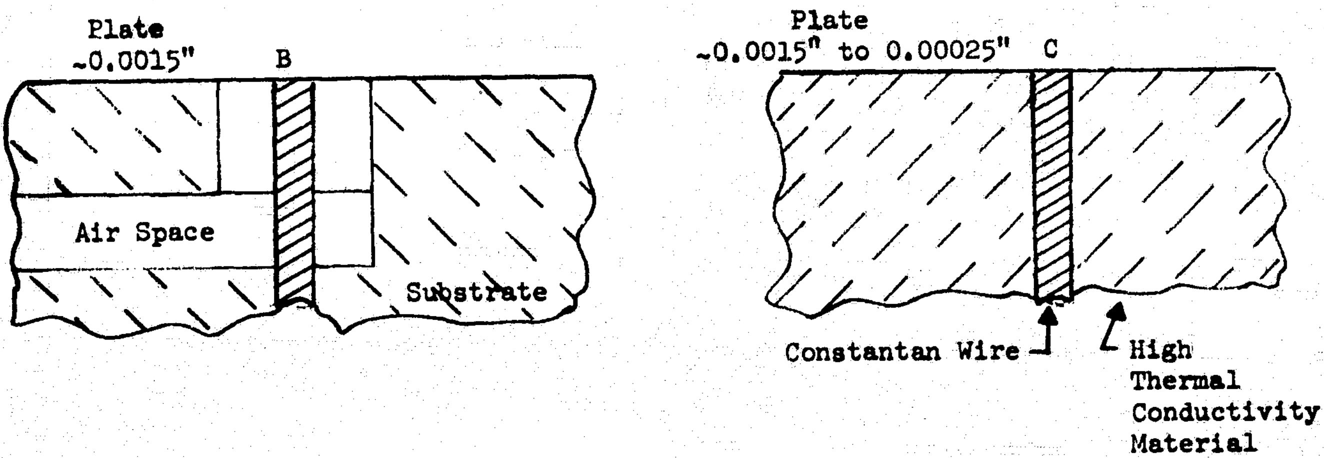

Figure 1 Model/Instrumentation Concepts Employing Electroless Nickel Surface c. Semi-Infinite - Material Gages

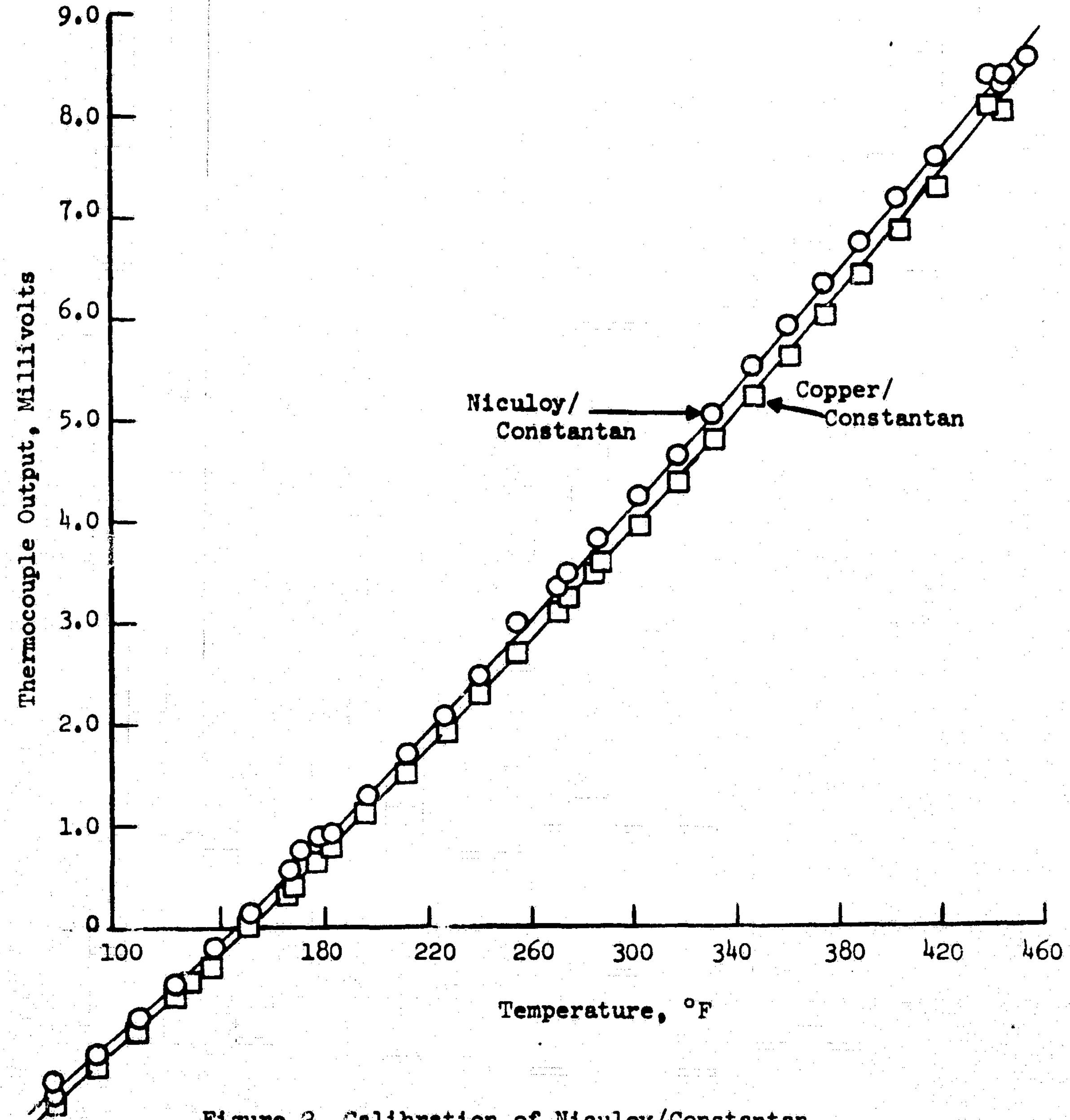

Figure 2 Calibration of Niculoy/Constantan and Copper/Constantan Thermocouples

	Thickness (in) Nickel Plate	Diameter (in) Constantan Wire	Air Gap (in) Around Wire	Substrate Material
◇	.0015	.010	0	Novimide 700/55
♢	.0015	.010	.010	Novimide 700/55
▽	.0015	.03125	0	Novimide 700/55
◁	.0015	.0325	.01625	Novimide 700/55
◊	.0015	∞	0	---

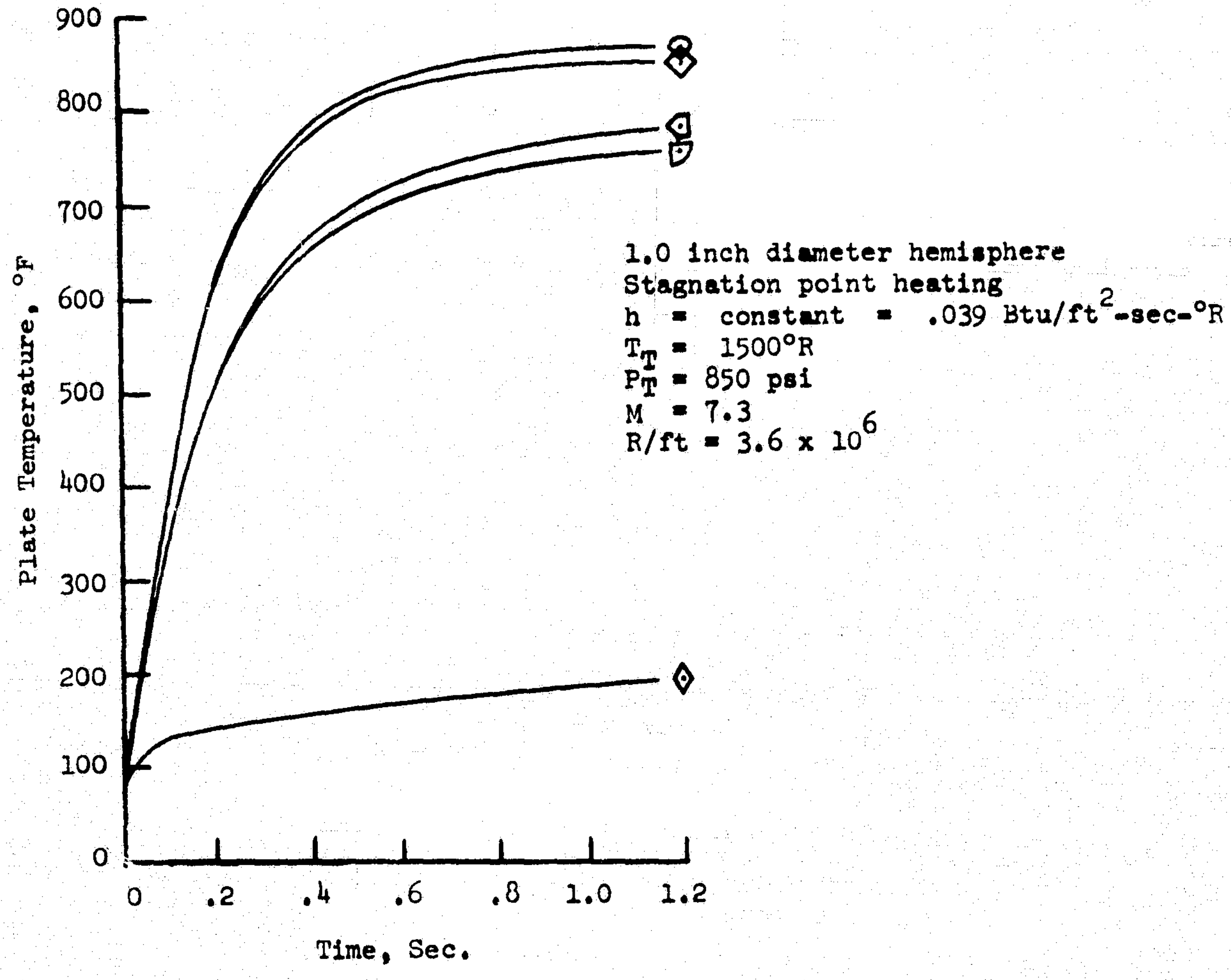

1.0 inch diameter hemisphere
Stagnation point heating
h = constant = .039 Btu/ft^2-sec-°R
T_T = 1500°R
P_T = 850 psi
M = 7.3
R/ft = 3.6 x 10^6

Figure 3 Temperature Response of Nickel Plated Novimide 700/55, Effect of Air Gap

	Thickness (in) Niculoy Plate	Diameter (in) Constantan Wire	Substrate Material
□	.001	0	Novimide 700/55
△	.001	.003	Novimide 700/55
◇	.001	.010	Novimide 700/55
D	.001	.032	Novimide 700/55
◊	.001	∞	---

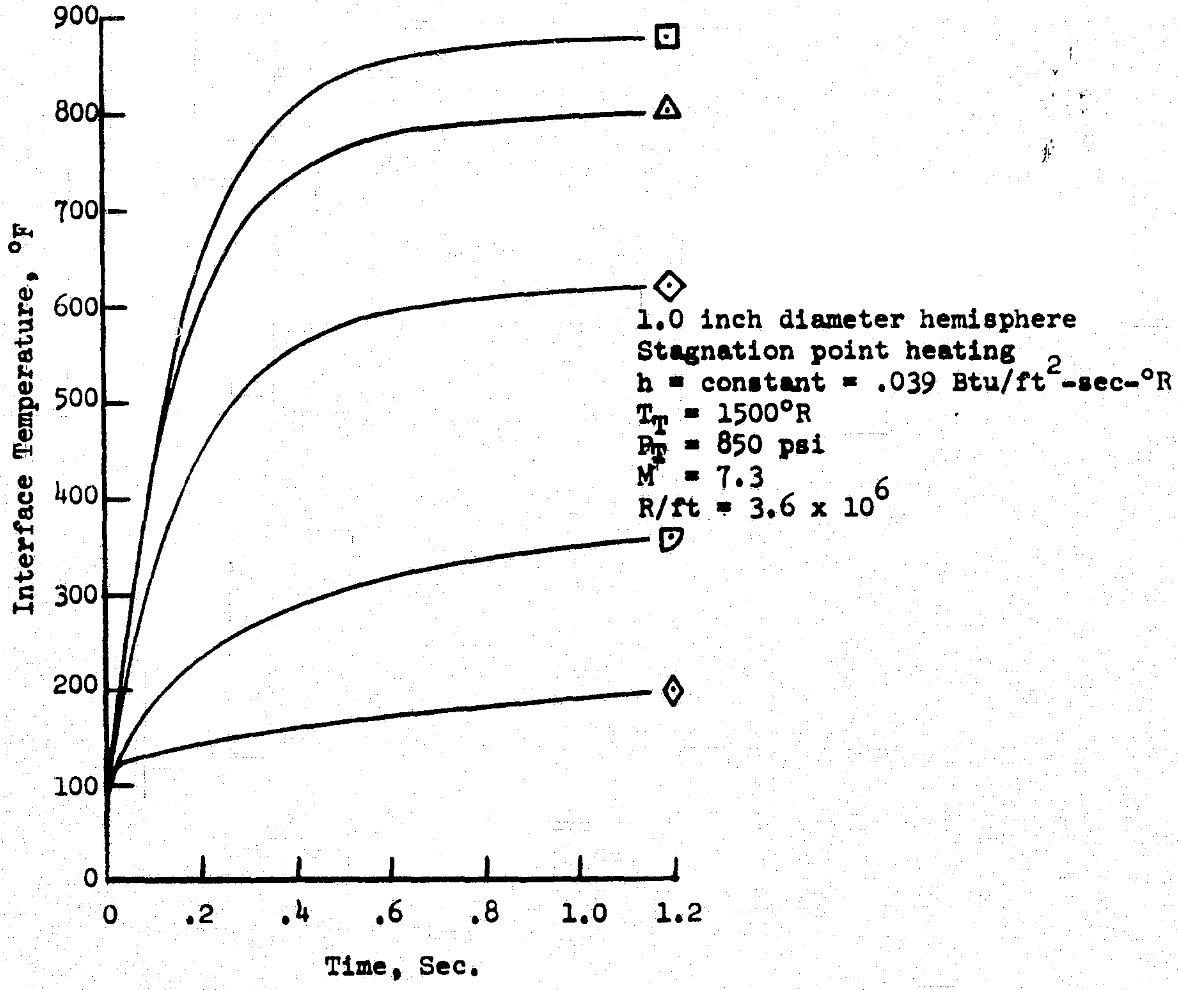

1.0 inch diameter hemisphere
Stagnation point heating
h = constant = .039 Btu/ft^2-sec-°R
T_T = 1500°R
P_T = 850 psi
M = 7.3
R/ft = 3.6 x 10^6

Figure 4 Temperature Response of Niculoy Plated Novimide 700/55, Effect of Wire Diameter

1.0 inch diameter hemisphere
Stagnation point heating
h = constant = .039 Btu/ft^2-sec-°R
T_T = 1500°R
P_T = 850 psi
M = 7.3
R/ft = 3.6 x 10^6

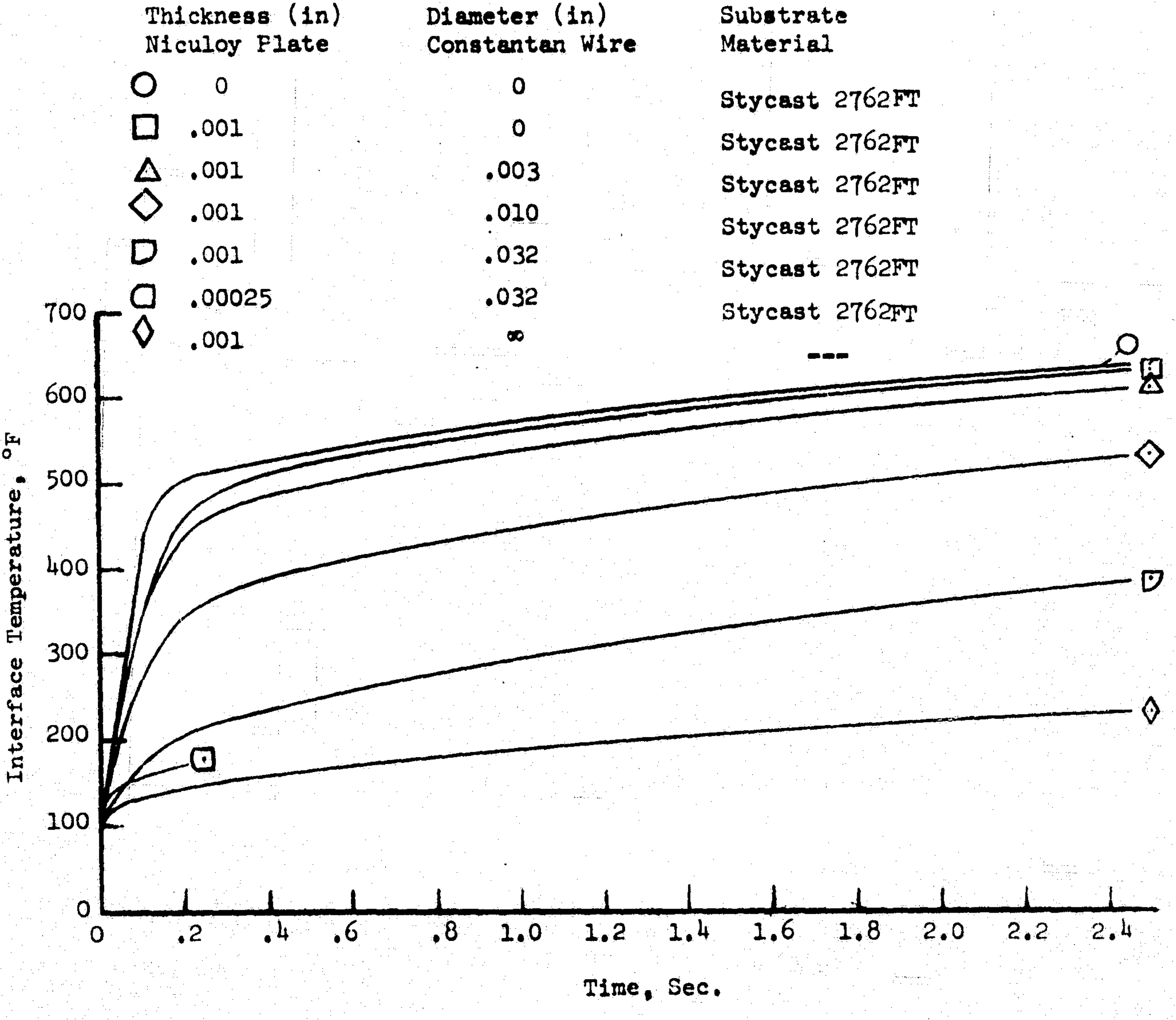

	Thickness (in) Niculoy Plate	Diameter (in) Constantan Wire	Substrate Material
○	0	0	Stycast 2762FT
□	.001	0	Stycast 2762FT
△	.001	.003	Stycast 2762FT
◇	.001	.010	Stycast 2762FT
D	.001	.032	Stycast 2762FT
▢	.00025	.032	Stycast 2762FT
◊	.001	∞	---

Figure 5 Temperature Response of Niculoy Plated Stycast 2762FT, Effects of Wire and Plate Dimensions

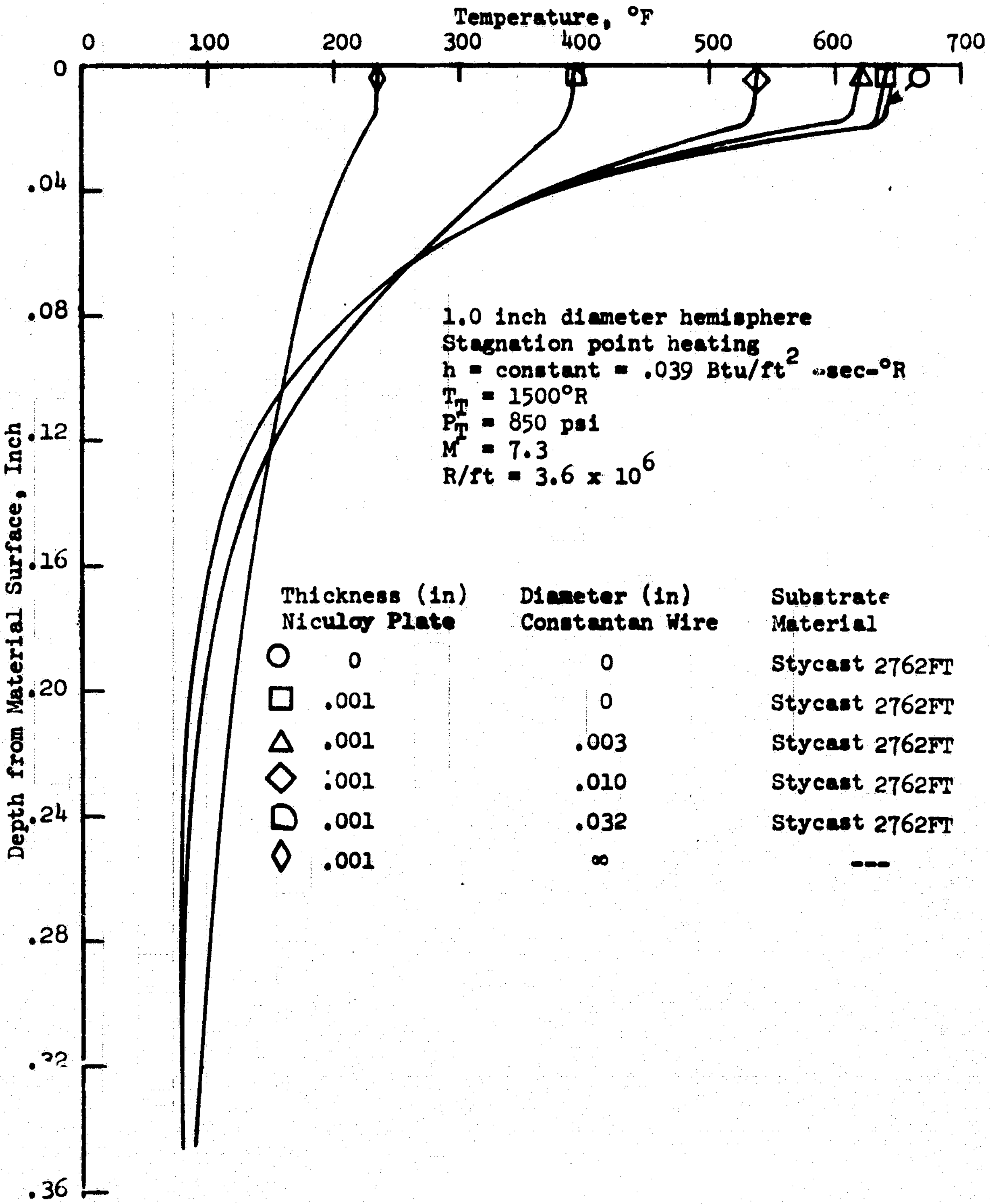

1.0 inch diameter hemisphere
Stagnation point heating
h = constant = .039 Btu/ft^2-sec-°R
T_T = 1500°R
P_T = 850 psi
M = 7.3
R/ft = 3.6 x 10^6

Figure 6 Temperature Gradients in Materials at Time 2.5 Seconds

1.0 inch diameter hemisphere
Stagnation point heating
h = constant = .039 Btu/ft^2-sec-°R
T_T = 1500°R
P_T = 850 psi
M = 7.3
R/ft = 3.6 x 10^6

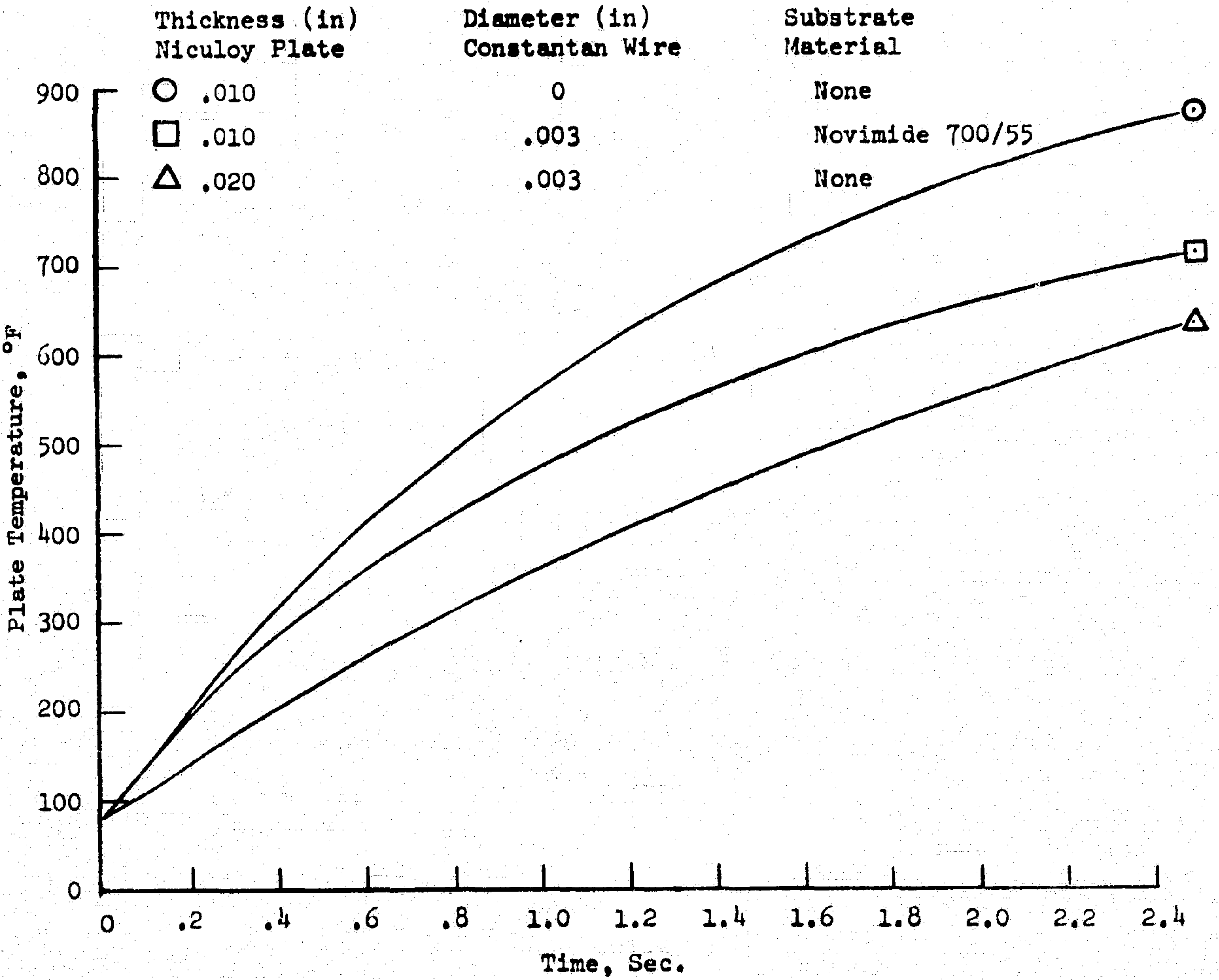

Figure 7 Temperature Response of Niculoy Plate Used As A Calorimeter

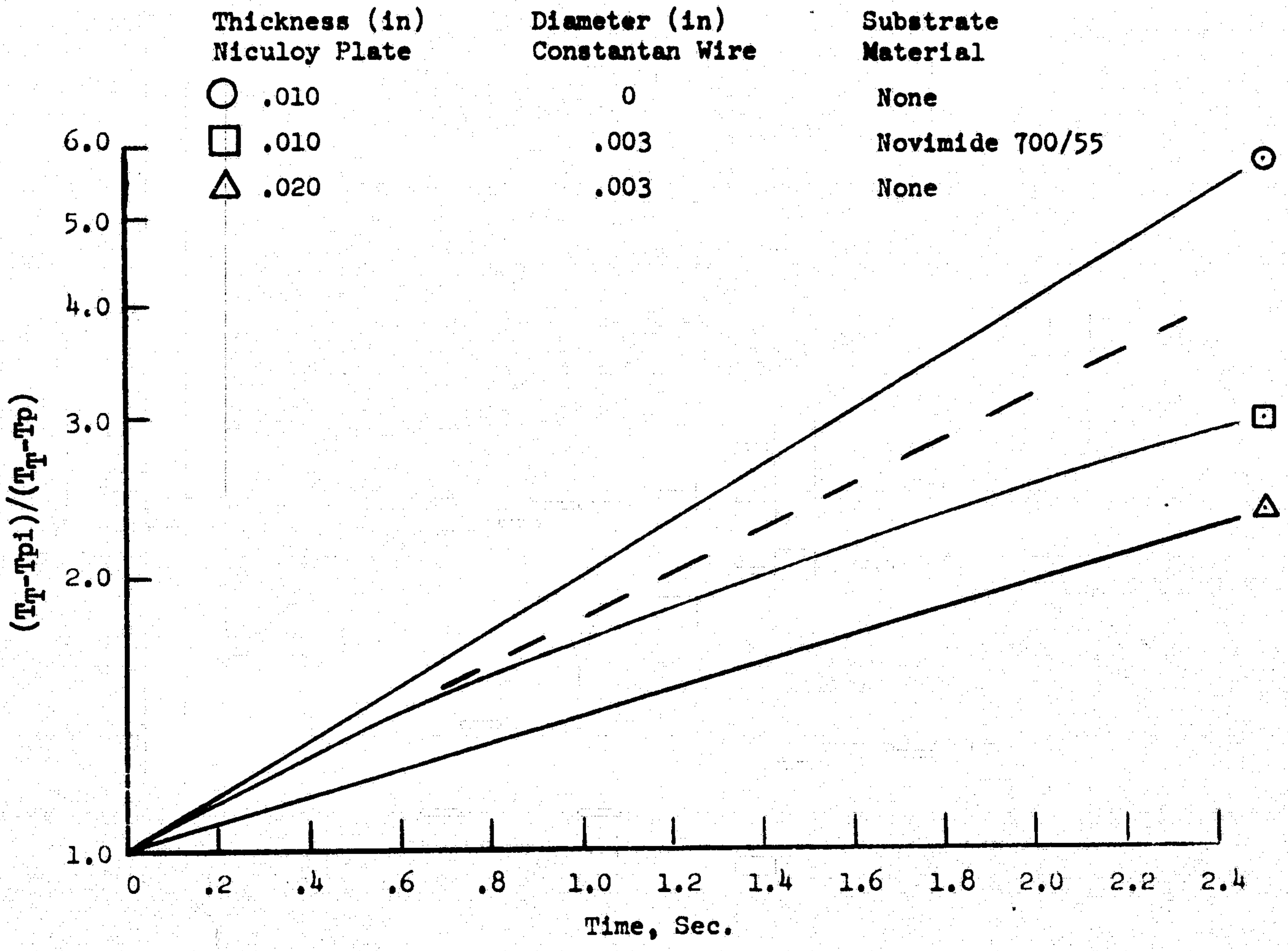

1.0 inch diameter hemisphere
Stagnation point heating
h = constant = .039 Btu/ft^2-sec-°R
T_T = 1500°R
P_T = 850 psi
M = 7.3
R/ft = 3.6 x 10^6

Figure 8 Effect of Substrate and Wire on Calorimeter Temperature History

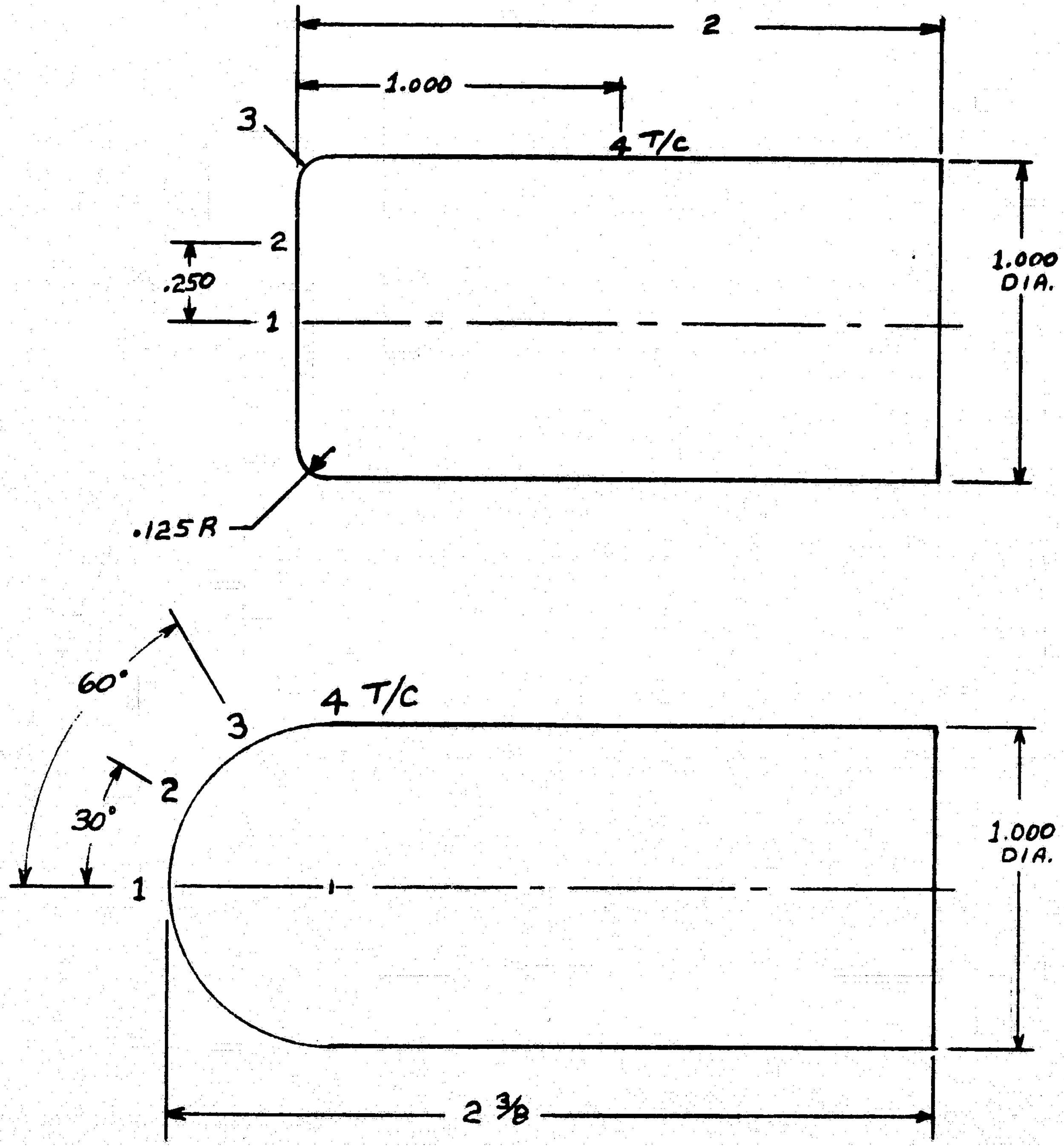

Figure 9 Geometry and Thermocouple Locations of Development Models

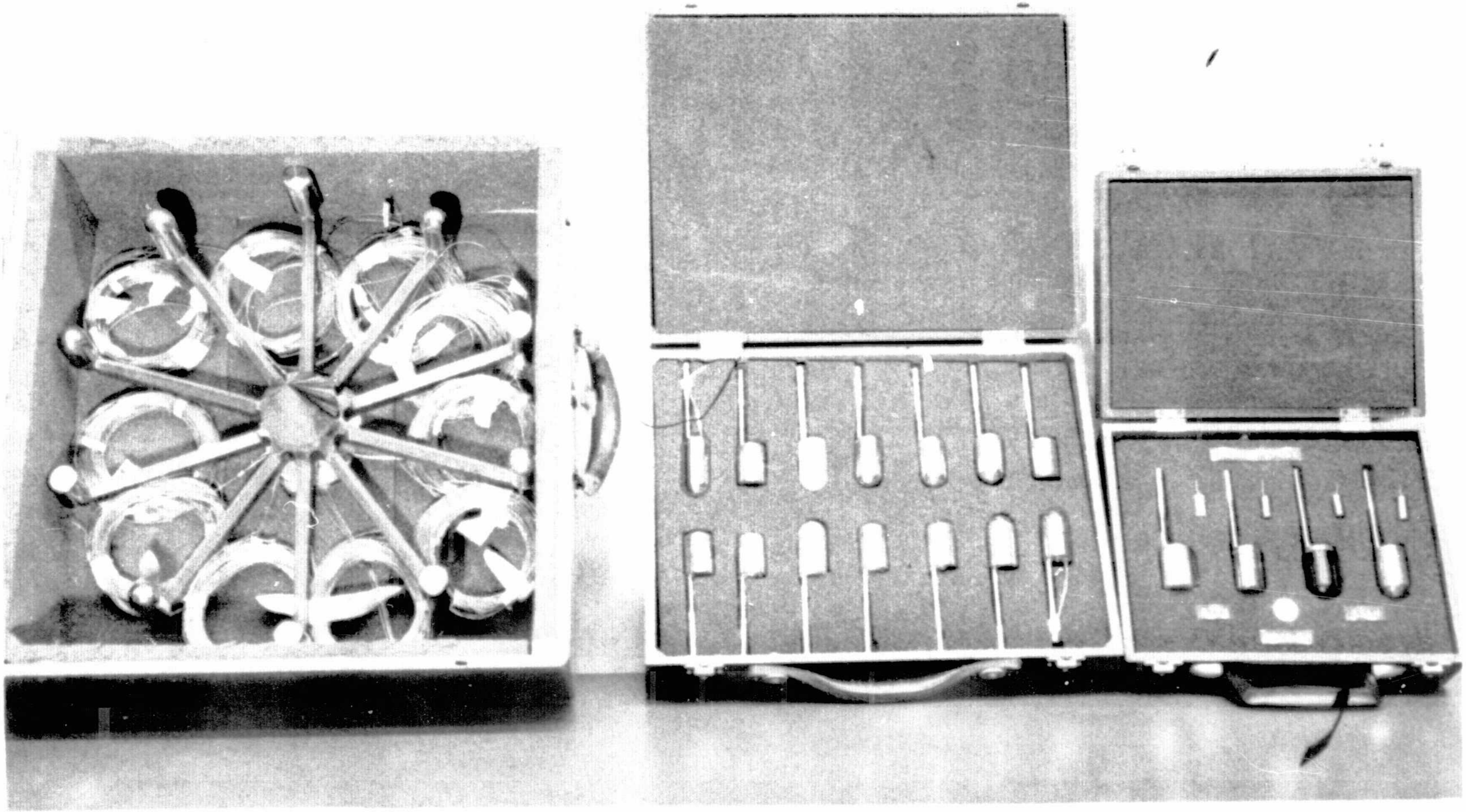

Figure 10 Phase A Models Prior to Tunnel Entry

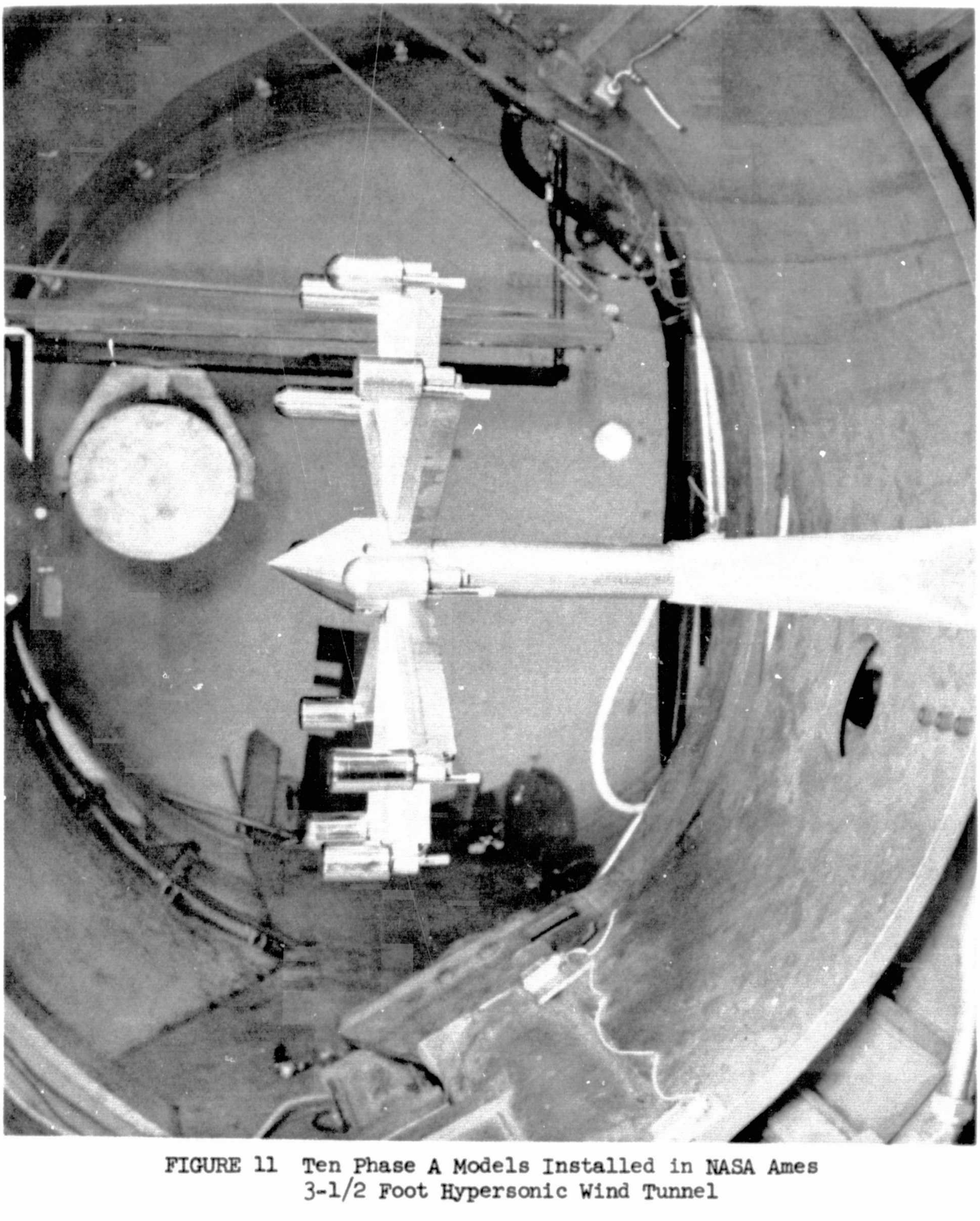

FIGURE 11 Ten Phase A Models Installed in NASA Ames 3-1/2 Foot Hypersonic Wind Tunnel

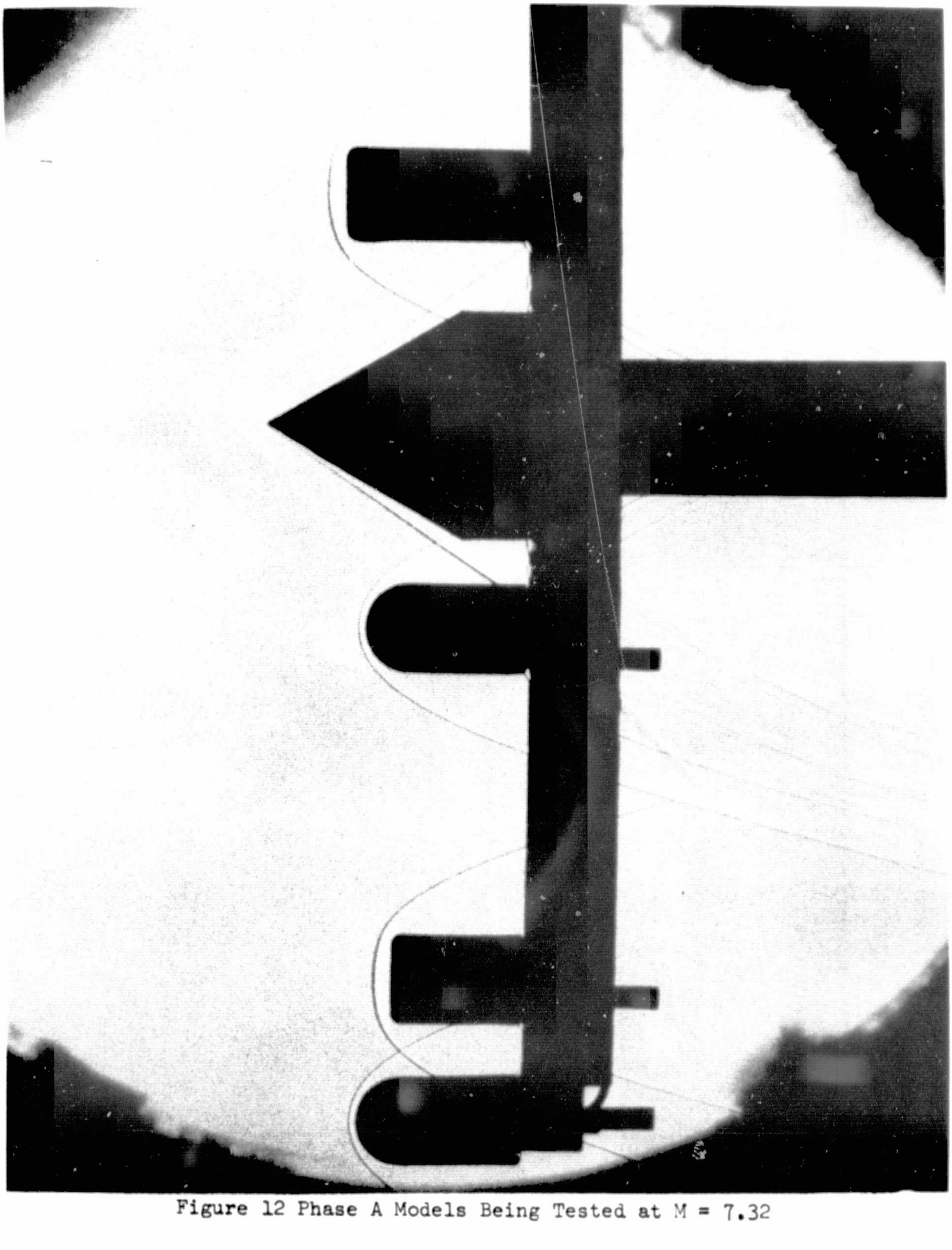

Figure 12 Phase A Models Being Tested at M = 7.32

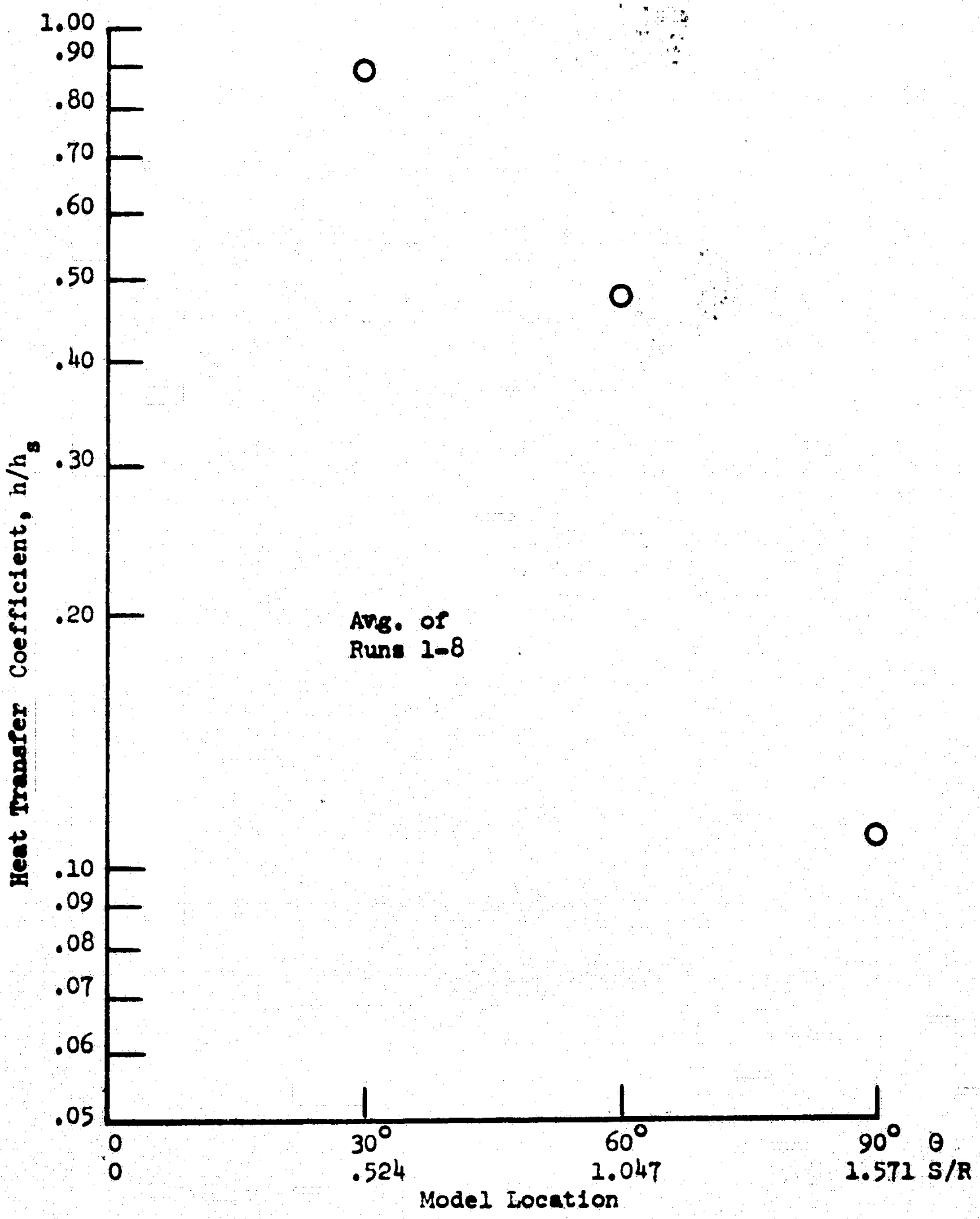

Figure 13 Distribution of Film Coefficient
on Master Hemisphere Model

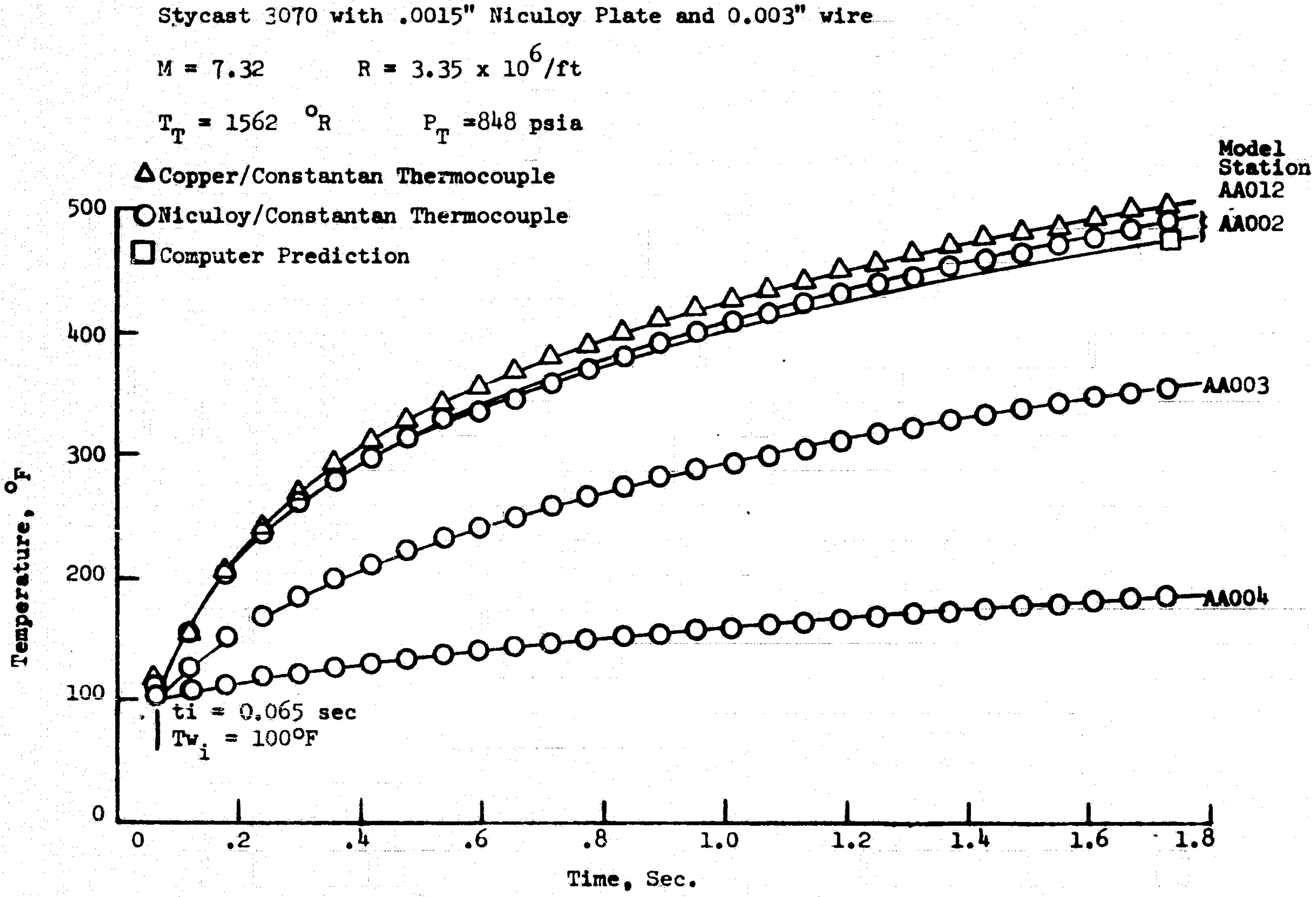

Figure 14 Temperature History of Model AA Hemisphere, Run 5

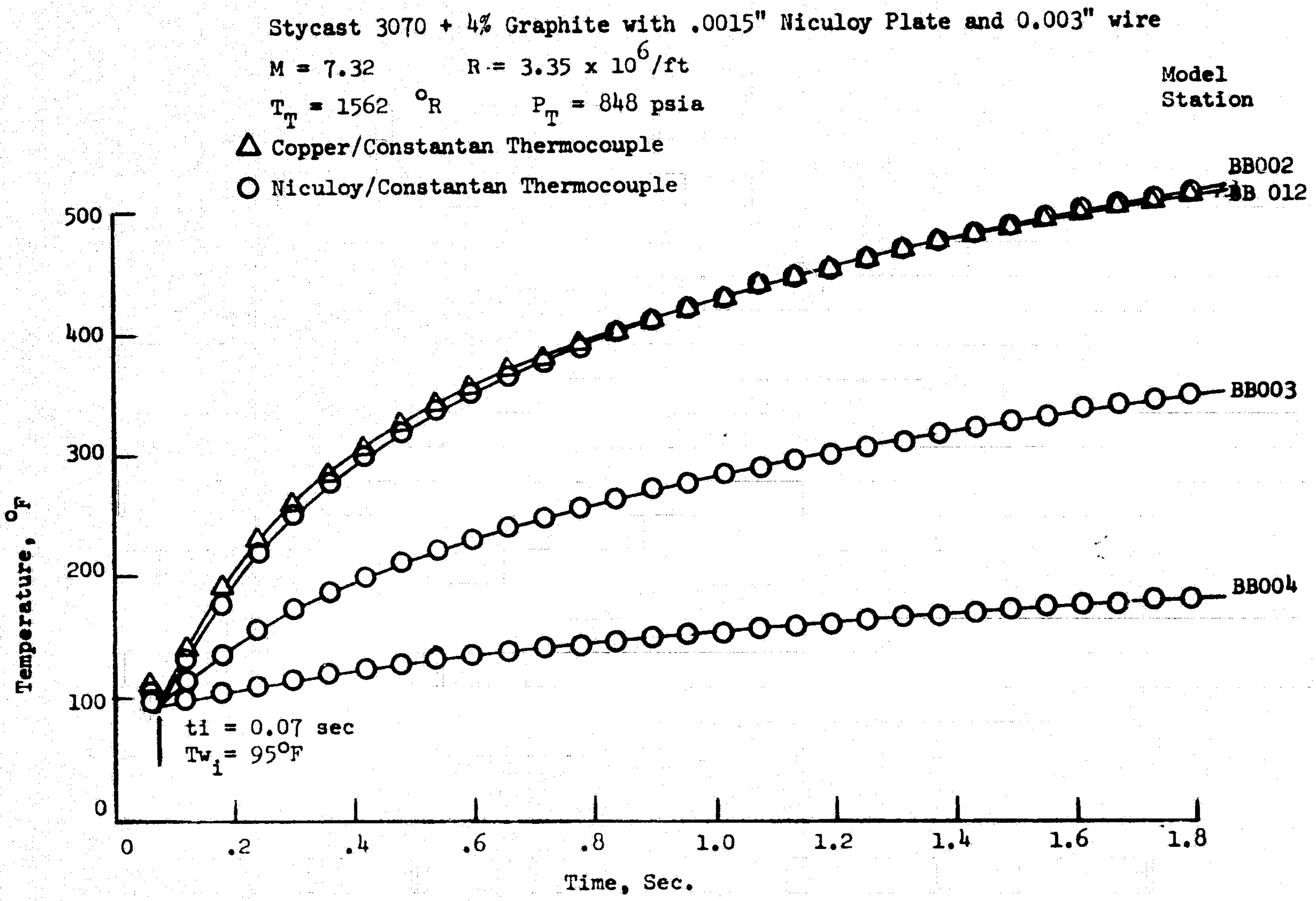

Figure 15 Temperature History of Model BB Hemisphere, Run 5

Stycast 3070 with .0015" Niculoy Plate and 0.003" wire
for all Runs 1-8, M = 7.32
Ranges: $.8 \times 10^6 < R/ft < 4.0 \times 10^6$
$202 < P_T$, Psia < 1000
$1415 < T_T$, °R < 1618

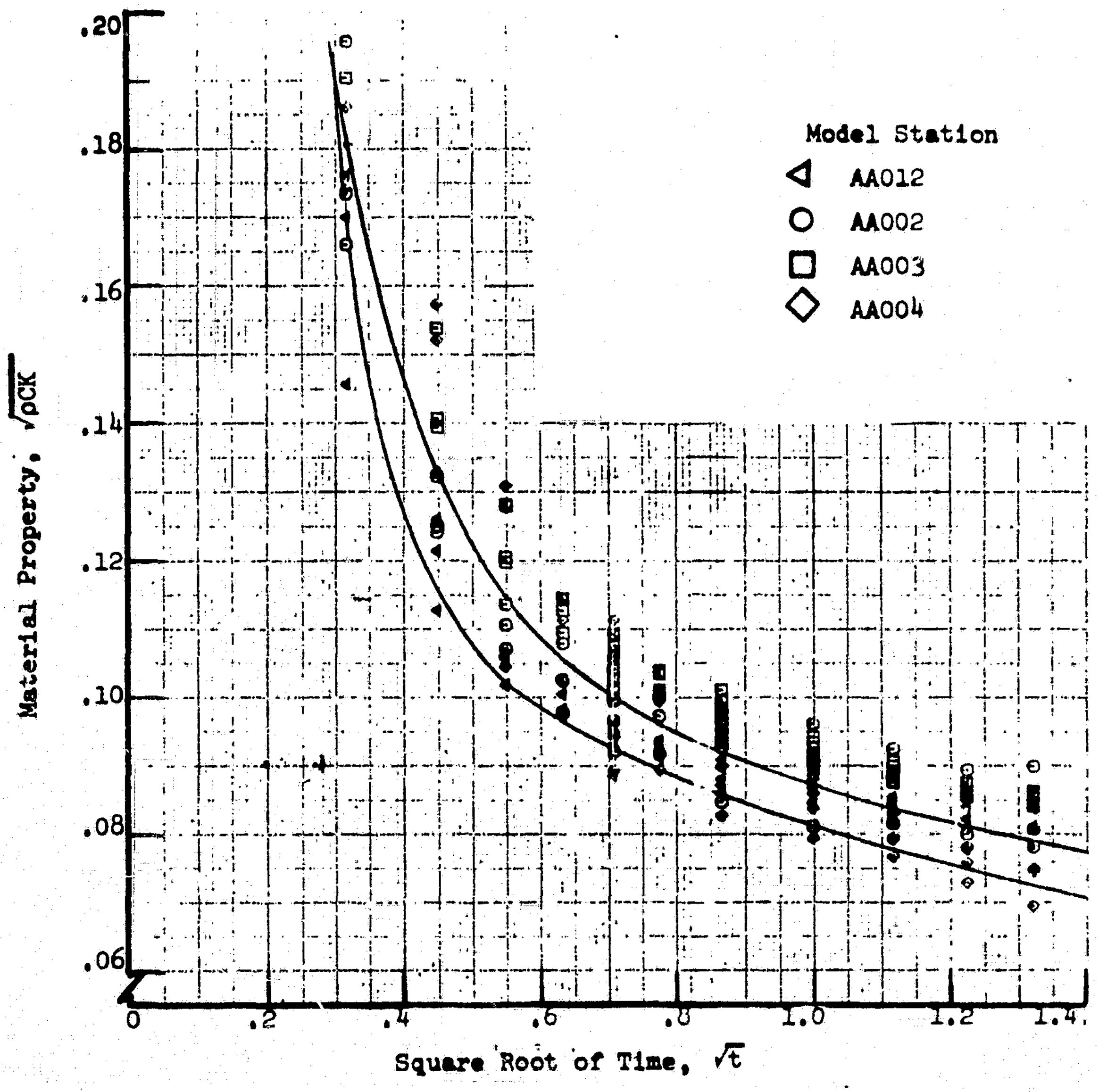

Figure 16 Material Property of Model AA Hemisphere

Stycast 3070 with .0015" Niculoy Plate and 0.003" wire
for all Runs 1-8, $M = 7.32$
Ranges: $.8 \times 10^6 < R/ft < 4.0 \times 10^6$
$202 < P_T, Psia < 1000$
$1415 < T_T, {}^{o}R < 1618$

○ - $t = .5$ sec., $\sqrt{t} = .707$
☐ - $t = 1.5$ sec., $\sqrt{t} = 1.225$

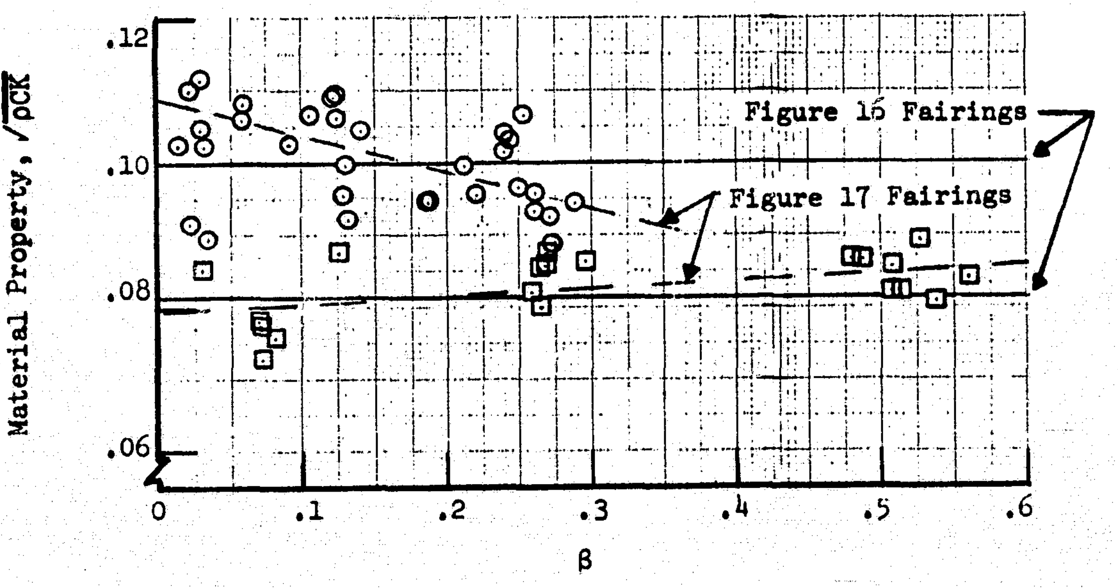

Figure 17 Material Property of Model AA as Function of β at Selected Times

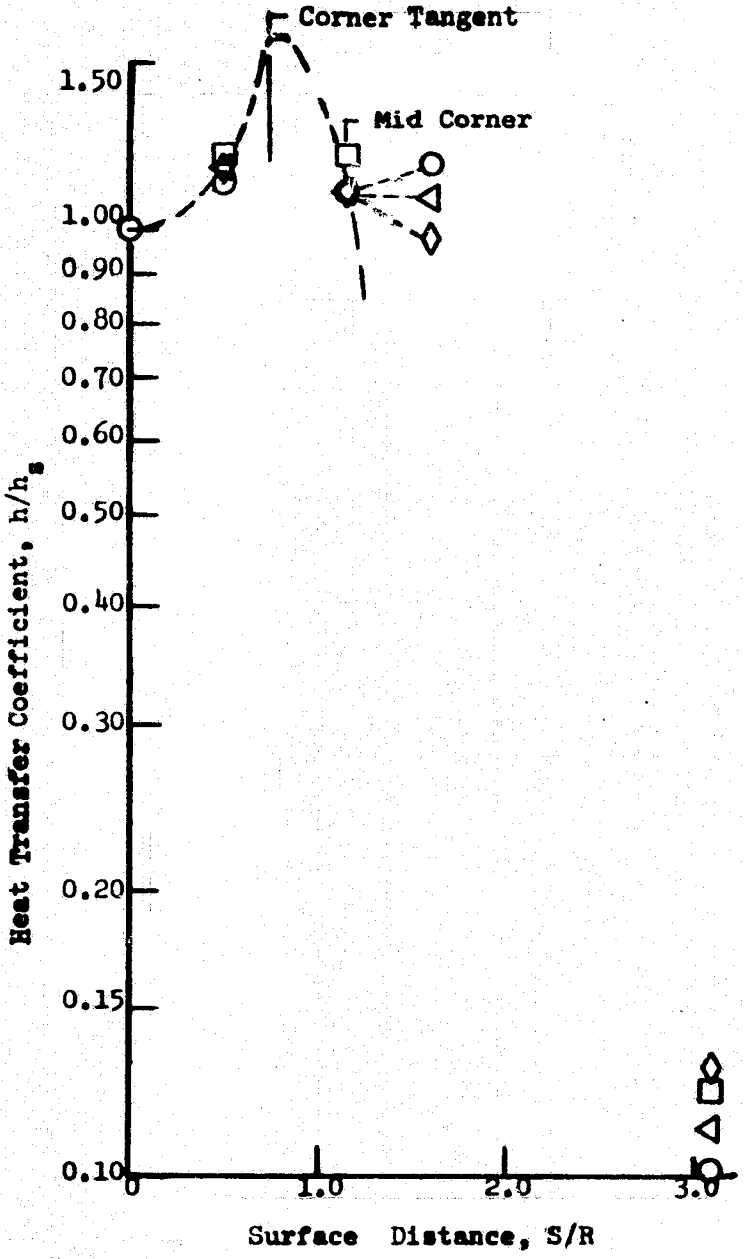

○ - Model A (Master), Avg. of Runs 1-8
□ - Model CC (ECAN), Avg. of Runs 1-8
◁ - Model I (ATZN), Avg. of Runs 1-2
◊ - Model G (ATZN), Run 1

Range of Conditions for Runs 1-8, $M = 7.32$:

$.8 \times 10^6 < R/ft < 4.0 \times 10^6$

$202 < P_T$, Psia < 1000

$1415 < T_T$, $^oR < 1618$

Notes: (1) Values at $S/R = .50$ are averages of two thermocouples (12 and 02) for each model

(2) Experimental fairing guided by Reference 12

Figure 18 Distribution of Film Coefficient on Flat Face Cylinder

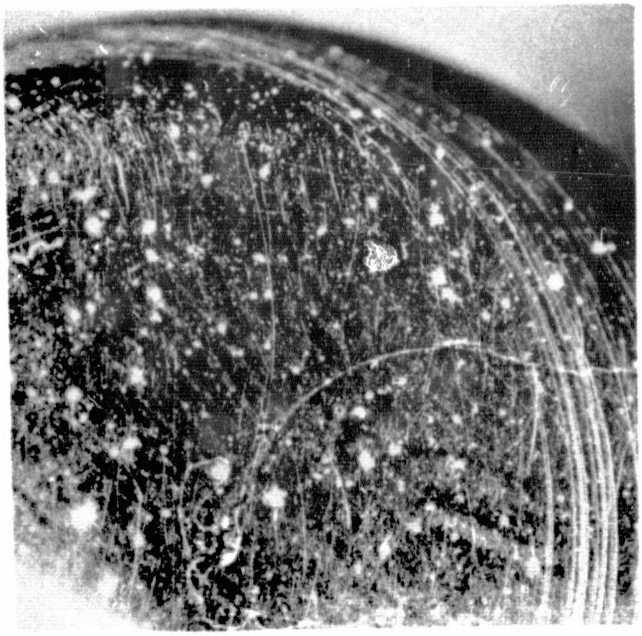

Model A
Steel Master
Flat Face
8 x Magnification

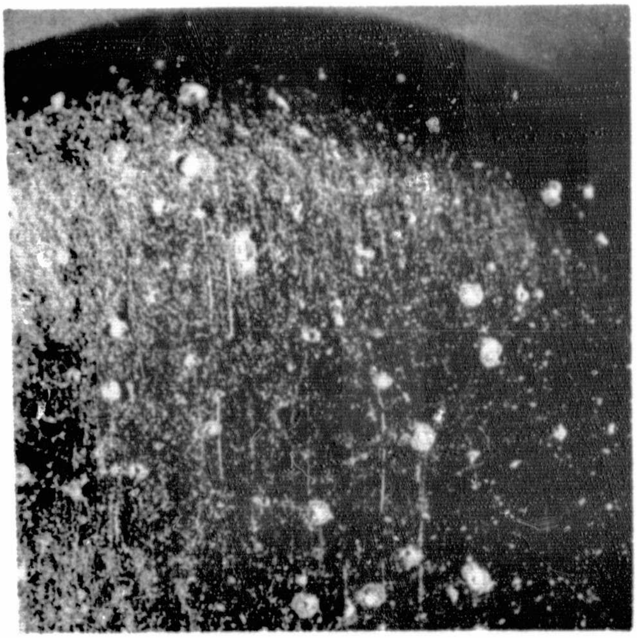

Model CC
ECAN (Phase A)
Flat Face
8 x Magnification

FIGURE 19 Comparison of Particle Damage Between Steel and Plated Epoxy Models After Eight Tunnel Runs

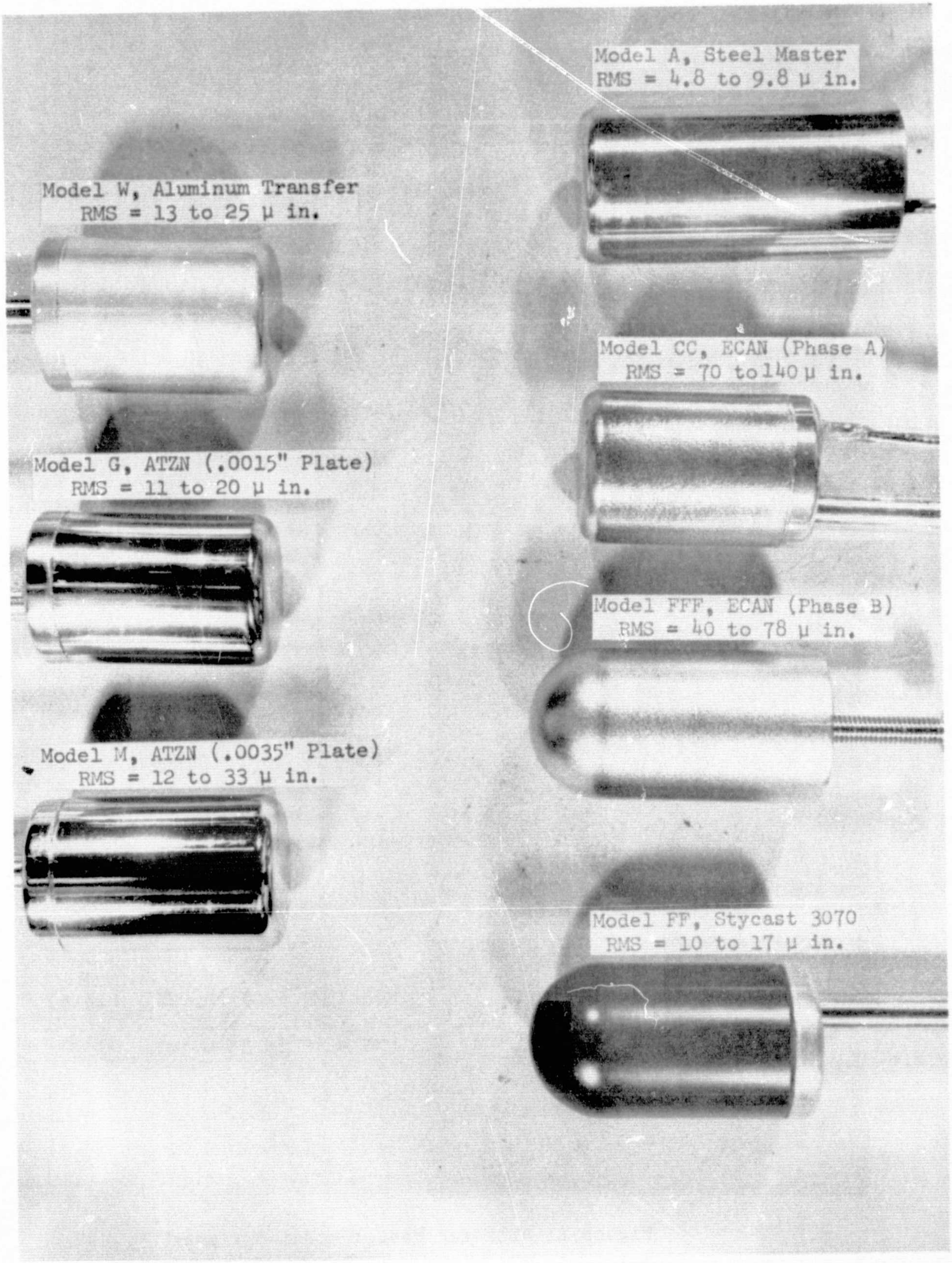

Figure 20 Representative Development Models

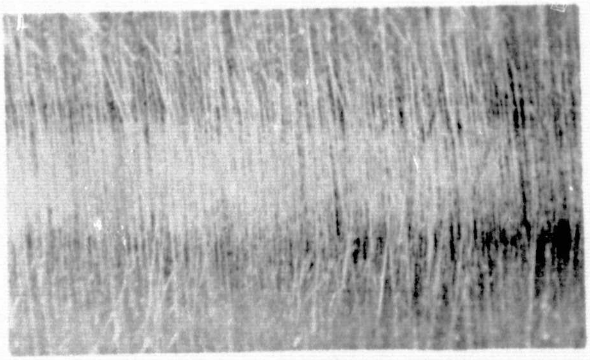

Model A, Steel Master
8 x Magnification
RMS = 4.8 to 9.8 μ in.

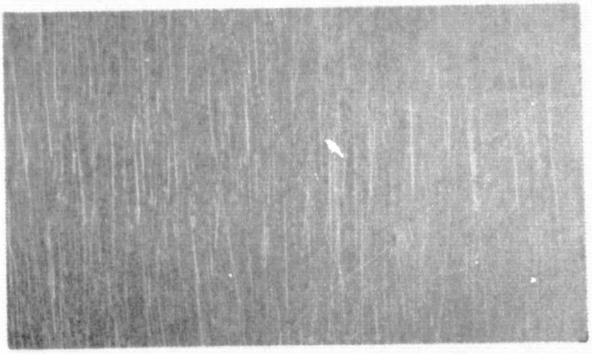

Model W, Aluminum Transfer
8 x Magnification
RMS = 13 to 25 μ in.

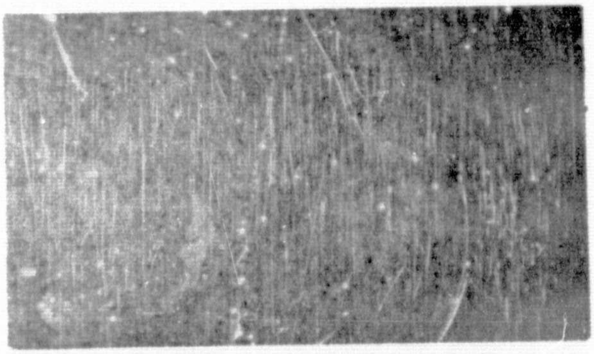

Model G, ATZN (0.0015" Plate)
8 x Magnification
RMS = 11 to 20 μ in.

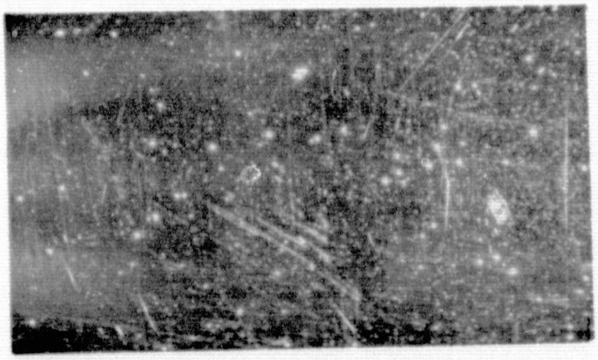

Model M, ATZN (0.0035" Plate)
8 x Magnification
RMS = 12 to 33 μ in.

Figure 21 ATZN and Master Model Surfaces

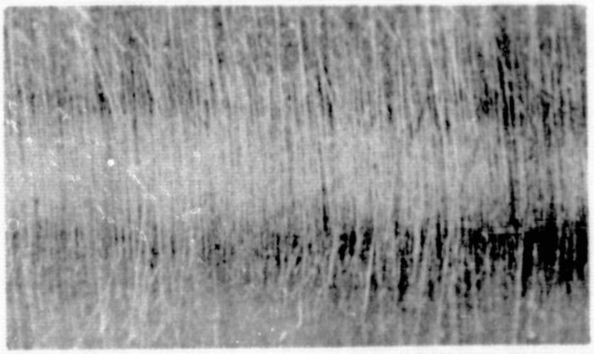

Model A, Steel Master
8 x Magnification
RMS = 4.8 to 9.8 μ in.

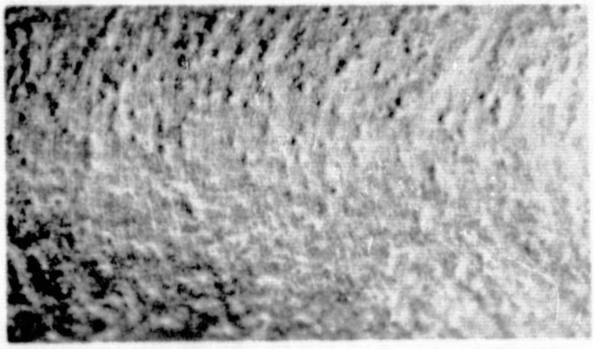

Model CC, ECAN (Phase A)
8 x Magnification
RMS = 70 to 140 μ in.

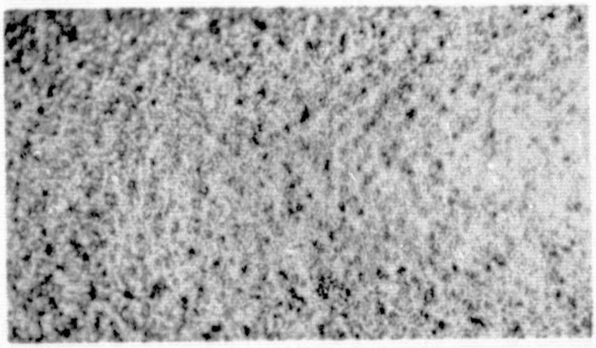

Model FFF, ECAN (Phase B)
8 x Magnification
RMS = 40 to 78 μ in.

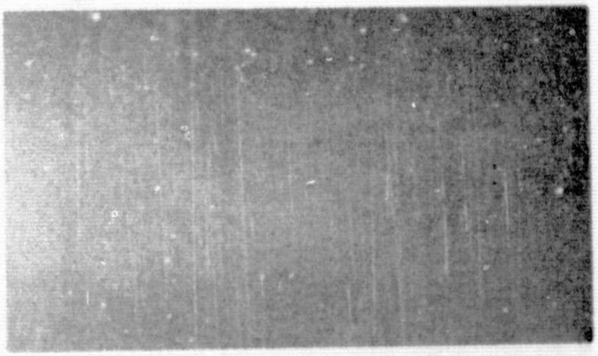

Model FF, Stycast 3070
8 x Magnification
RMS = 10 to 17 μ in.

Figure 22 ECAN and Master Model Surfaces

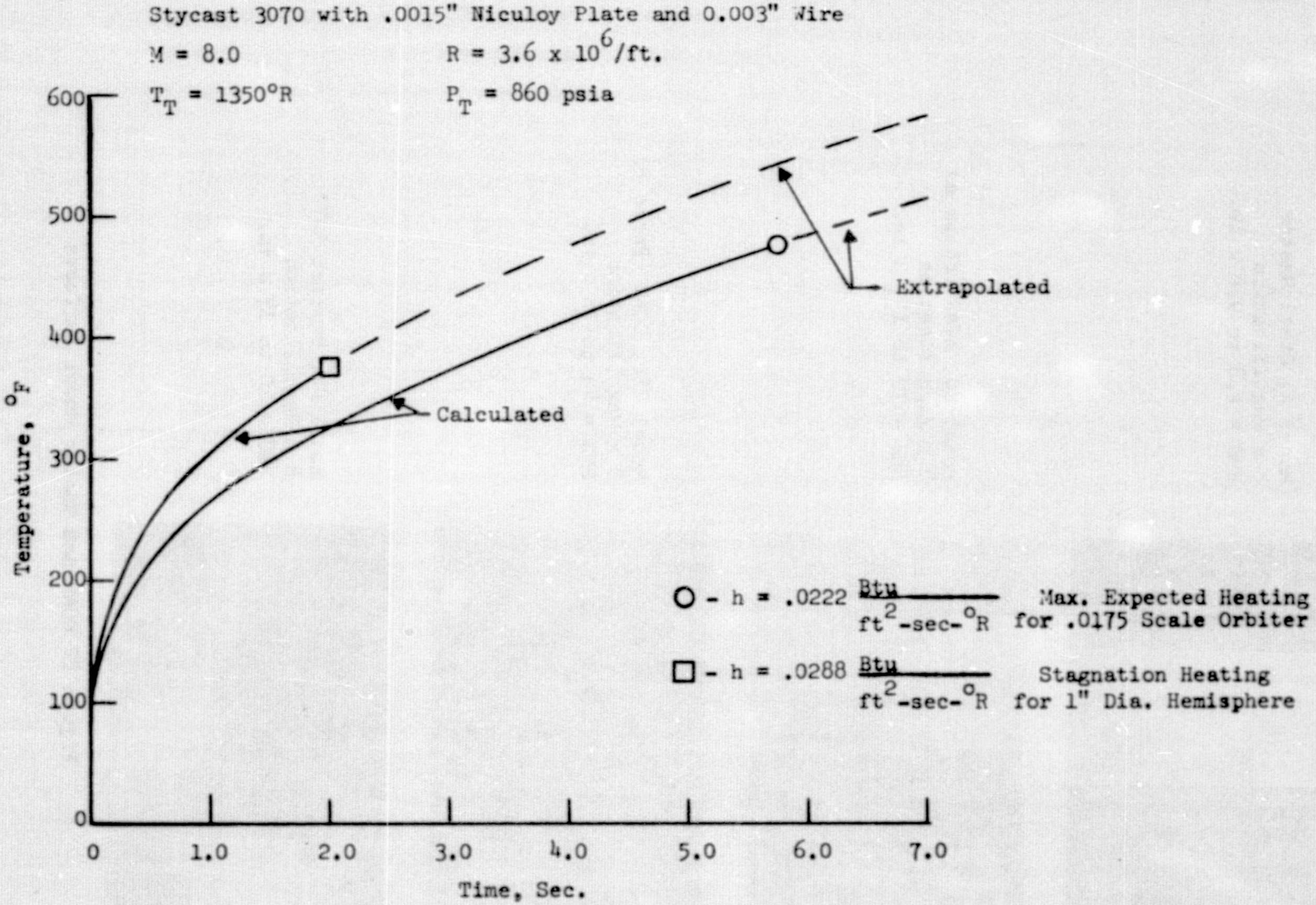

Figure 23 Temperature Predictions for Epoxy Models if Tested in AF Tunnel B at Maximum Reynolds Number

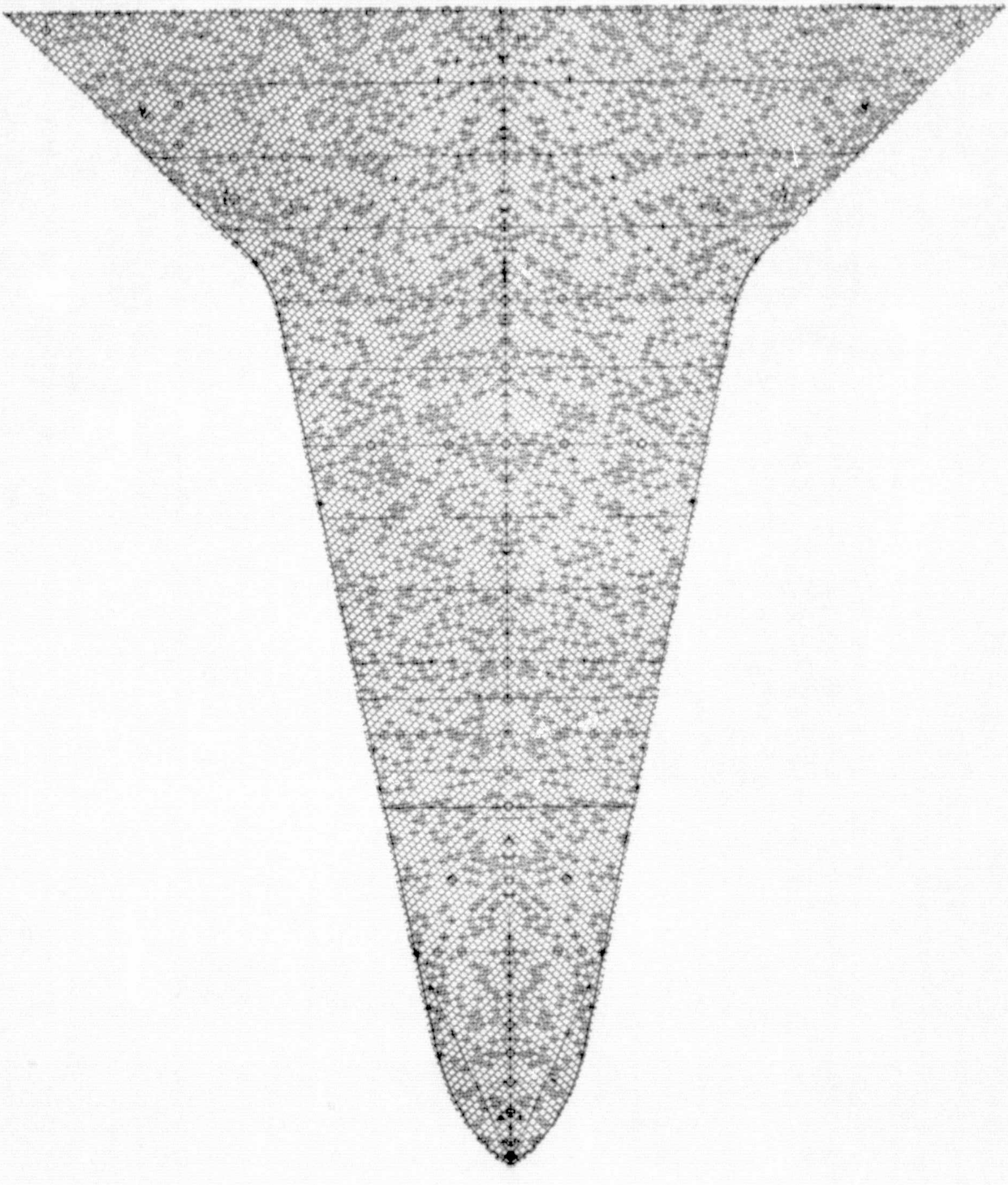

FIGURE 24 Heatshield Tile Pattern Showing Selection of Raised Tiles

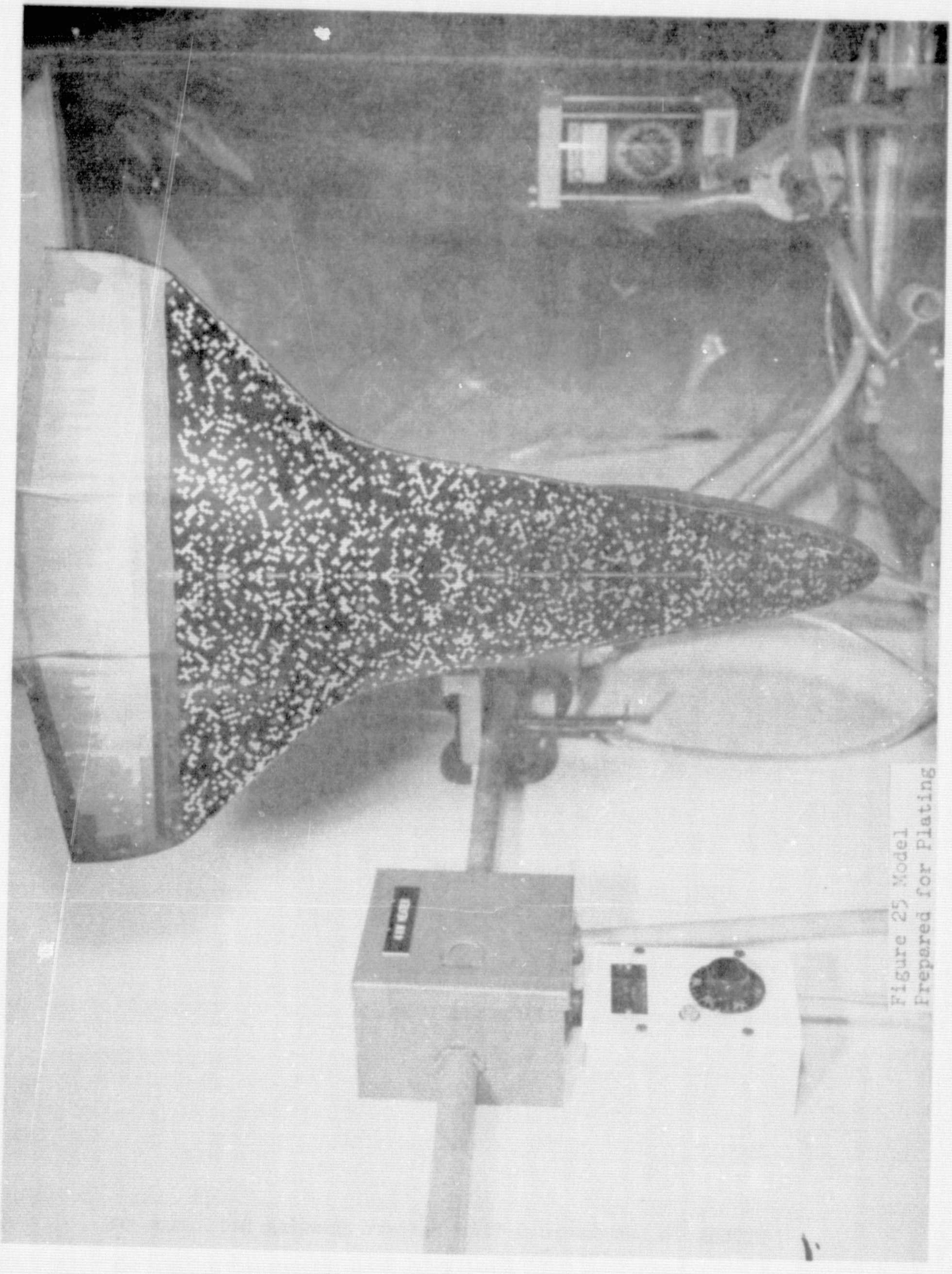

Figure 25 Model Prepared for Plating

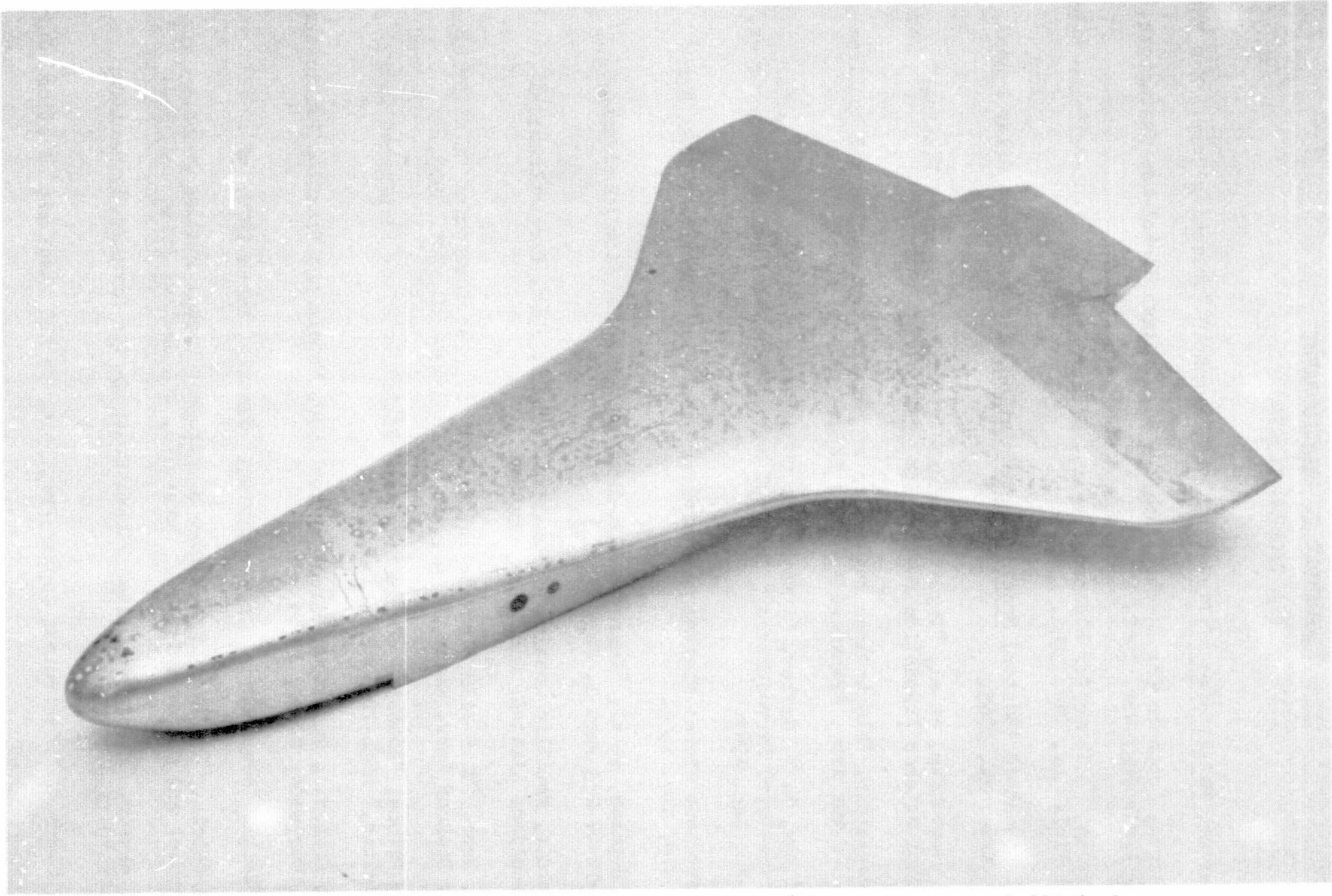

Figure 26 0.0175 scale Orbiter Model with 25% Tiles Plated to 0.001 inch

APPENDIX I. BIBLIOGRAPHY

ELECTROLESS PLATING

1. H. Narcus, Metallizing of Plastics, 1960, Reinhold Publishing Corp., New York.

2. L. Serota, "Science for Electroplaters - Electroless Nickel-Non Conductors," Metal Finishing, Oct. 1962.

3. L. Serota, "Science for Electroplaters - Electroless Nickel-Disposition Rate," Metal Finishing, Dec. 1962.

4. F. A. Lowenheim (Editor) Modern Electroplating, 2nd Ed., John Wiley & Sons, Inc., New York, 1963.

5. K. M. Gorbunova, et al, "Physicochemical Principles of Nickel Plating," National Science Foundation Publication, TT63-11003, 1963.

6. F. Pearlstein, "Electroless Deposition of Metals - Principles and Applications," Dept. of the Army, Frankford Arsenal, Report A68-11, March 1968.

7. L. E. Fox, B. V. Gerber, "A Method of Copper Plating Glass and Plastic (Styrene-Type) Microspheres," Chemical Research & Development Laboratories, TM-5-20, Dec. 1965.

8. "Electroless Nickel Plating on Stainless Steels and Aluminum," NASA Brief 66-10479, Nov. 1966.

9. Vern Hopkins, et al, "Improved High-Temperature Solid Film Lubricants," AFML-TR-67-223 Part 1, July 1967.

10. W. Goldie, Metallic Coating of Plastics, Vol. I, 1968, Electrochemical Publications Limited, Middlesex, England.

11. E. L. Hebb, "Thin-Film Electric Initiator: 1. Fabrication of Cu/Ni Bridges," Harry Diamond Labs, Wash., D. C., Proj: DA-1-L-01300, Nov. 1968.

12. D. E. Prince, "Adhesion of Electroplated Nickel to Fiber Reinforced Epoxy Composites," AFML-TR-69-282, Jan. 1970.

13. Metal Finishing Guidebook Directory for 1970, Metals and Plastics Publication, Inc., Westwood, N. J., 1970.

14. F. O'Neill, "Advances in Electroforming," Plating, March 1970.

15. N. Feldstein, "Two Room-Temperature Electroless Nickel Plating Baths - Properties and Characteristics," June 1970, RCA Review, Princeton, N.J.

16. J. H. Weaver, "Electrodeposited Nickel Coatings for Errosion Protection," AFML-TR-70-111, 1970.

17. R. L. Coombes, "Electroless Copper Preplating on ABS Plastics," Plating, July 1970.

18. N. Feldstein, "Selective Electroless Plating Techniques: A Survey," Plating, August 1970.

19. J. B. Burhawitz and V. H. Emerson, "Plating Methods, A Survey," NASA SP 5114, 1972.

20. D. J. Butler, "Improved Corrosion Protection for Solid Rocket Propulsion Systems," North American Rockwell Corp., Vol. 4, April 1973.

21. "Uniformly Thick Nickel Shells Produced by Vapor Deposition," Nickel Topics, Vol. 26, #1, 1973 by International Nickel Co., Inc.

22. E. W. Turns and J. W. Browning, "Properties of Electroless Nickel Coatings on High Strength Steels" Plating, May 1973.

CASTING OF WIND TUNNEL MODELS

1. "Selected Casting Techniques," NASA SP-5044, April 1965.

2. J. A. Payne, "Techniques and Facilities for Aeroelastic Modeling," Royal Aircraft Establishment, TR 68227, Sept. 1968.

3. J. A. Payne, "The Manufacture of Aeroelastic Models Using Glass Reinforced Plastics," Royal Aircraft Est. TR 71101, May 1971.

4. W. G. Dean and L. F. Connor, "A Study for Development of Aerothermodynamic Test Model Materials and Fabrication Technique," prepared under Contract NAS 1-9983 by Lockheed Missiles and Space Company.

5. C. E. DeRose and L. Yee, "Techniques for Producing Wind-Tunnel Heat Transfer Models," NASA Tech Brief B72-10349, NASA Ames Research Center, December 1972.

6. W. J. Gander, Brochure on Grumman Model Design and Fabrication Using Electroformed Nickel, June 1973.

7. Donald J. Collins, "An Inexpensive Technique for the Fabrication of Two-Dimensional Wind Tunnel Models," Rev. Sci. Instrum. Vol. 44, No. 7, July 1973.

HEAT TRANSFER INSTRUMENTATION

1. H. S. Carslaw and J. C. Jaeger, Conduction of Heat in Solids, Clarendon Press, 1950.
2. M. W. Zemansky, Heat and Thermodynamics, McGraw-Hill, 1951.
3. M. W. Rubesin, "The Effect of an Arbitrary Surface-Temperature Variation Along a Flat Plate on the Convective Heat Transfer in an Incompressible Turbulent Boundary Layer," NACA TN 2345, April 1951.
4. R. Gardon, "An Instrument for the Direct Measurement of Intense Thermal Radiation," The Review of Scientific Instruments, Vol. 24, No. 5, May 1953.
5. R. J. Conti, "Heat-Transfer Measurements at a Mach Number of 2 in the Turbulent Boundary Layer on a Flat Plate Having a Stepwise Temperature Distribution," NASA TN D-159, Nov. 1959.
6. J. C. Westkaemper, "An Analysis of Slug-Type Calorimeters for Measuring Heat Transfer From Exhaust Gases," AEDC-TN-60-202, Nov. 1960.
7. H. D. Baker, et al, Temperature Measurement In Engineering, Vol. I and Vol. II, John Wiley and Sons, Inc., 1961.
8. R. J. Conti, "Approximate Temperature Distributions and Streamwise Heat Conduction Effects in the Transient Aerodynamic Heating of Thin-Skinned Bodies," NASA TN D-895, Sept. 1961.
9. D. R. Burnett, "Transient Temperature Measurement Errors in Heated Slabs for Thermocouples Located at the Insulated Surface," Journal of Heat Transfer, Nov. 1961.
10. R. L. Ledford, "A Device for Measuring Heat Transfer Rates in Arc-Discharge Hypervelocity Wind Tunnels," AEDC-TDR-62-64, May, 1962.
11. E. T. Meleason and G. L. Burke, "Experimental Determination of Conduction Errors in Aerodynamic Heating Test Date," ASRMDF-TM62-37, FDL, Wright-Patterson Air Force Base, Ohio, June 1962.
12. J. W. Kurzrock, "Selection of Surface Thermometers for Measuring Heat Flux," Cornell Aero Lab, Report No. 124, Feb. 1963.
13. J. L. Lindsey and C. J. Stalmach, Jr., "Heat-Transfer-Rate Measurement Using a Thin-Continuous-Skin Technique in a Hypervelocity Wind Tunnel," Chance Vought Corporation Report 2-59740/3R-445, Feb. 1963.
14. E. A. Laumann, "Determining Aerodynamic Heating Rates Using Calorimetric Models in the Jet Propulsion Laboratory Hypersonic Wind Tunnel," Jet Propulsion Laboratory TM 33-121, March 1963.

15. W. D. Harvey, "Continuous Skin Construction Techniques for Fabricating Models for Aerodynamic Heat-Transfer Studies Involving Very Small Transient Heating Rates," Presented at Instrument Society of America 20th Annual ISA Conference and Exhibit, October 1965.

16. R. A. Jones and J. L. Hunt, "Use of Fusible Temperature Indicators for Obtaining Quantitative Aerodynamic Heat-Transfer Data," NASA TR R-230, Feb. 1966.

17. J. W. Reece, "Nonlinear Effects Due to High Heat Flux in Thin Film Thermometry and Means for Their Compensation," Proceedings of the 2nd International Congress on Instrumentation in Aerospace Simulation Facilities, August 1966.

18. C. R. Spitzer, "A Comparative Performance Analysis of Pyroelectric Heat-Transfer Sensors for Use in Hypersonic Impulse Facilities," Proceedings of the 2nd International Congress on Instrumentation in Aerospace Simulation Facilities, August 1966.

19. D. N. Kendall, et al, "Semiconductor Surface Thermocouples for Determining Heat Transfer Rates," Proceedings of the 2nd International Congress on Instrumentation in Aerospace Simulation Facilities, August 1966.

20. P. Czysz and D. Kendall, "Testing Technology Advances Associated with Development of an Arc Heated Impulse Tunnel," AIAA Paper 66-759, Sept. 1966.

21. E. O. Doebelin, Measurement Systems: Application and Design, McGraw-Hill, 1966.

22. D. S. Bynum, "Instrumentation for the AEDC/VKF 100-in. Hotshot (Tunnel F)," AEDC-TR-66-209, Jan. '67.

23. K. L. Ledford, W. E. Smotherman and C. T. Kidd, "Recent Developments in Heat-Transfer-Rate, Pressure, and Force Measurements for Hotshot Tunnels," AEDC-TR-66-220, Jan. 1967.

24. L. Bogdan, "Instrumentation Techniques for Short-Duration Test Facilities," Cornell Aeronautical Laboratory, Aerosciences Div. Report No. WTH-030, March 1967.

25. C. T. Kidd, "A Theoretical and Experimental Analysis of Slug Calorimeter Heat Losses for Continuous and Impulse Wind Tunnel Heat Flux Measurements," AEDC-TR-67-66, August 1967.

26. E. A. Laumann, "Determining Aerodynamic Heating Rates Using Calorimeter Models in the Jet Propulsion Laboratory Hypersonic Wind Tunnel," Jet Propulsion Laboratory TM No. 33-121.

27. P. A. Czysy and D. N. Kendall, "Improved Methods in Wind Tunnel Technology," McDonnell Co. Engineering Laboratories, Report F938, 15 April 1968.

28. W. P. Dixon, "Precise Heat Transfer Measurements with Surface Thermocouples," Presented at 8th Annual Conference on Thermal Conductivity, Purdue University, October, 1968.

29. E. H. Schulte, E. O. Puromen, W. P. Dixon, "Calibration Apparatus for Surface Thermocouples," International Congress on Instrumentation in Aerospace Simulation Facilities, 1969.

30. F. K. Hube, "An Experimental Method for Determining Heat Transfer Distributions on Blunt Bodies at Hypersonic Mach Numbers," AEDC-TR-69-20, June 1969.

31. Jean Maulard, "Calibration Method Used at ONERA for Hotshot and Shock Tube Heat Transfer Transducers," International Congress on Instrumentation in Aerospace Simulation Facilities, 1969.

32. E. H. Schulte and R. F. Stahl, "A High Heat Flux Sensor Employing Semiconductors," International Congress on Instrumentation in Aerospace Simulation Facilities, 1969.

33. J. P. Chevallier, J. Ponteziere and A. Betremiux, "Calorimeter Method of Heat Flux Measurement in Wind-Tunnels," Office National D'Etudes Et De Recherches Aerospatiales, Note Technique No. 159 (1970).

34. L. B. Garrett and J. I. Pitts, "A General Transient Heat-Transfer Computer Program for Thermally Thick Walls," NASA TM X-2058, August 1970.

35. Manual on the Use of Thermocouples in Temperature Measurement, ASTM Special Technical Publication 470, American Society for Testing and Materials, August 1970.

36. J. L. Hunt and J. I. Pitts, "Application of Phase-Change Technique to Thin Sections with Heating on Both Surfaces," informal information presented at Supersonic Tunnel Association, March 1971.

37. D. D. Pollock, The Theory and Properties of Thermocouple Elements, ASTM Special Technical Publication 492, American Society for Testing and Materials, Phil. Pa., May 1971.

38. "Test Facilities Handbook (9th Edition)" Arnold Engineering Development Center, July 1971.

39. C. B. Johnson, "High Reynolds Number Turbulent Heating to Two Simplified Shuttle Configurations," in NASA TM X-2507 Space Shuttle Aerothermodynamic Technology Conference Vol. II - Heating, Feb. 1972.

40. H. L. Seegmiller and G. G. Mateer, "Effects of Roughness on Heating and Boundary-Layer Transition," in NASA TM X -2507, Space Shuttle Aerothermodynamics Technology Conference, Vol. II - Heating, Feb. 1972.

41. J. J. Bertin, et. al., "Aerothermodynamic Measurements for Space Shuttle Configuration in Hypersonic Wind Tunnels," in NASA TM X-2507, Space Shuttle Aerothermodynamics Technology Conference, Vol. II - Heating, Feb. 1972.

42. D. L. Compton, "Convective Heating Measurements by Means of an Infared Camera," in NASA TM X-2507, Space Shuttle Aerothermodynamics Technology Conference, Vol. II - Heating, Feb. 1972.

43. D. A. Throckmorton, "Heat-Transfer Testing Procedures in Phase B Shuttle Studies With Emphasis on Phase-Change Data Improvement," in NASA TMX - 207, Space Shuttle Aerothermodynamics Technology Conference, Vol. II - Heating, Feb. 1972.

44. C. J. Stalmach, Jr., "Plating Methods for Thin-Skin Heat-Transfer Models," LTV Aerospace Corp., VSD Report 2-59700/2R-2986, Feb. 1972, Rev. A, May 1972.

45. R. K. Matthews, et. al., "Heat-Transfer and Flow-Field Tests of the McDonnell-Douglas-Martin Marietta Space Shuttle Configurations," AEDC-TR-73-53, April 1973.

46. C. E. Rogers, et.al., "A Thermal Mapping Technique for Shock Tunnels and a Practical Data-Reduction Procedure," AIAA Paper 72-1031, Spet. 1972.

47. Stone, et. al., "Factors Affecting Phase-Change Paint Heat-Transfer Data Reduction with Emphasis on Wall Temperatures Approaching Adiabatic Conditions," AIAA 72-1030, Sept. 1972.

48. D. L. Schultz and T. V. Jones, "Heat-Transfer Measurements in Short-Duration Hypersonic Facilities," AGARD -AG-165, February 1973.

49. L. L. Trimmer, R. K. Matthews and T. D. Buchanan, "Measurement of Aerodynamic Heat Rates at the Von Karman Facility," International Congress on Instrumentation in Aerospace Simulation Facilities, Sept. 1973.

50. R. K. Matthews, "Aerothermal Mapping and Photographic Data Processing at AEDC," International Congress on Instrumentation in Aerospace Simulation Facilities, 19[illegible]

51. S. C. Metcalf, "An Evaluation of Heat Transfer Measurement Techniques for use in a Low Density Tunnel," Aerodynamic Dept., RAE Farnborough, presented at 40th Semi-Annual STA Meeting, Sept. 1973.

Appendix II

Description of a Computer Routine for the Analysis of a Two-Dimensional Conductive Heat Transfer

By: T. C. Pope

A simplified heat transfer routine has been developed for the analysis of two-dimensional conductive heating in a body comprised of as many as four materials. The heat source for the system was conductive heating, represented by $\dot{Q} = HA\,(T_{\substack{\text{adiabatic} \\ \text{wall}}} - T_{\text{wall}})$, to which one side of the body was exposed. Although the routine was coded for a specific problem, it is adaptable and can be used for other applications involving conductive heating.

The program was developed under NASA contract NAS9-13692 for the purpose of determining the effects of the geometric and thermal-property variations which could be affected in the design of heat transfer instrumentation. The basic configuration is illustrated in Figure 1 and consists of a thin, metallic film to which a wire is butted to the backside; the remainder of the backside volume consists of a low-conductivity substrate and, if desired, an air gap around the wire.

Since the problem was two-dimensional, the model configuration was sliced in half and divided into finite elements as shown in Figure 2. (The arrangement and number of elements in this figure, 4 by 10, is for illustrative purposes only; the routine is capable of handling 11 by 44 elements if computation time is not a consideration.) A single element is shown in Figure 3 and the various conductive areas are defined. The two-dimensional elements which were modeled in the computer routine are illustrated in Figure 4 with the areas designated and the heat flow sign convention defined.

By modifying the three-dimensional elements of Figures 2 and 3 to the two-dimensional form of Figure 4, the model matrix becomes that of Figure 5. The dimensions of the elements may be varied; however, with the present arrangement the first two layers have a width of half the wire diameter and a depth or thickness equal to the film thickness; the remaining layers have the same width and a thickness of 0.05 inches. The program is a finite-interval computation of the heat balance equation given in Figure 4 for each of the elements. The incremental heat conduction is calculated from

$$\frac{(\text{thermal conductivity})(\text{conduction area})(\text{temperature difference between elements})(\text{time increment})}{(\text{conduction length})}$$

for each of the four heat flux components. The temperature increment for each element is caluclated from

$$\frac{(\text{heat stored})}{(\text{specific heat})(\text{density})(\text{element volume})}$$

The boundary conditions slightly alter the heat balance equation in Figure 4. For instance, for elements on the surface (the first layer) Q_1 would be replaced by HA $(T_{\text{adiabatic wall}} - T_{\text{wall}})$. Similarly, the sides and bottom are adiabatic boundaries so that the appropriate Q in each case would be set to zero. The selection of the time increment is most important from two aspects not related to accuracy. If the increment is too small, the computer time can become prohibitive. If the time increment is too large, the computed temperatures will begin to oscillate, rather than continuously rise, and subsequently diverge. An estimate of the magnitude of the largest increment that can be used, and divergence avoided, is given by

$$\frac{(\text{specific heat})(\text{density})(\text{element thickness})^2}{\text{thermal conductivity}}$$

The above expression must be evaluated for each material and the minimum value obtained selected for use.

With regard to the simplification of the routine it should be noted that radiation has been neglected in the heat balance equation. Similarly, corrections for joints (interfaces between materials) have been omitted. This was done because of the ill defined joints which would probably exist and the complexity which would be required in establishing the model matrix for the routine. Finally, in the runs that were made with an air gap separating the wire from the substrate, convection was ignored.

The results which were generated for the aforementioned contract are difficult to check. Thus, to provide some verification of the routine and procedures upon which it was based, a classical, constant-property, semi-infinite-slab problem was run, and a series of hand calculations were made using the information presented in *Temperature Response Charts* by P. J. Schneider © 1963, John Wiley & Sons, Inc. A comparison of these results is shown in Figure 6. The agreement between the two methods at 3 seconds (the problem termination time) was within 0.1°F. This extremely small difference is particularly impressive or perhaps fortuitous since in the course of this solution the computer performed 30,000 finite-interval approximations without the benefit of extended precision. This feature was not available due to the limitation of the storage capacity.

Other applications of the routine may be effected by varying the material properties and element dimensions as desired. Cases ranging from the basic semi-infinite homogenous slab to the more complex four-material problem can be handled.

Enclosure 1 defines some of the more prominent terms used in Enclosure 2, a listing of the FORTRAN program. A sample of the output format is given in Enclosure 3.

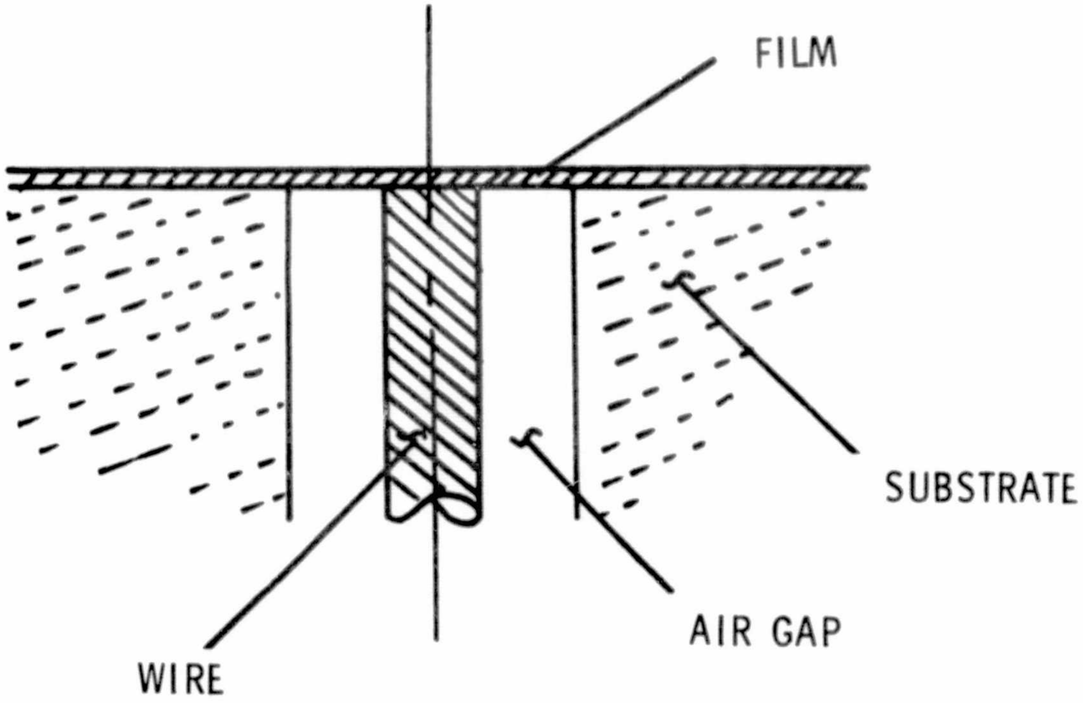

FIGURE I GENERAL CONFIGURATION
(CROSS SECTION)

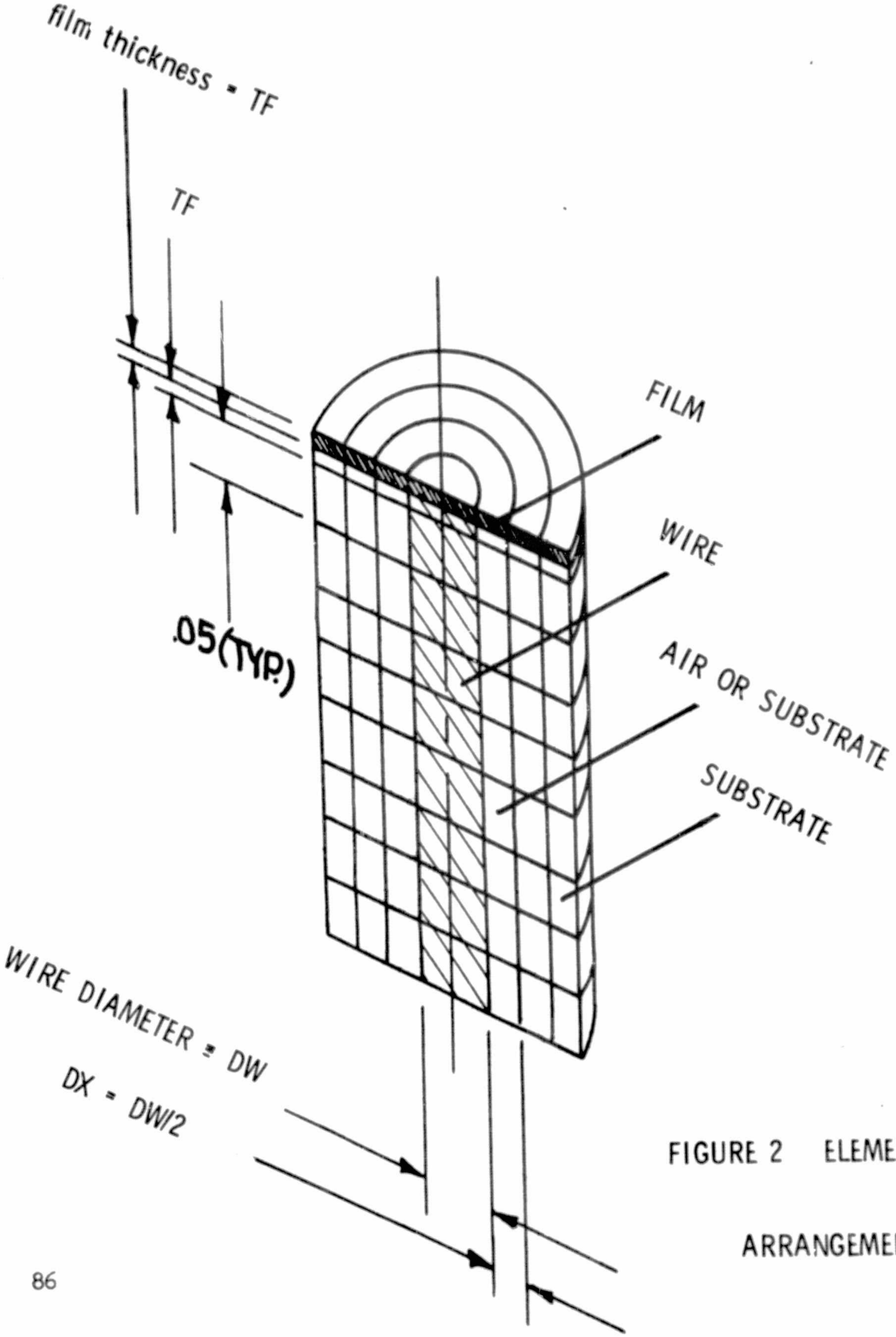

FIGURE 2 ELEMENT ARRANGEMENT

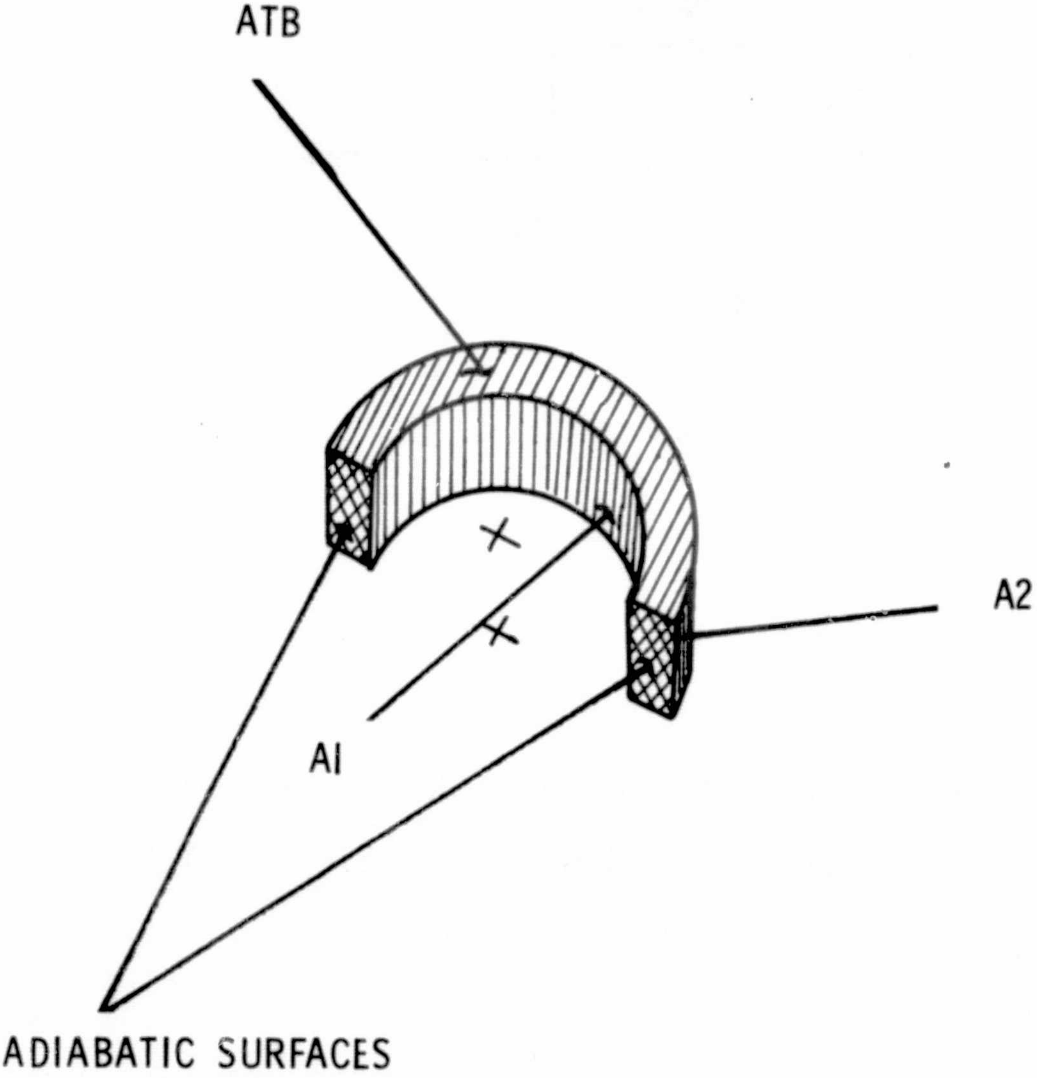

FIGURE 3 DEFINITION OF AREAS ON TYPICAL ELEMENT

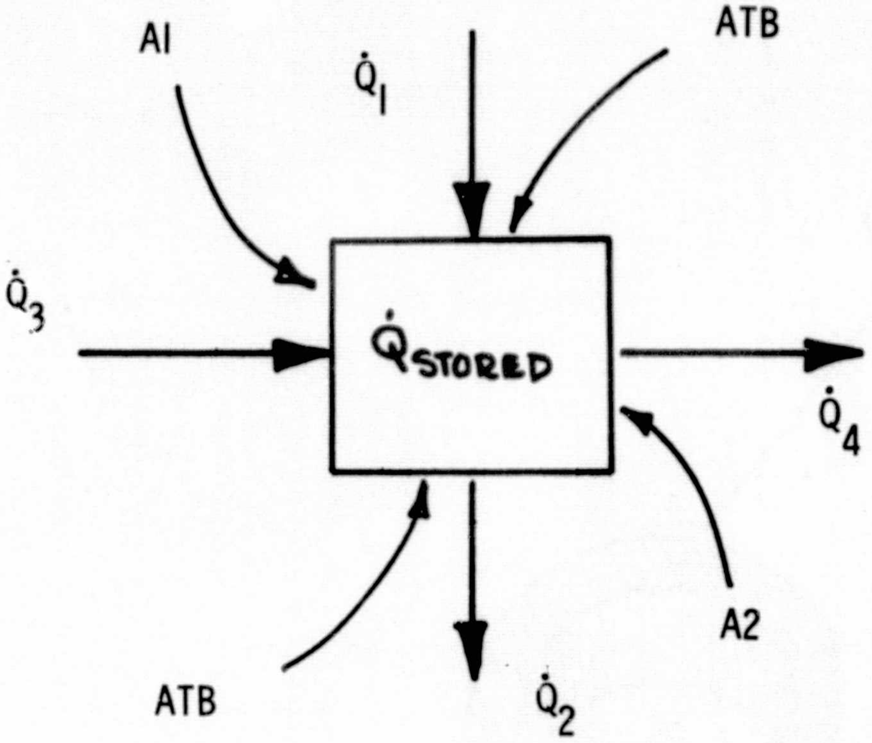

$$\dot{Q}_{STORED} = \dot{Q}_1 - \dot{Q}_2 + \dot{Q}_3 - \dot{Q}_4$$

FIGURE 4 TWO-DIMENSIONAL VERSION OF TYPICAL ELEMENT AND HEAT FLUX SIGN CONVENTION

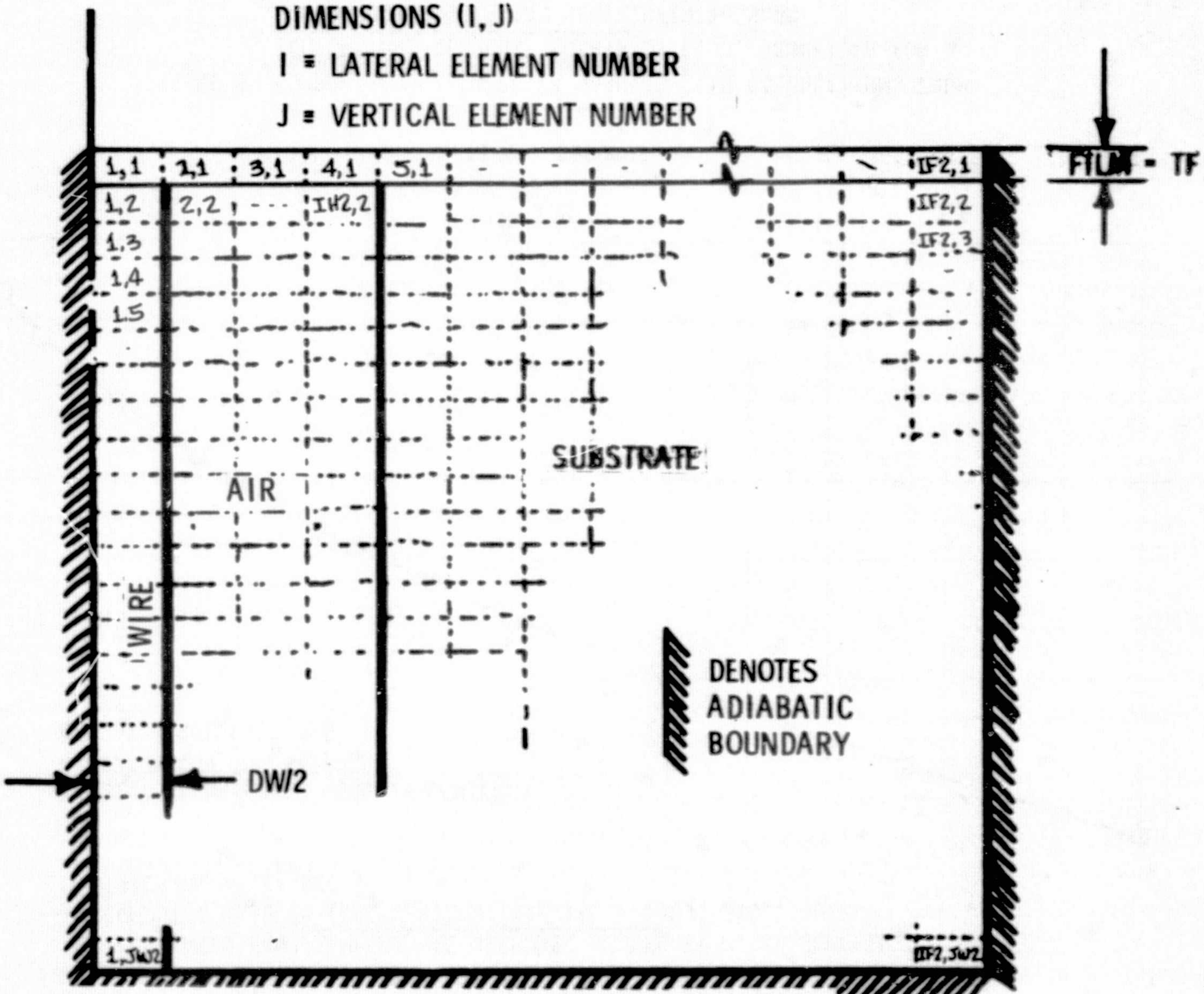

FIGURE 5 ELEMENT DEFINITION IN COMPUTER PROGRAM

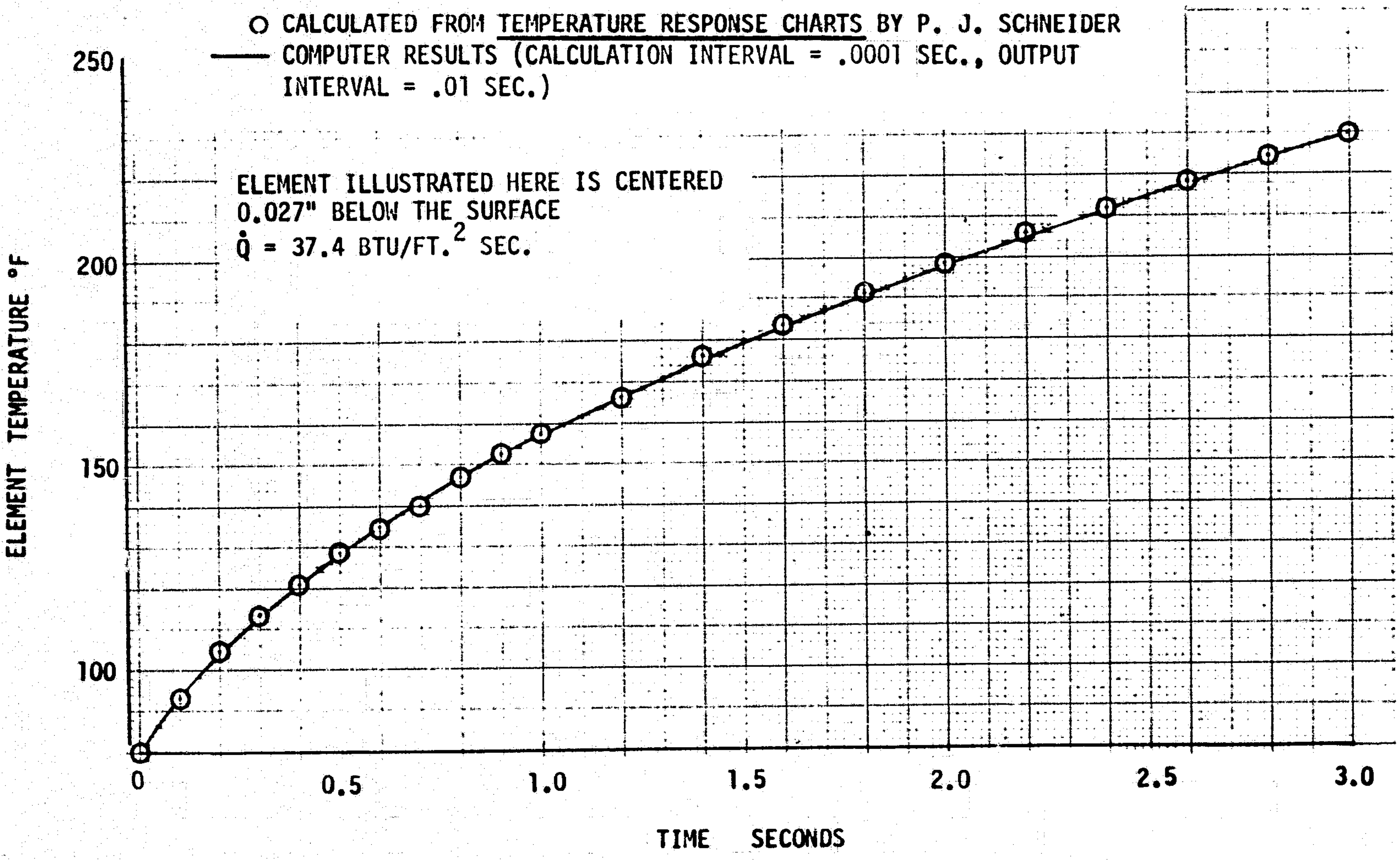

FIGURE 6 COMPARISON OF COMPUTER RESULTS WITH CALCULATIONS FROM TEMPERATURE RESPONSE CHARTS BY P. J. SCHNEIDER FOR A HOMOGENOUS CONSTANTAN SEMI-INFINITE SLAB

CPA, CPF, CPS and CPW	specific heat of air, film, substrate and wire, respectively, BTU/lb.$^{\circ}$F
DENA, DENF, DENS and DENW	density of air, film, substrate and wire, respectively, lb./ft.^{3}
DW	wire diameter, in.
DX	DW/2, the width of an element, in.
DYF	the height of elements in the first two layers, in.
DYW	the height of elements in layers below the first two layers, in.
H	heat transfer coefficient, BTU/ft.^{2} sec. $^{\circ}$F
I	lateral element number (see Figure 5)
IF2	the number of elements in the horizontal plane (see Figure 5)
J	vertical element number (see Figure 5)
JW2	the number of elements in the vertical plane (see Figure 5)
KA, KF, KS and KW	thermal conductivity of air, film, substrate and wire, respectively, BTU/ft.$^{\circ}$F sec.
TAW	adiabatic wall temperature, $^{\circ}$F
TF	film thickness, in.
T(I,J)	temperature of element(I,J) $^{\circ}$F.

Enclosure 1 - Definition of Some Terms Used in Program

```
      REAL KF,KA,KM,KS,K(11,44)
      DIMENSION T(11,44),TAVG(11) ,DEM(11,44),CP(11,44),ATM(11),
     1C1(11,44),C2(11,44),C3(11,44),C4(11,44),
     2              A1(11,44),A2(11,44),ONET(11,44)
      IPUCH=0
      H=.039
      TM=1040.
      TF=.001
      DW=.01
      DX=DW/2.
      DYF=TF
      TIME=0.
      ICT=0
      DO 100 J=1,44
      DO 100 I=1,11
  100 T(I,J)=80.
      CPA=.24
      DEMA=.07675
      KA=.0000038
      KF=.0009
      DENF=515.
      CPF=.13
      DEMM=556.6
      CPM=.094
      KM=.00337
      CPS=.2
      DEMS=131.
      KS=.0002132
      IF2=7
      JF2=1.
      JM2=3
      JM22=JM2-1
      IM2=3
      IS=IF2+1
      IA=2
      DT=.0001
      DO 110 J=1,JF2
      DO 110 I=1,IF2
      CP(I,J)=CPF
      DEM(I,J)=DENF
  110 K(I,J)=KF
      DO 111 J=2,20
      DO 111 I=IA,IM2
      CP(I,J)=CPA
      DEM(I,J)=DEMA
  111 K(I,J)=KA
      DO 112 J=2,20
      DO 112 I=1,1
      CP(I,J)=CPM
      DEM(I,J)=DEMM
  112 K(I,J)=KM
      DO 113 J=2,20
      DO 113 I=IS,IF2
      CP(I,J)=CPS
      DEM(I,J)=DEMS
  113 K(I,J)=KS
      DO 152 I=1,IF2
```

Enclosure 2 (Con't.)

Page 2 of 3

```
 152 ATB(I)=3.1416*DX**2*(2.*I-1)/2./144.
     DO 150 J=1,1
     DO 150 I=1,IF2
     A1(I,J)=3.1416*DX*DYF*(I-1)/144.
     A2(I,J)=3.1416*DX*DYF*I/144.
     C1(I,J)=12.*K(I,J)*ATB(I)/DYF
     C2(I,J)=12.*K(I,J)*A1(I,J)/DX
     C3(I,J)=12.*K(I,J)*A2(I,J)/DX
 150 C4(I,J)=CP(I,J)*DEN(I,J)*ATB(I)*DYF/12.
     DO 151 J=2,20
     DO 151 I=1,IF2
     IF(J-2)157,155,156
 155 DYW=.05
     GO TO 157
 156 DYW=.05
 157 A1(I,J)=3.1416*DX*DYW*(I-1)/144.
     A2(I,J)=3.1416*DX*DYW*I/144.
     C1(I,J)=12.*K(I,J)*ATB(I)/DYW
     C2(I,J)=12.*K(I,J)*A1(I,J)/DY
     C3(I,J)=12.*K(I,J)*A2(I,J)/DX
 151 C4(I,J)=CP(I,J)*DEN(I,J)*ATB(I)*DYW/12.
 933 FORMAT(     5E20.6)
     DO 932 J=1,20
 932 WRITE(6,933)CP(1,J),CP(2,J),CP(3,J),CP(4,J),CP(5,J)
     DO 934 J=1,20
 934 WRITE(6,933)DEN(1,J),DEN(2,J),DEN(3,J),DEN(4,J),DEN(5,J),DEN(6,J),
    1DEN(7,J)
     DO 935 J=1,20
 935 WRITE(6,933)K(1,J),K(2,J),K(3,J),K(4,J),K(5,J),K(6,J),K(7,J)
     DO 936 J=1,20
 936 WRITE(6,933)A1(1,J),A1(2,J),A1(3,J),A1(4,J),A1(5,J),A1(6,J),
    1A1(7,J)
     DO 937 J=1,20
 937 WRITE(6,933)A2(1,J),A2(2,J),A2(3,J),A2(4,J),A2(5,J),A2(6,J),
    1A2(7,J)
     DO 938 J=1,20
 938 WRITE(6,933)C1(1,J),C1(2,J),C1(3,J),C1(4,J),C1(5,J),C1(6,J),
    1C1(7,J)
     DO 939 J=1,20
 939 WRITE(6,933)C2(1,J),C2(2,J),C2(3,J),C2(4,J),C2(5,J),C2(6,J),
    1C2(7,J)
     DO 941 J=1,20
     DO 940 J=1,20
 940 WRITE(6,933)C3(1,J),C3(2,J),C3(3,J),C3(4,J),C3(5,J),C3(6,J),
    1C3(7,J)
 941 WRITE(6,933)C4(1,J),C4(2,J),C3(3,J),C4(4,J),C4(5,J),C4(6,J),
    1C4(7,J)
 169 QNET(1,1)=DT*(H*ATB(1)*(TAW-T(1,1))-          C1(1,2)    *(T(1,1)
    1-T(1,2))-C3(2,1)*(T(1,1)-T(2,1)))
     DO 800 I=2,IF2
 800 QNET(I,1)=DT*(H*ATB(I)*(TAW-T(I,1))+C2(I   ,1)*(T(I-1,1)-T(I,1))
    1-C1(I,2)*(T(I,1)-T(I,2))-C3(I+1,1)*(T(I,1)-T(I+1,1)))
     JW22=JW2-1
     DO 802 J=2,JW22
     DO 802 I=2,IF2
 802 QNET(I,J)=DT*(          C1(I,J)     *(T(I,J-1)-T(I,J))
    1-C1(I,J+1)*(T(I,J)-T(I,J+1))+          C2(I,J)     *(T(I-1,J)
```

(1) No surface joints
(2) Good surface detail reproduction
(4) Accurate instrument location
(6) Sufficient strength
(8) Instrument placement anywhere
(9) Effective in areas of high thermal gradients

The plated slab possesses a very hard surface that is resistant to particle damage and therefore meets in principal the model objective number (5). However, particle damage did occur in the pebble-bed heater facility used in this evaluation. Figure 19 shows post-test magnified views of the flat face of ECAN Model CC compared to the heat treated (190,000 psi) flat face of the master Model A. Both models were subjected to all eight runs in the hypersonic tunnel and both were still providing data without any loss of instrumentation. Figure 19 and Table IX indicate particle damage resistance of the ECAN models is comparable to a heat treated stainless steel model. The softer copper coating of the ATZC process had more severe particle damage as noted in Table IX.

The customization of sensor sensitivity, objective (7), was restricted to materials that provided good plate-to-substrate bond strength. The best materials for bond strength fortunately also provided good data sensitivity. Areas of low heating impose less demand on the plate bond and therefore less restriction on the choice of materials for increased sensitivity (if required).

Data accuracy (not listed as a specific objective) obviously must be adequate if the plated slab concept is to be practiced. The tunnel results of this preliminary test proved that this model method will provide accurate data. Further improvements in accuracy can be expected as material, process and data reduction improvements are made. Discovery of the Niculoy/constantan thermocouple greatly enhances the data accuracy and overall attractiveness of this modeling approach.

<u>Problem Areas</u>. - A smooth surface finish (objective (3)) could be provided, however, for marginal operating temperatures. The principal problem area was finding an acceptable compromise between surface smoothness, plate hardness and maximum operating temperature of the model.

Figure 20 is a photograph comparing the surface smoothness of master, ATZN and ECAN models. The smoothness of ATZN models are considered adequate for applications involving natural hypersonic boundary layer transition. Figure 21 shows magnified views of the ATZN surfaces compared to the master and the aluminum transfer film. Note that polishing marks of the master are reproduced in the plated plastic models which attests to the faithful reproduction of surface detail of this process. The thicker plate of Model M shows some pores caused by hydrogen bubbles forming on the surface during plating. This problem can be reduced by better control of the nitrogen agitation in the plating solution.

Enclosure 2 (Con't.)

Page 2 of 3

```
 152 ATB(I)=3.1416*DX**2*(2.*I-1)/2./144.
     DO 150 J=1,1
     DO 150 I=1,IF2
     A1(I,J)=3.1416*DX*DYF*(I-1)/144.
     A2(I,J)=3.1416*DX*DYF*I/144.
     C1(I,J)=12.*K(I,J)*ATB(I)/DYF
     C2(I,J)=12.*K(I,J)*A1(I,J)/DX
     C3(I,J)=12.*K(I,J)*A2(I,J)/DX
 150 C4(I,J)=CP(I,J)*DEN(I,J)*ATB(I)*DYF/12.
     DO 151 J=2,20
     DO 151 I=1,IF2
     IF(J-2)157,155,156
 155 DYW=.05
     GO TO 157
 156 DYW=.05
 157 A1(I,J)=3.1416*DX*DYW*(I-1)/144.
     A2(I,J)=3.1416*DX*DYW*I/144.
     C1(I,J)=12.*K(I,J)*ATB(I)/DYW
     C2(I,J)=12.*K(I,J)*A1(I,J)/DX
     C3(I,J)=12.*K(I,J)*A2(I,J)/DX
 151 C4(I,J)=CP(I,J)*DEN(I,J)*ATB(I)*DYW/12.
 933 FORMAT(     5E20.6)
     DO 932 J=1,20
 932 WRITE(6,933)CP(1,J).CP(2,J),CP(3,J),CP(4,J),CP(5,J)
     DO 934 J=1,20
 934 WRITE(6,933)DEN(1,J),DEN(2,J),DEN(3,J),DEN(4,J),DEN(5,J),DEN(6,J).
    1DEN(7,J)
     DO 935 J=1,20
 935 WRITE(6,933)K(1,J),K(2,J),K(3,J),K(4,J),K(5,J),K(6,J),K(7,J)
     DO 936 J=1,20
 936 WRITE(6,933)A1(1,J).A1(2,J),A1(3,J),A1(4,J),A1(5,J),A1(6,J),
    1A1(7,J)
     DO 937 J=1,20
 937 WRITE(6,933)A2(1,J),A2(2,J),A2(3,J),A2(4,J),A2(5,J),A2(6,J).
    1A2(7,J)
     DO 938 J=1,20
 938 WRITE(6,933)C1(1,J),C1(2,J),C1(3,J),C1(4,J),C1(5,J),C1(6,J),
    1C1(7,J)
     DO 939 J=1,20
 939 WRITE(6,933)C2(1,J).C2(2,J),C2(3,J),C2(4,J),C2(5,J),C2(6,J).
    1C2(7,J)
     DO 941 J=1,20
     DO 940 J=1,20
 940 WRITE(6,933)C3(1,J).C3(2,J),C3(3,J),C3(4,J),C3(5,J),C3(6,J),
    1C3(7,J)
 941 WRITE(6,933)C4(1,J),C4(2,J),C3(3,J),C4(4,J),C4(5,J),C4(6,J).
    1C4(7,J)
 169 QNET(1,1)=DT*(H*ATB(1)*(TAW-T(1,1))-          C1(1,2)     *(T(1,1)
    1-T(1,2))-C3(2,1)*(T(1,1)-T(2,1)))
     DO 800 I=2,IF2
 800 QNET(I,1)=DT*(H*ATB(I)*(TAW-T(I,1))+C2(I   ,1)*(T(I-1,1)-T(I,1))
    1-C1(I,2)*(T(I,1)-T(I,2))-C3(I+1,1)*(T(I,1)-T(I+1,1)))
     JW22=JW2-1
     DO 802 J=2,JW22
     DO 802 I=2,IF2
 802 QNET(I,J)=DT*(           C1(I,J)     *(T(I,J-1)-T(I,J))
    1-C1(I,J+1)*(T(I,J)-T(I,J+1))+           C2(I,J)     *(T(I-1,J)
```

Enclosure 2 (Con't)

Page 3 of 3

```
     2-T(I.J))-C3(I+1,J)*(T(I,J)-T(I+1,J)))
      DO 801 J=2,JW2
  801 QNET(1,J)=DT*(             C1(1,J)     *(T(1,J-1)-T(1,J))
     1-C1(1,J+1)*(T(1,J)-T(1,J+1))-            C3(2,J)      *(T(1,J)-T(2,J)))
      DO 806 I=1,IF2
  806 QNET(I,JW2)=DT*(C1(I,JW2  )*(T(I,JW2-1)-T(I,JW2))
     1+             C2(I+1.JW2)     *(T(I,JW2)-T(I+1,JW2))
     2-             C3(I+1,JW2)     *(T(I,JW2)-T(I+1,JW2)))
      DO 813 J=2,JW2
  813 QNET(11,J)=DT*(              +C1(11,J)     *(T(11,J-1)-T(11,J))
     1+C2(11,J)*(T(10,J)-T(11,J))-C1(11,J+1)*(T(11,J)-T(11,J+1)))
      QNET(11,1)=DT*(H*ATR(11)*(TAW-T(11,1))-             C1(11,2)      *
     1(T(11,1)-T(11,2))+C2(11,1)*(T(10,1)-T(11,1)))
      DO 803 J=1,JW2
      DO 803 I=1,IF2
  803 T(I,J)=T(I,J)+QNET(I,J)/C4(I,J)
      IF(T(1,JW2)-81.)835,835,832
  832 JW2=JW2+1
  835 CONTINUE
      IF(JW2-12)833,833,834
  834 JW2=12
  833 CONTINUE
      TIME=TIME+DT
      ICT=ICT+1
   56 ICT=0
      WRITE(6,49)TIME
   49 FORMAT(///,5X,E20.10)
      DO 45 J=1,JW2
   45 WRITE(6,44)T(1,J),T(2,J),T(3,J),T(4,J),T(5,J),T(6,J),T(7,J)
   44 FORMAT(5X, 7E11.4)
      DO 2000 I=1,IF2
 2000 TAVG(I)=(T(I,1)+T(I,2))/2.
      WRITE(6,2001)TAVG(1),TAVG(2),TAVG(3),TAVG(4),TAVG(5),TAVG(6).
     1TAVG(7)
 2001 FORMAT(/,5X,7E11.4)
      IPUCH=IPUCH+1
      IF(IPUCH-20)2499,2502,2502
 2502 IPUCH=0
      WRITE(5,2498)JW2
 2498 FORMAT(I5)
      DO 2500 J=1,JW2
 2500 WRITE(5,2501)TIME,T(1,J),T(2,J),T(3,J),T(4,J),T(5,J),T(6,J),T(7,J)
 2501 FORMAT(8F8.4)
 2499 CONTINUE
      IF(TIME-3.0)169,169,970
  970 STOP
      END
00A1
```

ORIGINAL PAGE IS
OF POOR QUALITY

C-2

OUTPUT FORMAT

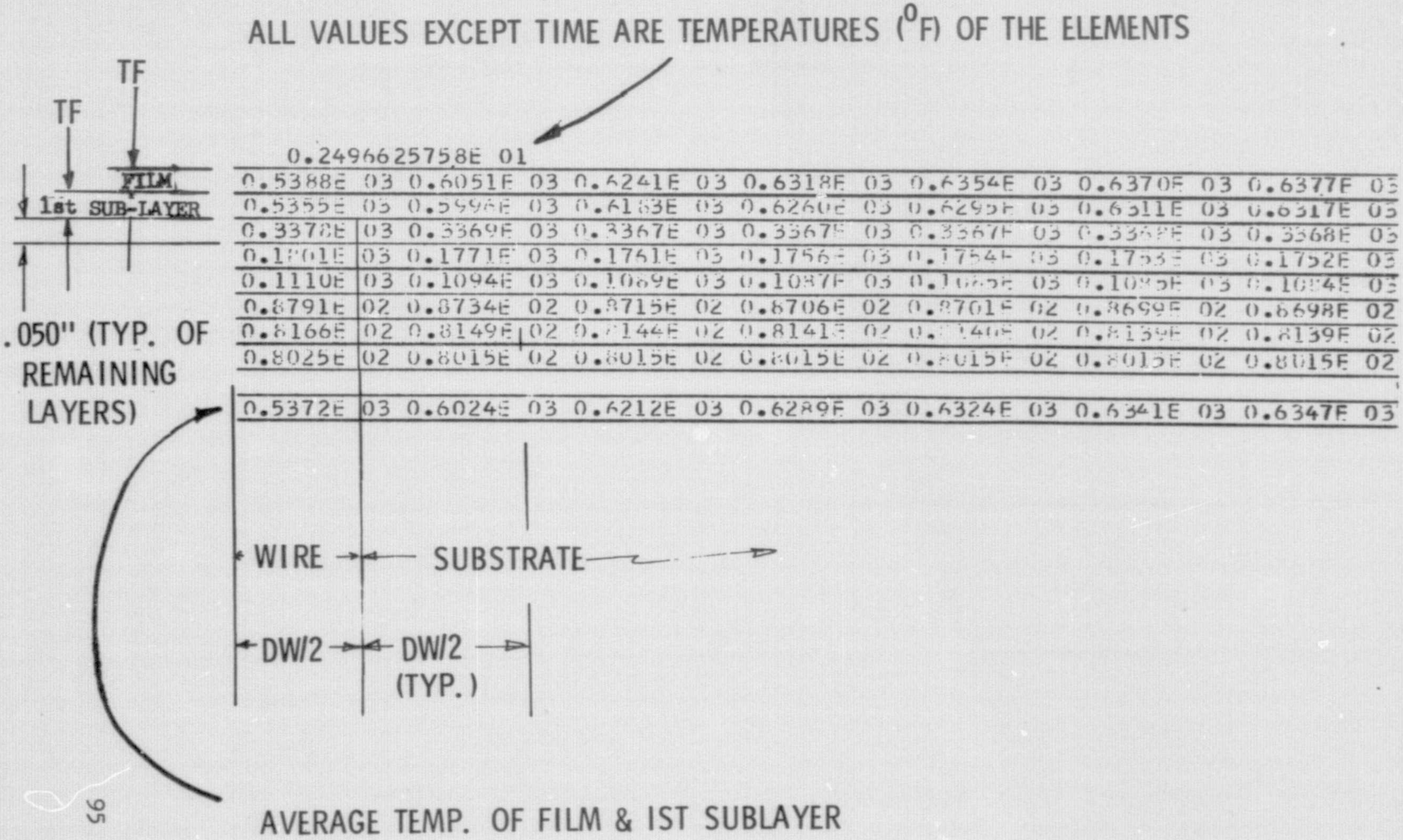

```
      0.2496625758E 01
0.5388E 03 0.6051E 03 0.6241E 03 0.6318E 03 0.6354E 03 0.6370E 03 0.6377E 03
0.5355E 03 0.5996E 03 0.6183E 03 0.6260E 03 0.6295E 03 0.6311E 03 0.6317E 03
0.3378E 03 0.3369E 03 0.3367E 03 0.3367E 03 0.3367E 03 0.3368E 03 0.3368E 03
0.1801E 03 0.1771E 03 0.1761E 03 0.1756E 03 0.1754E 03 0.1753E 03 0.1752E 03
0.1110E 03 0.1094E 03 0.1089E 03 0.1087E 03 0.1085E 03 0.1085E 03 0.1084E 03
0.8791E 02 0.8734E 02 0.8715E 02 0.8706E 02 0.8701E 02 0.8699E 02 0.8698E 02
0.8166E 02 0.8149E 02 0.8144E 02 0.8141E 02 0.8140E 02 0.8139E 02 0.8139E 02
0.8025E 02 0.8015E 02 0.8015E 02 0.8015E 02 0.8015E 02 0.8015E 02 0.8015E 02

0.5372E 03 0.6024E 03 0.6212E 03 0.6289E 03 0.6324E 03 0.6341E 03 0.6347E 03
```

ENCLOSURE 3